INVESTIGATION OF THE *HELICOBACTER PYLORI* CAG TYPE IV SECRETION SYSTEM *IN VITRO* AND *IN VIVO*

By

Aung Soe Lin

Dissertation

Submitted to the Faculty of the Graduate School

of Vanderbilt University in partial fulfillment of the

requirements for the degree of

DOCTOR OF PHILOSOPHY

In

MICROBIOLOGY AND IMMUNOLOGY

December 12th, 2020

Nashville, Tennessee

Approved by:

D. Borden Lacy, Ph.D.

Holly M. Algood, Ph.D.

David M. Aronoff, M.D.

Matthew J. Tyska, Ph.D.

Mary Kay Washington, M.D., Ph.D.

Timothy L. Cover, M.D.

To my parents and sister.

ACKNOWLEDGEMENTS

First and foremost, I would like to thank Tim Cover for being such a wonderful and supportive mentor. I have learned so much: for example, developing hypotheses, discussing ideas, and designing and executing experiments under your mentorship and guidance. You have taught me to not only become a better scientist trainee, but also be a team player and collaborator. I cannot thank you enough for providing me a nurturing laboratory environment which I called my home away from home. I could not have asked for a better boss. Thanks very much for welcoming me into your lab. I hope that I have lived up to your expectations during my Ph.D. journey.

I would also like to thank all the Cover lab members for fostering such a positive dynamic laboratory environment in which I could grow and learn. I would like to thank Mark and John for all your advice on designing and troubleshooting the experiments. Without your guidance, I would not have been able to have 'beautiful' data. I would like to thank Lorena for your friendship, for always being there for me for literally anything. I am glad that we joined the laboratory in the same year. I would also like to thank Rhonda for being my gym buddy and breakfast pal, and for always checking on me so that I do not 'over-exhaust myself'. I would also like to thank new additions to the lab – Georgia, Jennie, Mandy, and Sirena for making this lab exciting and interesting.

Finally, I would like to thank my family. My mom had always been so supportive. You are a guiding star in my life. I truly appreciate all your sacrifices. I would like to thank my dad for having set an example. Even though you would not be able to witness your son receiving Ph.D., I hope that I make you proud. I cannot thank you enough for teaching me to be kind, generous and genuine no matter what. I would also like to thank my sister for always being there whenever I need you, listening to me and supporting me. I always feel replenished and energetic after talking to you. My aunts and uncles have always been supportive of my education in Myanmar and the States. Talking and video chatting with you has always been a cure to my homesickness. Last, I would like to acknowledge my grandparents. You have molded me at an early age to be who I am today.

TABLE OF CONTENTS

Page

DEDICATION ii

ACKNOWLEDGEMENTS iii

LIST OF TABLES vii

LIST OF FIGURES viii

CHAPTER

I. INTRODUCTION 1

Prevalence of *Helicobacter pylori* infection and its role in gastric disease 1
The *cag* pathogenicity island (*cag* PAI) 2
Effector protein CagA 2
Prototypical type IV secretion systems (T4SSs) 3
The Cag type IV secretion system of *H. pylori* 3
Structural organization of the Cag type IV secretion system 4
Comparison of Cag T4SS to prototypical T4SS 5
Animal models for study of *H. pylori* 6
Gaps in knowledge 7

II. ATPASES ASSOCIATED WITH THE *HELICOBACTER PYLORI* CAG TYPE IV SECRETION SYSTEM 8

Introduction 8
Materials and methods 9
Growth of *H. pylori* strains 9
Generation of *H. pylori* mutant strains 10
Cryo-electron tomography (cryo-ET) analysis 10
Proteomic analysis of *H. pylori* membrane fractions 11
Isolation of the *H. pylori* Cag T4SS outer membrane core complex 12
CagA translocation assay 13
IL-8 induction assay 13
NF-κB activation assay 13
TLR9 activation assay 13
Results 14
ATPases associated with the Cag T4SS 14
Cag ATPases are not required for outer membrane core complex assembly 14
Visualization of the inner membrane via cryo-ET 18
Localization of the individual Cag ATPases in the inner membrane complex 20
Individual Cag ATPases are required for CagA translocation 22
Cagβ is dispensable for *H. pylori*-induced NF-κB activation and IL-8 production 26
Cagα and CagE are required for *H. pylori*-induced TLR9 activation 26
Putative ATP-binding motifs in Cag ATPases 29

Functional ATP-binding motifs in the Cag ATPases are required for CagA translocation 32
Functional ATP-binding motifs in Cagα and CagE are required for NF-κB activation, IL-8 induction, and TLR9 activation 34
Discussion 36

III. TEMPORAL CONTROL OF THE *HELICOBACTER PYLORI* CAG TYPE IV SECRETION SYSTEM IN A MONGOLIAN GERBIL MODEL OF GASTRIC CARCINOGENESIS 41

Introduction 41
Materials and methods 42
H. pylori culture methods 42
Generation of *H. pylori* strains in which Cag T4SS activity can be conditionally regulated 43
Animal infection 43
Processing of gastric tissue 44
Bacterial colonization density 44
Histology 44
Analysis of *cagUT* expression 45
Western blot analysis 46
NF-κB activation 46
CagA translocation assay 47
Statistical analyses 47
Results 48
Regulation of Cag T4SS activity *in vitro* 48
Regulation of *cagUT* expression *in vivo* 54
Stability of the TetR/*tetO* system *in vivo* 58
Gastric inflammation in response to Cag T4SS activity 60
Temporal regulation of Cag T4SS activity 63
Discussion 72

IV. GASTRIC LIPID ALTERATIONS IN RESPONSE TO *HELICOBACTER PYLORI* 78

Introduction 78
Materials and methods 79
Animal infection 79
Processing of gastric tissue 79
Histology 81
Mass spectrometry imaging 81
Chemicals 81
Lipid extraction for liquid chromatography-mass spectrometry (LC-MS/MS) procedure 82
Data processing for LC-MS/MS 83
Results 83
Gastric inflammation and disease outcomes in response to *H. pylori* 83

Visualization of gastric lipids by Imaging Mass Spectrometry (IMS) 89
Identification of lipids by Liquid Chromatography-Mass Spectrometry (LC-MS/MS) 89
Spatial distribution of differentially abundant lipids identified by LC-MS/MS and IMS 91
Spatial distribution of additional lipids by IMS 95
Discussion 99

V. PROJECTS IN PROGRESS 102

Filamentous structures 102
Structure of Cagα 108
Structure of Cagβ 112
Structure of CagE 116

VI. CONCLUSIONS AND FUTURE DIRECTIONS 120

Conclusions 120
Cag ATPases 120
Temporal control of the Cag T4SS *in vivo* 122
H. pylori-induced alterations of gastric lipids 123
Future directions 123

PUBLICATIONS 128

REFERENCES 129

LIST OF TABLES

Table Page

2.1 *H. pylori* strains used in this study 23

2.2 Mass spectrometric detection of Cag ATPases in wild-type and mutant strains..... 31

3.1 *H. pylori* strains used in this study 51

3.2 Frequency of most severe diagnosis in uninfected and infected animals receiving various concentrations of doxycycline 62

4.1 Quantification of parietal cell loss and chief cell loss 88

4.2 Lipids observed in positive or negative ion mode imaging mass spectrometry (IMS) and correlated with liquid chromatography mass spectrometry (LC-MS/MS) 90

LIST OF FIGURES

Figure Page

2.1 Individual Cag ATPases are not required for formation of the Cag T4SS core complex 16

2.2 Cryo-ET analyses reveal that individual Cag ATPases are not required for the assembly of outer membrane core complex 17

2.3 The inner membrane complex of the Cag T4SS 19

2.4 Localization of the individual Cag ATPases in the inner membrane complex 21

2.5 Individual Cag T4SS ATPases are essential for CagA translocation into AGS gastric epithelial cells 25

2.6 Cagα and CagE, but not Cagβ, are required for three Cag T4SS-dependent alterations in host cells 27

2.7 Functional Walker motifs in individual Cag T4SS ATPases are required for CagA translocation into AGS gastric epithelial cells 33

2.8 Functional Walker motifs in Cagα and CagE are required for three Cag T4SS-dependent phenotypes 35

3.1 Introduction of *tetR* and *tetO* in the engineered strain VM202-203 50

3.2 Regulatory control of *cagU* expression and Cag T4SS activity *in vitro* 52

3.3 Pilot experiment analyzing transcript abundance of *cagU* and a control gene (*lpxD*) in stomach tissues of infected gerbils receiving chow containing 0 mg/kg doxycycline 55

3.4 Regulatory control of *cagU* expression *in vivo* 57

3.5 Stability of the Cag T4SS *in vivo* 59

3.6 Gastric inflammation in *H. pylori*-infected animals in response to Cag T4SS activity 61

3.7 Gastric inflammation in response to Cag T4SS activity during specific stages of infection 65

3.8 Stability of the TetR/*tetO* system *in vivo* 66

3.9 Dysplasia and gastric cancer in response to Cag T4SS activity 68

3.10 Gastric inflammation and gastric cancer in response to Cag T4SS

activity during the initial 6 weeks of a 3-month infection 70

4.1 Processing of stomachs from Mongolian gerbils 80

4.2 Gastric histology from representative animals 85

4.3 Gastric inflammation in response to *Helicobacter pylori* 86

4.4 Loss of parietal cells and chief cells in response to *H. pylori* infection 87

4.5 Imaging mass spectrometry analysis showing reduced abundance of multiple sphingomyelin species in gastric tissue from infected animals 92

4.6 Imaging mass spectrometry analysis showing increased abundance of multiple phosphatidylcholine species in gastric tissues from infected animals 93

4.7 Imaging mass spectrometry analysis showing corpus localization of lysophosphatidylethanolamine 18:1 that is reduced in abundance in gastric tissues from infected animals 94

4.8 Imaging mass spectrometry analysis showing triglyceride 48:8 is reduced in abundance in gastric tissues from infected animals 96

4.9 Imaging mass spectrometry analysis showing phosphatidylcholine and phosphatidylserine species are increased in abundance in gastric tissues in infected animals 97

4.10 Imaging mass spectrometry analysis showing phosphatidylethanolamine species are increased in abundance in gastric tissues from infected animals 98

5.1 Individual Cag ATPases are not required for formation of "filamentous structures" 103

5.2 "Filamentous structures" are observed in images of a Δ*cag* PAI mutant strain when in contact with gastric epithelial cells 104

5.3 "Filamentous structures" are produced by the TetR/*tetO* strain in the presence or absence of anhydrotetracycline (ATc) 105

5.4 Modification of Cagα with an HA tag does not disrupt Cag T4SS function and allows affinity purification of Cagα via immunoprecipitation 108

5.5 Crosslinking and immuno-precipitation of HA- Cagα from a ΔCagα/HA-Cagα strain 109

5.6 Immuno-precipitation of HA-Cagβ 112

5.7 Purification of Cagβ from *H. pylori* 113

5.8 CagE purification via two steps using GST column and size exclusion column 115

5.9 2D class average of CagE structure showing spike features with a globular core at the center..... 116

5.10 Purification of CagE from *H. pylori*..... 117

Chapter I

Introduction

Prevalence of *Helicobacter pylori* infection and its role in gastric disease

Helicobacter pylori is a Gram-negative, helical-shaped, and microaerophilic bacterium that persistently colonizes the human stomach (1, 2). *H. pylori* infection is present in about half of the global population (1). The prevalence of *H. pylori* is higher in developing countries (for example, >80% prevalence in Brazil, Libya, Egypt, and Nigeria) than in developed countries (for example, less than 20% prevalence in Australia, Sweden, and Finland) (3). Low socio-economic status during childhood is one of the risk factors for *H. pylori* acquisition (4).

Relatively little is known about *H. pylori* transmission, but interpersonal transmission through the faeco-oral, oro-oral, or gastro-oral routes is likely (5). Transmission through consumption of contaminated water and food has been suggested as a possibility, especially in developing countries with poor sanitation systems (4), but there is relatively little direct evidence of transmission by this route.

H. pylori infection causes gastric inflammation in most infected persons, and long-term infection significantly increases the risk of developing peptic ulcer disease and gastric cancer (6, 7). It has been estimated that peptic ulcer disease develops in about 5% of *H. pylori*-positive individuals, gastric adenocarcinoma develops in about 1%, and mucosa-associated lymphoid tissue lymphoma develops in fewer than 0.1% (8-10). However, most infected individuals remain asymptomatic throughout their lives (10). The variable gastric disease outcomes are influenced by several factors, including environmental influences (smoking, high-salt diet), variation in host genetic characteristics, and *H. pylori* strain-specific virulence factors (*cag* pathogenicity island, VacA toxin, and specific outer membrane protein adhesins) (10).

The *cag* pathogenicity island (*cag* PAI)

The *cag* pathogenicity island (*cag* PAI) is a 40-kb chromosomal region that contains the *cagA* gene (encoding the secreted effector protein CagA) and genes that encode components of the Cag type IV secretion system (Cag T4SS) (11-15). The *cag* PAI was likely introduced into the *H. pylori* genome by a single horizontal DNA transfer event about 60,000 years ago. The *H. pylori* strains currently colonizing humans can be either *cag* PAI-positive or *cag* PAI-negative. The *cag* PAI is present in 90-100% of East Asian strains and about 50% of *H. pylori* strains found in the United States (16, 17). Individuals colonized with *H. pylori* strains containing the *cag* PAI have a higher risk of gastric adenocarcinoma or peptic ulcer disease than individuals colonized with *cag* PAI-negative strains (16, 17).

Effector protein CagA

CagA is the only effector protein known to be translocated into host cells by the Cag T4SS (18, 19). Upon entry into host cells, CagA undergoes phosphorylation of Glu-Pro-Ile-Tyr-Ala (EPIYA) motifs localized in the C-terminal portion of the protein, mediated by eukaryotic Src and Abl kinases (18-22). Phosphorylated CagA then interacts with multiple signaling molecules and alters their cellular activities (18-21). One of the host proteins that interacts with CagA is the pro-oncogenic phosphatase SHP2 (22, 23). CagA activates SHP2 and initiates a signaling cascade, resulting in the activation of the MAPK/ERK pathway and stimulation of cellular proliferation (22, 23). Non-phosphorylated CagA can also interact with multiple host cell proteins and alter their functions (18-20). These cellular alterations caused by CagA contribute to neoplastic transformation, and therefore, CagA has been designated as a “bacterial oncoprotein” (18, 19, 24).

Prototypical type IV secretion systems (T4SSs)

Type IV secretion systems (T4SSs) are found in many Gram-negative bacteria, Gram-positive bacteria and some Archaea (25-27). They are a versatile family of secretion systems that translocate effector proteins into host cells, import DNA, or export DNA into the extracellular milieu or host cells (25-27). Examples of effector-translocating T4SSs include the Dot/Icm system in *Legionella pneumophila* and *Coxiella burnetii* (28, 29), and the Cag T4SS in *H. pylori* (27). *Agrobacterium tumefaciens* utilizes the VirB/VirD T4SS to deliver T-DNA into plant cells, causing crown-gall disease, and *Escherichia coli* utilizes an F plasmid transfer system for conjugation and DNA transfer (30, 31).

The well-characterized VirB/VirD4 T4SS of *A. tumefaciens* is assembled from 12 subunits (VirB1- VirB11 and VirD4) and is composed of three main subassemblies (30, 31). There is an inner membrane complex, composed of multiple ATPases and other components (30, 31). The ATPases are predicted to provide energy for substrate translocation and secretion of pilus subunits (30, 31). The core complex is localized within the periplasm and extends from the inner membrane to the outer membrane (30, 31). The pilus is an extracellular structure, composed of multiple pilin subunits, which contacts target cells (30, 31).

The Cag type IV secretion system of *H. pylori*

H. pylori can potentially harbor as many as four different type IV secretion systems (T4SSs) (32, 33). One of them, the ComB T4SS, is present in nearly all *H. pylori* strains and mediates uptake of DNA (33, 34). T4SSs known as TFS3 and TFS4 are present in some *H. pylori* strains but absent from others; their functions are unknown (32, 33).

The Cag T4SS is encoded by a cluster of genes in the *cag* PAI (11-15). The Cag T4SS is required for several *H. pylori*-induced alterations of host cells, including CagA translocation, transcription factor (NF-κB) activation, cytokine (IL-8) production and toll-like receptor 9 (TLR9)

activation. About 17 of the 27 genes in the *cag* PAI are essential for CagA translocation into gastric epithelial cells, and about 14 are essential for *H. pylori*-induced IL-8 production by host cells (35). Interestingly, there are 3 genes (*cagβ*, *cagF*, *cagG*) that are dispensable for IL-8 induction but required for CagA translocation (35).

H. pylori-induced NF-κB activation and IL-8 production are attributed to the intracellular entry of non-protein bacterial constituents [lipopolysaccharide metabolites (36-39) and/or peptidoglycan (40)] into host cells. Activation of TLR9 is attributed to the entry of *H. pylori* DNA into host cells (41, 42). Several publications reported that CagA can contribute to IL-8 induction and NF-κB activation (43-46). Conversely, these two cellular responses are elicited by mutant strains that do not produce CagA (47-49), which indicates that *H. pylori* can stimulate these responses through CagA-independent pathways.

Structural organization of the Cag type IV secretion system

The Cag type IV secretion system is a macromolecular machine spanning both the inner and outer membranes of *H. pylori*. A large membrane-spanning core complex was isolated and shown to be composed of multiple copies of five proteins (CagM, CagT, Cag3, CagX, and CagY) (50-52). High resolution cryo-EM structural analysis of the transmembrane core complex revealed that the core complex has a mushroom-like shape and exhibits three main features – an outer membrane cap, a periplasmic ring, and central stalk (50-52). The structure of isolated core complex particles observed by single particle cryo-EM closely resembles the structure of this portion of the Cag T4SS observed in intact *H. pylori* by cryo-electron tomography (cryo-ET) (53). Cryo-ET analysis of the Cag T4SS in intact bacteria also revealed the presence of a Cag T4SS inner membrane complex (53, 54).

This inner membrane complex is predicted to be composed of multiple ATPases (Cagα, Cagβ, CagE) as well as additional Cag proteins. A previous study reported the crystal structure of

Cagα recombinantly expressed in *Escherichia coli* and provided evidence that Cagα assembles into hexameric structures (55). There has been relatively little effort to investigate the structures of Cagβ or CagE.

Comparison of Cag T4SS to prototypical T4SS

Several components of the Cag T4SS have detectable sequence similarities to counterparts in the VirB/VirD system. For example, CagE has sequence similarity to VirB4, CagX to VirB9, CagY to VirB10, Cagα to VirB11 and Cagβ to VirD4 (30, 31). Based on the topology predictions, localization, and functional studies, Cag4 is predicted to be homologous to VirB1, CagC to VirB2, CagL to VirB5, CagW to VirB6, CagT to VirB7 and CagV to VirB8 (30, 31). However, there are five Cag proteins that do not have any sequence similarity to other bacterial proteins and that are unique to the Cag T4SS (30, 56).

Both the Cag T4SS and the VirB/VirD4 T4SS contain an inner membrane complex and core complex. In both systems, the core complex has 14-fold symmetry, but the core complex of the Cag T4SS (~400 Å in width and ~250 Å in height) is much larger than that of the VirB/VirD4 T4SS (typically ~250 Å and ~150 Å in height). The VirB/VirD4 T4SS core complex contains three proteins – VirB7, VirB9 and VirB10 (26). On the other hand, the Cag T4SS core complex contains not only three VirB homologs [CagT (VirB7), CagX (VirB9) and CagY (VirB10)], but also additional CagT4SS-specific proteins (Cag 3 and CagM) (50-52). Recently, the Cag T4SS was reported to have a periplasmic ring feature, which is absent in the VirB/VirD T4SS (51, 52).

The T4SSs (including VirB/VirD system) in multiple bacterial species (*Escherichia, Legionella, Helicobacter, Agrobacterium)* have more than one ATPase. Maintaining more than one ATPase is an energetically expensive process. The existence of multiple ATPases associated with T4SSs suggests that this provides evolutionary advantage to the bacteria and implies that the

functions of individual ATPases are non-redundant. In *H. pylori*, the specific functions of individual Cag ATPases have not yet been investigated in detail.

Animal models for study of *H. pylori*

Several *in vivo* models have been utilized to study *H. pylori*-induced gastric pathology, ranging from rodents (mice, Mongolian gerbils) to larger animals (beagle dogs, rhesus monkeys and gnotobiotic pigs).

The mouse model has been one of the popular choices of *in vivo* models due to its availability, economic cost, and the availability of many genetically manipulated strains. Mice have been used extensively to study gastritis caused by *H. pylori* infection (57). However, there are some limitations. The fact that wild-type mice do not usually develop gastric cancer (57) makes it difficult to study gastric carcinogenesis using this model. Furthermore, the genes in the *cag* PAI commonly undergo inactivating mutations during long-term infections of mice with *H. pylori* (58). Thus, it is difficult to investigate the Cag T4SS using the mouse model.

One of the most popular and commonly used *in vivo* models is the Mongolian gerbil. Mongolian gerbils can develop *H. pylori*-induced gastric pathologies, ranging from superficial gastritis to intestinal-type metaplasia and gastric cancer (57). Several studies have used Mongolian gerbils to demonstrate that environmental factors influence the disease outcomes of *H. pylori* infection. High-salt and/or low-iron diets accelerate the development of gastric disease (59, 60), consistent with human epidemiologic studies, and influence the severity of iron deficiency anemia in gerbils (61). Furthermore, Mongolian gerbils have been used to study the roles of specific *H. pylori* virulence factors in gastric pathogenesis. Multiple studies of *H. pylori cag* PAI mutant strains have reported that the Cag T4SS contributes to gastric cancer pathogenesis in the Mongolian gerbil model (37, 62-66).

Previous multiple studies have examined the role of the Cag T4SS in pathogenesis in Mongolian gerbil models using simple knock-out mutant strains. However, comparisons of wild-type and mutant strains provide limited insight into the temporal features of processes by which gastric disease develops.

Gaps in knowledge

There are several gaps in our understanding of the Cag T4SS that this dissertation addresses. First, there are gaps in our understanding of the molecular mechanisms by which the Cag T4SS translocates substrates across the bacterial inner and outer membranes and into host cells. Second, there are gaps in our understanding of temporal features of the process by which the Cag T4SS activity contributes to gastric carcinogenesis. Finally, there are gaps in our understanding of Cag T4SS-dependent alterations in gastric tissue. Therefore, my first goal was to investigate the functional roles of three proteins in the *H. pylori* Cag T4SS that have predicted ATPase activity. My second goal was to understand the contribution of Cag T4SS activity to carcinogenesis during specific stages of *H. pylori* infection. My third goal was to detect T4SS-dependent molecular alterations in gastric tissue.

Chapter II

ATPases associated with the *Helicobacter pylori* Cag type IV secretion system

A modified version was previously published as:

Lin AS, Dooyema SDR, Frick-Cheng AE, Harvey ML, Suarez G, Loh JT, McDonald WH, McClain MS, Peek Jr. RM, Cover TL. Bacterial energetic requirements for *Helicobacter pylori* cag type IV secretion system-dependent alterations in gastric epithelial cells. Infect Immun. Jan 2020. 88:e00790-19.

Hu B, Khara P, Song L, **Lin AS**, Frick-Cheng AE, Harvey ML, Cover TL, Christie PJ. In situ molecular architecture of the *Helicobacter pylori* cag type IV secretion system. mBio. May 2019. 10:e00849-19.

Introduction

The Cag T4SS is responsible for translocating the effector protein CagA into host cells (18, 19). The cellular alterations caused by CagA contribute to neoplastic transformation. Thus, CagA is termed a “bacterial oncoprotein” (18, 19, 24).

In additional to its role in CagA translocation, the Cag T4SS is required for entry of non-protein bacterial constituents into host cells. Specifically, there is evidence that Cag T4SS activity is required for entry of lipopolysaccharide metabolites (36-39), peptidoglycan (40) and DNA into host cells. Upon entry into host cells, lipopolysaccharide metabolites and peptidoglycan stimulate NF-κB activation and IL-8 induction and bacterial DNA is recognized by TLR9 in the host cells (41, 42). Several publications reported that CagA can contribute to IL-8 induction and NF-κB activation (43-46). Conversely, these two cellular responses are elicited by mutant strains that do not produce CagA (47-49), indicating that *H. pylori* can stimulate these responses through CagA-independent pathways.

H. pylori CagA, lipopolysaccharide metabolites, peptidoglycan and DNA all enter host cells through Cag T4SS-dependent processes, but we speculate that these bacterial components are

recruited and delivered into host cells through disparate mechanisms. In support of this view, a previous study showed that translocation of CagA into gastric epithelial cells requires several *cag* PAI-encoded proteins that are not required for *H. pylori*-induced IL-8 induction (35). One of such protein is Cagβ (a VirD4 homolog) (35, 67). In *E. coli* conjugation systems and the *A. tumefaciens* VirB/VirD4 system, VirD4 acts as a coupling protein that recruits DNA and relaxosome from the cytoplasm to the T4SS (30, 68, 69). The role of Cagβ in TLR9 activation (a phenotype attributed to entry of bacterial DNA into host cells) has not yet been determined. Since VirD4 acts as a coupling protein required for recruitment and translocation of DNA in prototypical VirB/VirD4 system (30, 31, 70), we hypothesized that Cagβ might be essential for recruitment and delivery of *H. pylori* DNA into host cells.

In the current study, we sought to further investigate the bacterial energetic requirements for T4SS-dependent, *H. pylori*-induced alterations in host cells. We generated unmarked *cagα*, *cagβ*, and *cagE* deletion mutants, along with the corresponding mutants containing restored intact genes, as well as mutant strains containing substitution mutations in putative ATP-binding motifs (Walker-A and Walker-B boxes) of these ATPases. We then tested these mutants in cell culture assays to assess CagA translocation and CagA-independent cellular alterations (stimulation of IL-8 production, NF-B activation, and TLR9 activation). In addition, we collaborated with the laboratories of Dr. Peter Christie and Dr. Bo Hu at McGovern Medical School, Houston, to analyze these mutant strains by cryo-electron tomography (cryo-ET).

Materials and methods

Growth of *H. pylori* strains

H. pylori 26695 and isogenic mutant strains were grown on Trypticase soy agar plates supplemented with 5% sheep blood at 37°C in room air containing 5% CO_2. Antibiotic concentrations for the selection of *H. pylori* mutant strains were as follows: chloramphenicol

(5 μg/ml), kanamycin (10 μg/ml), metronidazole (7.5 to 15 μg/ml), or streptomycin (25 or 50 μg/ml). The *E. coli* strain DH5α was used for plasmid propagation and was grown on Luria-Bertani agar plates or in Luria-Bertani liquid medium supplemented with appropriate antibiotics (ampicillin [50 μg/ml], kanamycin [25 μg/ml], or chloramphenicol [25 μg/ml]).

Generation of *H. pylori* mutant strains

Unmarked deletion mutant strains (Δ*cagα*, Δ*cagβ*, and Δ*cagE*) were generated as described previously. To generate ATP-binding motif mutant strains, we introduced point mutations into sites encoding amino acids in Walker-A and Walker-B motifs (specifically, K184A and E248A in *cagα*; K244A and D550A in *cagβ*; and K603A and D830A in *cagE*) (**Table 2.1**). The three *cag* ATPase genes, including the point mutations described above, along with 0.5-kb flanking DNA, were synthesized (GenScript) and cloned into a pUC57 vector. ATP-binding motif mutant strains were generated by introducing plasmids (containing both Walker box mutations) into *H. pylori* strains containing either a *cat-rdxA* cassette or a *cat-rpsL* cassette in the genes of interest (Table 1). In parallel, we used site-directed mutagenesis to change the point mutations in plasmids back to wild-type nucleotides. Plasmids containing the corrected point mutations were transformed into strains containing *cat-rdxA* or *cat-rpsL* cassettes inserted in the genes of interest, resulting in control strains containing wild-type-like ATPase gene sequences (Table 1). PCR and sequencing of PCR products were used to confirm that the desired sequences were introduced into the appropriate *cag* ATPase genes.

Cryo-electron tomography (cryo-ET) analysis

In preparation for cryo-ET analysis, *H. pylori* strains were grown 48 h on Trypticase soy agar plates supplemented with 5% sheep blood in room air supplemented with 5% CO_2. Bacteria were removed from the plates and suspended in phosphate-buffered saline (PBS) and were then mixed with 10-nm diameter colloidal gold particles and deposited onto freshly glow-

discharged, holey carbon grids for 1 min. The grids were blotted with filter paper and rapidly frozen in liquid ethane, using a gravity-driven plunger apparatus. The frozen-hydrated specimens were imaged at -170°C using a Polara G2 electron microscope (FEI company) equipped with a field emission gun and a direct detection device (Gatan K2 Summit). Further details about the cryo-ET analysis are available in a recent publication manuscript (54).

Proteomic analysis of *H. pylori* membrane fractions

H. pylori were cultured in *Brucella* broth containing 10% fetal bovine serum for 24 h at 37°C in room air containing 5% CO_2. The bacteria were harvested by centrifugation and then were washed in buffer (50 mM Tris, 100 mM NaCl, 27 mM KCl, 1 mM $CaCl_2$, 0.5 mM $MgCl_2$ [pH 7.4]) and centrifuged at 4,500 × *g* for 10 min. After two additional washing steps, the pelleted bacteria were resuspended in lysis buffer (50 mM Tris, 1 mM $MgCl_2$, protease inhibitor [cOmplete protease inhibitor cocktail tablets, Roche] [pH 7.4]) and then sonicated on ice. The lysate was centrifuged at 4,500 × *g* for 10 min to remove any remaining intact bacteria, and the resulting supernatant was centrifuged at 10,000 × *g* for 1 h at 4°C. The pellet (membrane fraction) was then resuspended in RIPA buffer (50 mM Tris-HCl, 150 mM NaCl, 1 mM EDTA, 1% NP40, 0.25% sodium deoxycholate, protease inhibitor [pH 8.0]). The membrane fraction was solubilized by rotating the sample for 1 h at 4°C. The solubilized membrane fraction was then collected after centrifugation at 21,000 × *g* for 10 min at 4°C. The membrane fraction was then subjected to proteomic analysis.

Samples prepared as described above were run 2 cm into a 10% Bis-Tris NuPAGE gel. Gels were stained with Coomassie blue, and an in-gel trypsin digest was performed. Single-dimensional liquid chromatography-tandem mass spectrometry (LC-MS/MS) was performed using Thermo Fisher QExactive Plus equipped with a nano-electrospray source and attached to an LC3000 (Thermo Fisher) high-pressure liquid chromatography (HPLC) unit with an autosampler. Peptides were resolved via reversed-phase separation (90 min total cycle time).

Full MS (MS1) were collected at 70,000 resolution with an automatic gain control (AGC) target of 3e6, and MS/MS were collected at 17,500 resolution with an AGC target of 1e5, excluding unassigned charge states and requiring an intensity threshold of 2e4. Fifteen MS/MS were collected for each MS1 with a dynamic exclusion window of 10 s. Peptides were resolved via reversed-phase separation (90-min total cycle time). Peptide MS/MS spectra were acquired data dependently with 2 full-scan MS followed by 5 MS/MS scans. The peptide MS/MS spectral data were queried using SEQUEST (full tryptic specificity) and searched against the *H. pylori* 26695 protein database, to which both common contaminants and reversed versions of *H. pylori* protein sequences had been added. Peptide identifications were filtered and collated to proteins using Scaffold 4 (Proteome Systems). Protein identifications required a minimum of 2 unique peptides per protein and were filtered to a 5% false discovery rate (both peptide and protein).

Isolation of the *H. pylori* Cag T4SS outer membrane core complex

The Cag T4SS outer membrane core complex was isolated from *H. pylori* strains producing HA-tagged forms of CagF (designated HA-CagF) using a previously described immunoprecipitation approach. We first transformed *Δcagα*, *Δcagβ*, or *cagE::kan* (kanamycin cassette inserted within the *cagE* gene) mutant strains with plasmids containing a gene encoding CagF with an HA-epitope tag at the N terminus and containing a chloramphenicol cassette. This approach introduced sequences encoding HA-tagged CagF into the *H. pylori ureAB* chromosomal locus. Outer membrane core complexes were isolated as previously described. Briefly, strains were grown in liquid cultures for 16 h, pelleted at 3,300 × *g* for 15 min at 4°C, resuspended in RIPA buffer (50 mM HEPES, 100 mM NaCl, 1% NP-40, and 0.25% deoxycholate supplemented with 1 mM phenylmethylsulfonyl fluoride and protease inhibitors [Roche]), sonicated on ice, and then incubated for 1 h at 4°C; bacterial lysates were collected and then incubated with anti-HA antibodies noncovalently linked to protein G Dynabeads for 30 min; HA peptide was utilized to

selectively elute the proteins. Samples were analyzed by negative-stain EM, as described previously.

CagA translocation assay

Translocation of oncoprotein CagA into AGS human gastric epithelial cells was assessed using previously described methodology (71-76). Briefly, we cocultured *H. pylori* strains with AGS cells at a multiplicity of infection (MOI) of 100:1 for 5 to 6 h at 37°C. CagA translocation was evaluated by detecting tyrosine phosphorylation of CagA, using an anti-phosphotyrosine antibody (α-PY99, Santa Cruz Biotechnology), and CagA was detected using anti-CagA antibody (Santa Cruz Biotechnology).

IL-8 induction assay

AGS cells were seeded at 2×10^5 cells per well in a 12-well culture dish overnight and then cocultured with *H. pylori* strains at an MOI of 100:1 for 5 to 6 h at 37°C with 5% CO_2. The supernatants were collected after being centrifuged at 15,000 × *g* for 5 min. IL-8 induction was quantified by using Human CXCL8 enzyme-linked immunosorbent assay (ELISA) (R&D systems), following the manufacturer's protocol.

NF-κB activation assay

NF-κB activity was quantified by coculturing an NF-κB luciferase reporter cell line (in an AGS gastric epithelial cell background) with *H. pylori* strains, as previously described. Briefly, the reporter cell line was seeded in a 96-well plate overnight and then infected with *H. pylori* strains at an MOI of 100:1 for 2.5 h. The luciferase activity of cell lysates was measured using a Steady-Glo luciferase assay substrate (Promega).

TLR9 activation assay

TLR9 activation by *H. pylori* strains was analyzed by coculturing the bacteria with TLR9 reporter cells for 24 h, using the approach described previously. Briefly, $TLR9^+$ (HEK-Blue-hTLR9) and parental (HEK-Blue-Null1) cells (InvivoGen) were seeded in 96-well plates and cocultured with *H. pylori* strains at an MOI of 100:1 at 37°C with 5% CO_2 for 24 h. The resulting supernatants were mixed with HEK-Blue detection media (InvivoGen), and the signals in the plates were measured by spectrophotometer at 650 nm.

Results

ATPases associated with the Cag T4SS

Three genes within the *cag* PAI are predicted to encode ATPases. Cagα (encoded by the gene HP0525 in *H. pylori* strain 26695) is a VirB11 homolog, Cagβ (HP0524) is a VirD4 homolog, and CagE (HP0544) is a VirB4 homolog. The sequence relatedness of these *H. pylori* proteins to homologs in T4SSs of other bacterial species is relatively low. For example, in comparisons of *H. pylori* sequences with the homologous *Agrobacterium* VirB/VirD4 sequences, Cagα exhibits about 21% amino acid identity with VirB11 (GenBank accession no. P0A3F9), CagE exhibits about 17% identity with VirB4 (GenBank accession no. P17794), and Cagβ exhibits about 13% identity with VirD4 (GenBank accession no. P18594). To facilitate analysis of the Cag T4SS ATPases, we generated *H. pylori* mutant strains in which genes encoding each of the ATPases were individually disrupted or deleted, as described in Materials and Methods.

Cag ATPases are not required for outer membrane core complex assembly

To evaluate whether the ATPases are required for T4SS core complex assembly, I collaborated with a former graduate student, Arwen Frick-Cheng, and conducted experiments to isolate core complexes from the ATPase mutants. We introduced a gene encoding HA-CagF into the *ureAB* chromosomal locus of strains harboring mutations in Cag ATPase-encoding genes. The resulting strains were designated FC1.1 (Δ*cagα*/HA-CagF), FC2.1 (Δ*cagβ*/HA-CagF), and

FC3.1 (*cagE*::Kan/HA-CagF) (**Table 2.1**). We then immunopurified HA-CagF from these strains, which allows copurification of core complexes. Negative-stain electron microscopy (EM) analysis revealed successful isolation of core complexes from each of the mutant strains (**Fig 2.1**). The structures of the core complexes isolated from the mutant strains appeared similar to structures of the core complex isolated from the corresponding strain containing a wild-type *cag* PAI (WT/HA-CagF) (**Fig 2.1**). These results indicate that the individual Cag ATPases are not required for formation of Cag T4SS outer membrane core complexes.

As another approach for investigating if Cag T4SS ATPases are required for core complex assembly, I collaborated with the labs of Drs Peter Christie and Bo Hu (McGovern Medical School, Houston) and visualized the molecular architecture of the Cag T4SS *in situ* via cryo-ET in wild-type (**Fig 2.2 A, B**). We observed outer membrane complexes in each of the Cag ATPase mutant strains, similar to the complexes observed in wild-type strains (**Fig 2.2 C-F**). These results indicate that individual Cag ATPases are not required for assembly of Cag T4SS outer membrane core complexes.

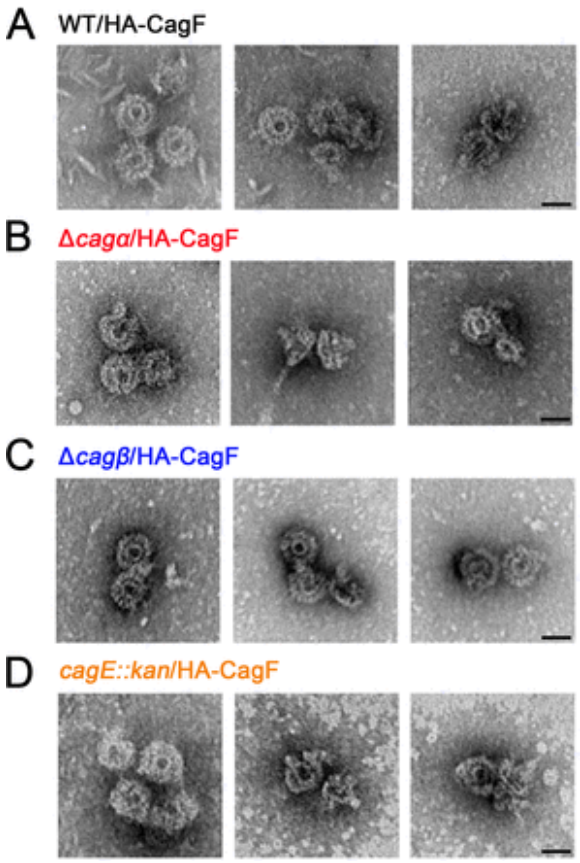

Figure 2.1: Individual Cag ATPases are not required for formation of the Cag T4SS core complex. *H. pylori* mutant strains lacking genes encoding individual ATPases (Δ*cagα*, Δ*cagβ*, and Δ*cagE*) were modified by introducing a gene encoding HA-CagF into the *ureAB* chromosomal locus, resulting in strains with the genotypes indicated in the figure (corresponding to FC1.1 [Δ*cagα*/HA-CagF], FC2.1 [Δ*cagβ*/HA-CagF], and FC3.1 [*cagE*::kan/HA-CagF] in **Table 2.1**). T4SS core complexes were immunopurified from these strains, and the preparations were analyzed and visualized by negative-stain electron microscopy (magnification, ×28,000). (A) Core complexes purified from a wild-type (WT) strain engineered to produce HA-CagF (WT/HA-CagF) (positive control). (B to D) Core complexes isolated from mutant strains engineered to produce HA-CagF (Δ*cagα*/HA-CagF, Δ*cagβ*/HA-CagF, and *cagE*::kan/HA-CagF). Scale bars, 25 nm.

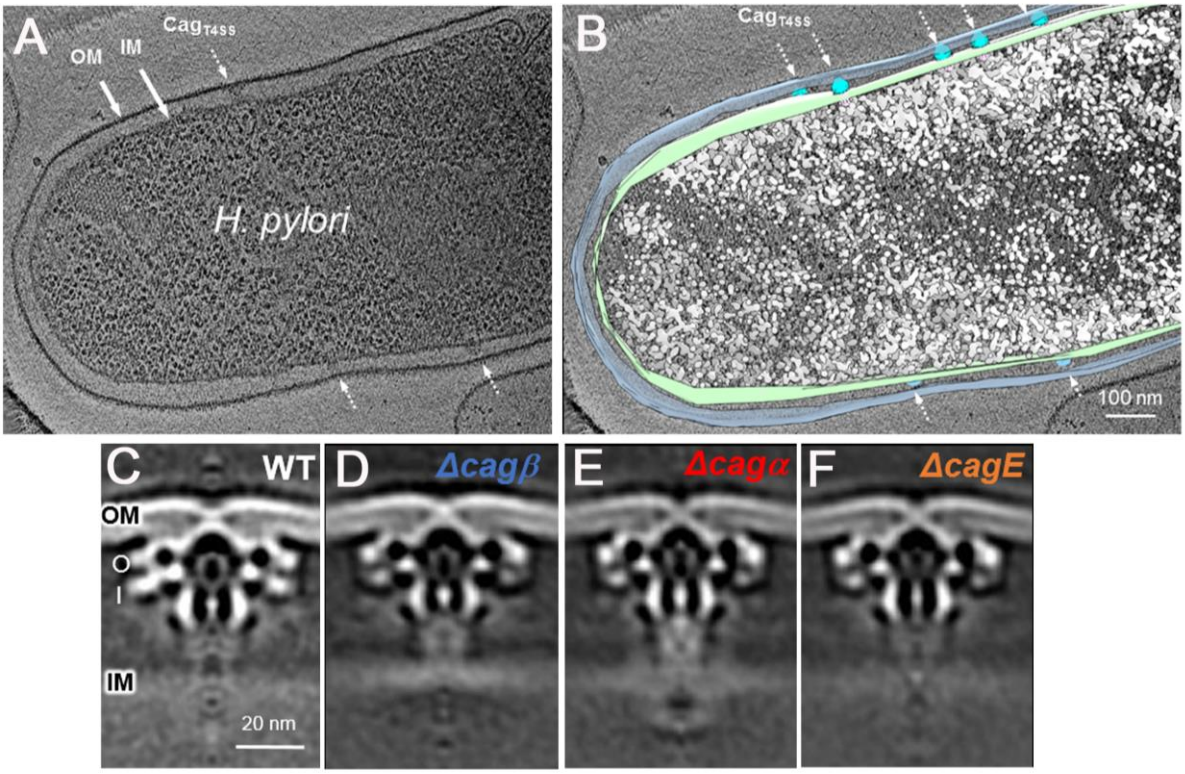

Figure 2.2: Cryo-ET analyses reveal that individual Cag ATPases are not required for the assembly of outer membrane core complex. (A, B) Slice of a tomographic reconstruction of a typical *H. pylori* cell (A) and its surface rendering (B), showing multiple Cag T4SSs (arrows) embedded in the cell envelope. (C to F) Core complex assembly visualized in wild-type and Cag ATPase mutant strains. OM, outer membrane; IM, inner membrane; O, outer-layer and I, inner-layer.

Visualization of the inner membrane complex via cryo-ET

As part of the same collaborative project, we visualized the inner membrane complex by locally defining the cytoplasmic regions from 1,280 Cag T4SS particle reconstructions (**Fig 2.3**). In side view, the complex is composed a central Chi (X) structure and two sets of vertical tiers on the side that extends into the cytoplasm (**Fig 2.3 B, C**). In end-on view, the complex presents as three concentric hexameric rings with 6 fold symmetry (**Fig 2.3 D**). 3D surface renderings clearly show the distinct 3-ring structure of the complex in side, central cut, and bottom views (**Fig 2.3 E-G**).

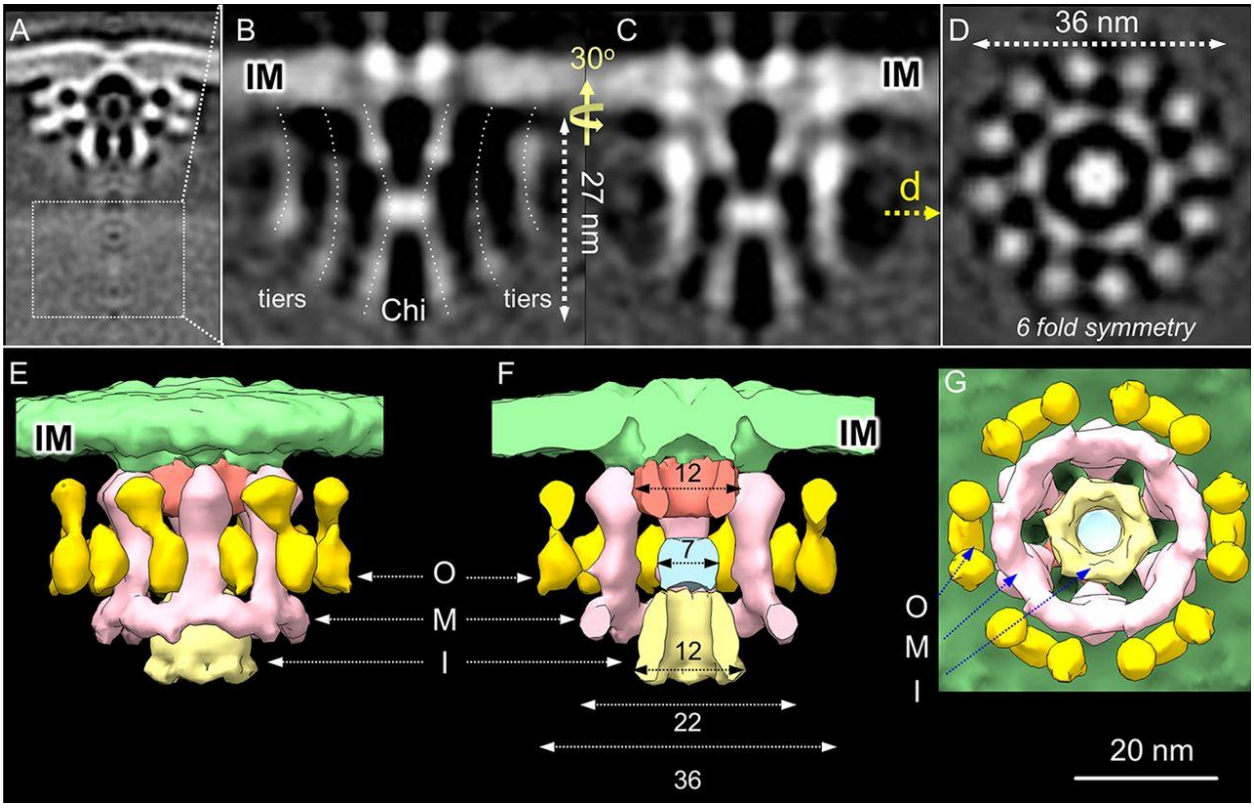

Figure 2.3: The inner membrane complex of the Cag T4SS. (A) A local refinement of the cytoplasmic portion of the Cag T4SS (boxed) revealed a detailed structure of the inner membrane complex. (B) Central section of the subtomogram average structure of the inner membrane complex. (C) The central section shown in panel B presented in a different view as indicated by the vertical and curved arrows shown between panel B and C. (D) Cross section of the inner membrane complex at the position indicated in panel C, revealing the 3-ring architecture and 6-fold symmetry. (E to G) 3D surface renderings of the inner membrane complex presented in side (E), central cut (F), and bottom (G) views. O, outer ring; M, middle ring; I, inner ring. Numbers correspond to the diameters (in nanometers) of respective regions showed in panel F.

Localization of the individual Cag ATPases in the inner membrane complex

First, we investigated the structure of the Δcagβ mutant by subtomogram averaging of 2,278 particles from 666 tomograms. Interestingly, several densities are missing in the inner membrane complex of the mutant strain compared to that of wild-type strain. The missing densities include the basal arms of the Chi structure, the basal halves of the first set of flanking tiers, and the entire second set of flanking tiers (**Fig 2.4 B, compared to Fig 2.4 A**). Thus, the data indicate that these missing densities are associated with the production of Cagβ in the inner membrane complex.

Second, we analyzed 1,135 particles from 419 tomograms of the Δcagα mutant strains. The analysis showed that the complex of Δcagα mutant strains are missing not only the densities accompanying deletion of Cagβ but also the central disc corresponding to the axis of the Chi structure in the wild-type complex (**Fig 2.4 C, compared to Fig 2.4 A**).

Last, we visualized the inner membrane complex of the ΔcagE mutant strains by subtomogram averaging of 465 particles from 242 tomograms. Strikingly, the ΔcagE mutant strains lack the entire inner membrane complex (**Fig 2.4 D, compared to Fig 2.4 A**). These data suggest that CagE contributes to the V-shaped densities and that CagE is important for assembly of the inner membrane complex.

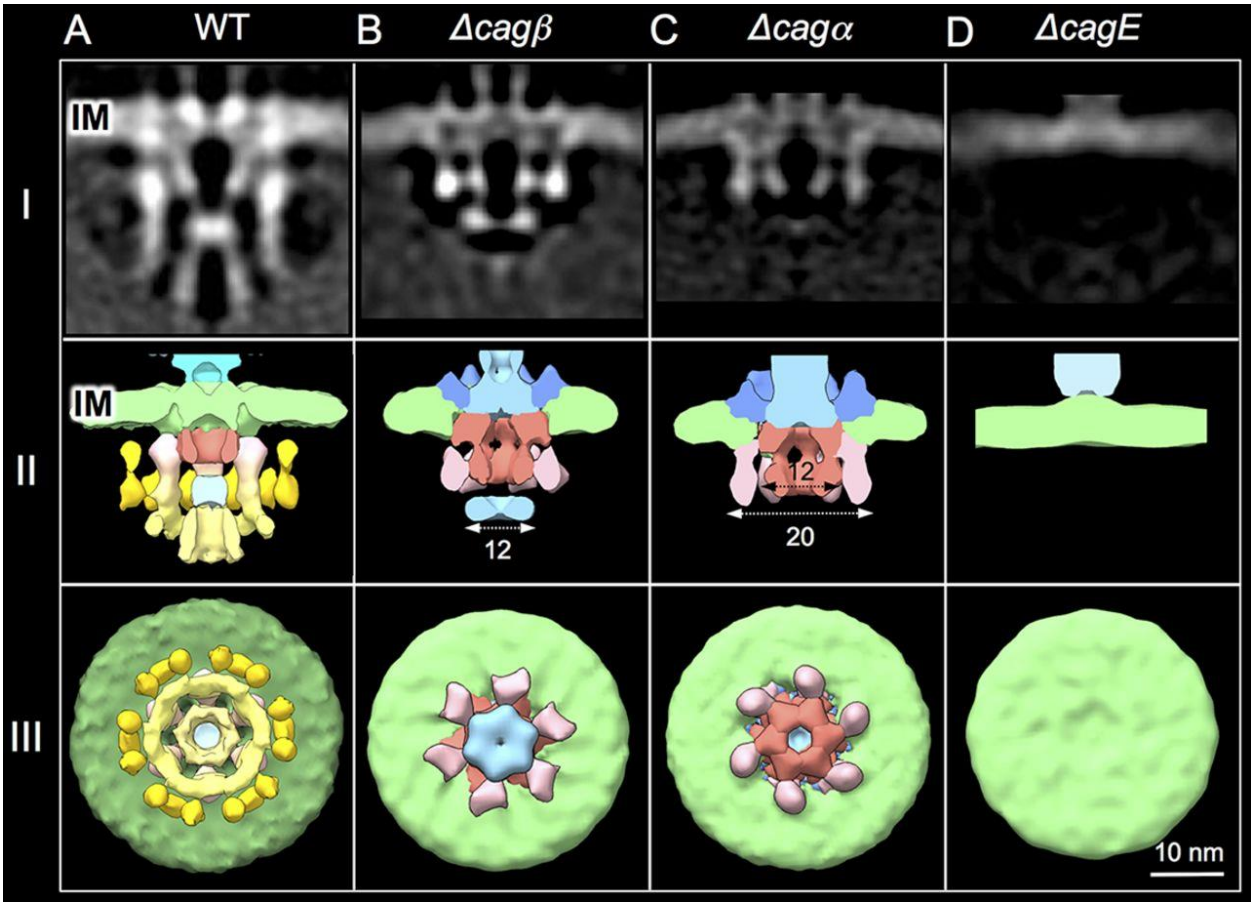

Figure 2.4: Localization of the individual Cag ATPases in the inner membrane complex. Columns A to D present structures of the inner membrane complexes from wild-type (WT) and Δcagβ, Δcagα, and ΔcagE mutant strains. (Row I) Central slices of the averaged inner membrane complex structures. (Row II) 3D surface renderings, cutaway side views. Numbers correspond to diameters (in nanometers) of the regions shown. (Row III) 3D surface renderings, bottom views.

Individual Cag ATPases are required for CagA translocation

To assess if the individual Cag ATPases are required for CagA translocation into host cells, we cocultured *H. pylori* strains with AGS gastric epithelial cells and analyzed phosphorylation of CagA. For these experiments, we analyzed unmarked ATPase deletion mutant strains (*Δcag*α, *Δcag*β, and *Δcag*E) along with genetically manipulated control strains containing restored wild-type *cag*α, *cag*β, and *cag*E sequences (named ASL12.1 [restored WT *cagα*], ASL14.1 [restored WT *cagβ*], and ASL16.1 [restored WT *cagE*]), generated as described in Materials and Methods (**Table 2.1**). Tyrosine-phosphorylated CagA was detected when the wild-type strain and control strains were cocultured with AGS cells but was not detected when any of the individual ATPase mutants were cocultured with AGS cells (**Fig 2.5**). These results indicate that all three ATPases are required for CagA translocation into AGS cells.

Table 2.1: *H. pylori* strains used in this study

***H. pylori* strains or plasmid**	**Description**	**Antibiotic resistance**	**Reference**
Strains[a]			
26695	Wild-type, intact *cag* PAI	None	(72)
ΔrdxA	Deletion of *rdxA*	Metronidazole	(75, 77)
rpsL-K43R	Codon 43 of *rpsL* harbors a lysine-to-arginine mutation	Streptomycin	(73, 78, 79)
Δ*cag* PAI	Deletion of *cag* PAI	Chloramphenicol	(72)
Δ*cagα*	Unmarked deletion of *cagα*	Metronidazole	(54)
ASL11.1 (*cagα* WB mutant)[b]	Introduced two point mutations in ATP-binding motifs of *cagα* (K184A, E248A)	Metronidazole	This study
ASL12.1 (restored WT *cagα)*	Restored two point mutations in *cagα*	Metronidazole	This study
Δ*cagβ*	Unmarked deletion of *cagβ*	Metronidazole	(54)
ASL13.1 (*cagβ* WB mutant)	Introduced two point mutations in ATP-binding motifs of *cagβ* (K244A, D550A)	Streptomycin	This study
ASL14.1 (restored WT *cagβ)*	Restored two point mutations in *cagβ*	Streptomycin	This study
Δ*cagE*	Unmarked deletion of *cagE*	Metronidazole	(54)
ASL15.1 (*cagE* WB mutant)	Introduced two point mutations in ATP-binding motifs of *cagE* (K603A, D830A)	Streptomycin	This study
ASL16.1 (restored WT *cagE*)	Restored two point mutations in *cagE*	Streptomycin	This study
WT/HA-CagF	Introduced HA-cagF into *ureAB* locus	Chloramphenicol	(50)
FC1.1 (Δ*cagα*/HA-CagF)	Introduced HA-cagF into *ureAB* locus	Metronidazole, chloramphenicol	This study
FC2.1 (Δ*cagβ*/HA-CagF)	Introduced HA-cagF into *ureAB* locus	Metronidazole, chloramphenicol	This study
FC3.1 (*cagE*::*kan*/HA-CagF)	Introduced HA-cagF into *ureAB* locus	kanamycin, chloramphenicol	This study
Plasmids			
pΔ*cagα*	Contain sequences from HP0524 and HP0526, and deletion of HP0525 (*cagα*)	Ampicillin	(54)

p∆*cagα::cat-rdxA*	*cat-rdxA* cassette cloned into BamHI site in HP0525 locus of p*∆cagα*	Ampicillin, chloramphenicol	(54)
pASL101.1	Contain sequences from HP0524 to HP0526 in which two point mutations in ATP-binding motifs are introduced (K184A, E248A)	Ampicillin	This study
pASL102.1	Restore the introduced point mutations in pΔcagα	Ampicillin	This study
p∆*cagβ*	Contain sequences from HP0523 and HP0525, and deletion of HP0524 (*cagβ*)	Ampicillin	(54)
p∆*cagβ::cat-rdxA*	*cat-rdxA* cassette cloned into BamHI site in HP0524 locus of p*∆cagβ*	Ampicillin, chloramphenicol	(54)
pASL103.1	*cat-rpsL* cassette cloned into ClaI site in HP0524 locus of p*∆cagβ*	Ampicillin, chloramphenicol	This study
pASL104.1	Contain sequences from HP0523 to HP0525 in which two point mutations in ATP-binding motifs are introduced (K244A, D550A)	Ampicillin	This study
pASL105.1	Restored the introduced point mutations in p∆*cagβ*	Ampicillin	This study
p∆*cagE*	Contain sequences from HP0543 and HP0545, and deletion of HP0544 (*cagE*)	Ampicillin	(54)
p∆*cagE::cat-rdxA*	*cat-rdxA* cassette cloned into BamHI site in HP0544 locus of p∆*cagE*	Ampicillin, chloramphenicol	(54)
pASL106.1	*cat-rpsL* cassette cloned into BamHI site in HP0544 locus of p∆*cagE*	Ampicillin, chloramphenicol	This study
pASL107.1	Contain sequences from HP0543 to HP0545 in which two point mutations in ATP-binding motifs are introduced (K603A, D830A)	Ampicillin	This study
pASL108.1	Restored the introduced point mutations in p*∆cagE*	Ampicillin	This study
pADN	Introduce HA tag on N-terminus of CagF on *ureAB* locus	Ampicillin, chloramphenicol	(50)

[a] All mutant strains were derived from *H. pylori* 26695.
[b] WB, Walker box.

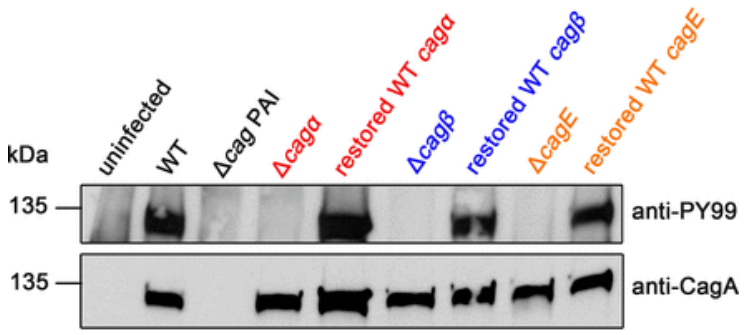

Figure 2.5: Individual Cag T4SS ATPases are essential for CagA translocation into AGS gastric epithelial cells. Wild-type (WT) strain 26695, a Δ*cag* PAI mutant strain, and the indicated unmarked deletion mutant strains (Δ*cagα*, Δ*cagβ*, and Δ*cagE*) were cocultured with AGS cells. Genetically manipulated strains containing restored wild-type ATPase sequences (named ASL12.1 [restored WT *cagα*], ASL14.1 [restored WT *cagβ*], and ASL16.1 [restored WT *cagE*]; **Table 2.1**) were tested as controls. Extracts from *H. pylori*-gastric epithelial cell cocultures were immunoblotted with an anti-CagA antibody to detect CagA and an anti-phosphotyrosine antibody (anti-PY99) to detect phosphorylated CagA.

Cagβ is dispensable for *H. pylori*-induced NF-κB activation and IL-8 production

When cocultured with gastric epithelial cells, *H. pylori* strains containing an intact *cag* PAI stimulate activation of NF-κB and production of proinflammatory cytokines such as interleukin-8 (IL-8). Multiple genes encoding components of the Cag T4SS are required for these phenotypes. To investigate whether the individual ATPases are required for these phenotypes, we cocultured the wild-type and mutant *H. pylori* strains with AGS cells or AGS-NF-κB reporter cells and quantified IL-8 induction and NF-κB activation as described in Materials and Methods. The *Δcag*α and *Δcag*E mutants were defective in both IL-8 induction and NF-κB activation, whereas the *Δcag*β mutant stimulated IL-8 induction and NF-κB activation similar to the wild-type strain (**Fig 2.6 A, B**). The IL-8 induction and NF-κB phenotypes were intact in each of the control strains containing wild-type ATPase sequences (**Fig 2.6 A, B**). These data indicate that Cagα and CagE are each required for IL-8 secretion and NF-κB activation in gastric epithelial cells, but Cagβ is not required.

Cagα and CagE are required for *H. pylori*-induced TLR9 activation

When cocultured with HEK293-hTLR9 reporter cells, *H. pylori* strains containing an intact *cag* PAI activate TLR9 through a process that requires multiple genes encoding components of the Cag T4SS. To determine if the individual ATPases are required for TLR9 activation, we cocultured the wild-type strain, mutant strains, and genetically manipulated control strains with the HEK293-hTLR9 reporter cells. The *Δcag*α and *Δcag*E mutants were defective in activating TLR9, whereas the *Δcag*β mutant retained the TLR9 activation phenotype (**Fig 2.6 C**). The genetically manipulated control strains containing restored wild-type ATPase sequences (ASL12.1, ASL14.1, and ASL16.1) exhibited an intact TLR9 activation phenotype (**Fig 2.6 C**). These data indicate that Cagα and CagE are required for *H. pylori*-induced TLR9 activation, but Cagβ is not required.

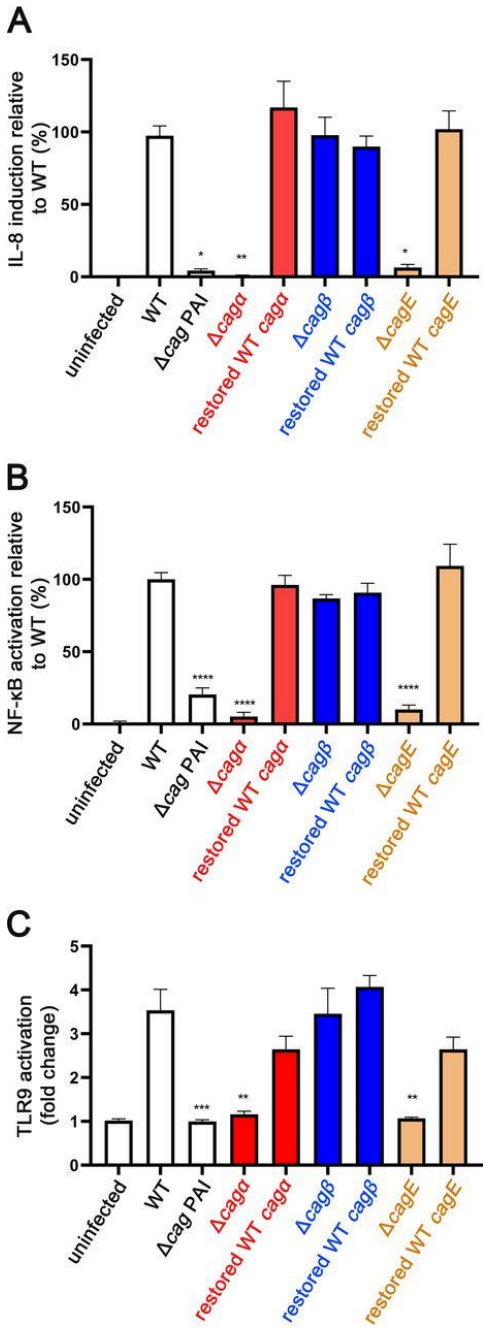

Figure 2.6: Cagα and CagE, but not Cagβ, are required for three Cag T4SS-dependent alterations in host cells. Wild-type (WT) strain 26695, a Δ*cag* PAI mutant strain, and the indicated unmarked deletion mutant strains (Δ*cagα*, Δ*cagβ*, and Δ*cagE*) were cocultured with AGS cells, AGS-NF-κB reporter cells, or HEK293-hTLR9 reporter cells. Genetically manipulated strains containing restored wild-type ATPase sequences (named ASL12.1, ASL14.1, and ASL16.1; **Table 2.1**) were tested as controls. IL-8 production, NF-κB activation, or TLR9 activation were quantified as described in Materials and Methods. (A, B) Cagα and CagE are required for IL-8 induction and NF-κB activation in AGS gastric epithelial cells. (C) Cagα and CagE are required for *H. pylori*-induced TLR9 activation in HEK293-hTLR9 reporter cells. The data represent results of three independent experiments with multiple technical replicates.

Values represent means ± standard error of the mean (SEM). Statistical significance among groups was determined by Kruskal-Wallis test with Dunnett's multiple comparison test.
*, $P \leq 0.05$; **, $P \leq 0.01$; ***, $P \leq 0.001$; ****, $P \leq 0.0001$ compared to WT.

Putative ATP-binding motifs in Cag ATPases

Previous cryo-electron tomography (cryo-ET) analyses revealed detectable differences in the structure of the Cag T4SS inner membrane complex in ATPase deletion mutants compared to the wild-type strain. Most notably, the inner membrane complex was almost completely absent in the ΔCagE mutant. This suggests that protein-protein interactions involving ATPases are important for assembly or stability of the Cag T4SS inner membrane complex. The ATPases (especially CagE) could potentially have important roles in assembly or stability of the T4SS inner membrane complex, independent of their enzymatic activity. Therefore, in addition to analyzing T4SS-dependent activities in ATPase deletion mutant strains, we undertook experiments to generate mutant strains containing substitution mutations in sites within the ATPases that are predicted to be required for enzymatic activity. By comparing the three *H. pylori* Cag ATPases to sequences of corresponding VirB11, VirB4, and VirD4 ATPases in T4SSs of other bacterial species, we identified putative ATP-binding motifs (Walker-A and Walker-B motifs) in Cagα, CagE, and Cagβ. We introduced point mutations into the corresponding regions of the 3 individual chromosomal ATPase genes encoding the Walker-A and Walker-B motifs. The point mutations resulted in a change from a conserved lysine to alanine in the Walker-A motifs and a change from a conserved aspartic acid or glutamic acid to alanine in the Walker-B motifs (**Table 2.1**). The resulting mutant strains were named ASL11.1 (*cagα* Walker box [WB] mutant), ASL13.1(*cagβ* WB mutant), and ASL15.1 (*cagE* WB mutant) (**Table 2.1**).

Proteomic analysis of membrane fractions allowed us to detect all three ATPase proteins in each of the mutant strains (**Table 2.2**). The proteomic data also allowed a semiquantitative assessment of ATPase abundance in the mutant strains compared to the WT strain. The number of CagE spectral counts detected in ASL15.1 was similar to the number of CagE spectral counts detected in the WT strain and other mutant strains (ASL11.1 and ASL13.1),

which suggests that the introduction of Walker box mutations into CagE did not substantially alter CagE stability. The number of Cagα spectral counts detected in ASL11.1 was lower than the number of Cagα spectral counts detected in the WT strain or other mutants, and similarly, the number of Cagβ spectral counts was somewhat lower in ASL13.1 than in the other strains. Therefore, the introduction of mutations into Cagα (and possibly Cagβ) might diminish the stability of these proteins. The phenotypes of the latter two mutants are potentially attributable to both reduced abundance of Cagα or Cagβ as well as loss of enzymatic activity.

Table 2.2: Mass spectrometric detection of Cag ATPases in wild-type and mutant strains

Protein	**Wild type**	**Δ *cag* PAI**	**Cagα WB mutant ASL11.1**	**Cagβ WB mutant ASL13.1**	**CagE WB mutant ASL15.1**
CagA[a]	265	0	309	263	327
Cagα	11	0	2	8	10
Cagβ	19	0	26	10	23
CagE	25	0	22	15	21
Fumarate reductase[a]	142	172	148	174	175
Acetyl-CoA synthetase[a]	67	71	71	54	67
Total spectral counts	17,477	18,500	21,735	17,865	21,139

[a] Number of spectral counts for CagA (encoded by the *cag* PAI), fumarate reductase, and acetyl-CoA synthetase (non-CagA proteins) are shown as controls for comparison.

Functional ATP-binding motifs in the Cag ATPases are required for CagA translocation

We then tested the capacity of the three Walker box mutant strains to translocate CagA into AGS gastric epithelial cells. None of the ATP-binding motif mutant strains (ASL11.1, ASL13.1, and ASL15.1) was able to translocate CagA into AGS cells (**Fig 2.7**). Similar to the results shown in **Fig 2.5**, all the engineered control strains containing wild-type ATPase sequences (ASL12.1, ASL14.1, and ASL16.1) exhibited an intact CagA translocation phenotype (**Fig 2.7**). These data indicate that functional Walker motifs in each of the individual ATPases (Cagα, CagE, and Cagβ) are required for CagA translocation into host cells.

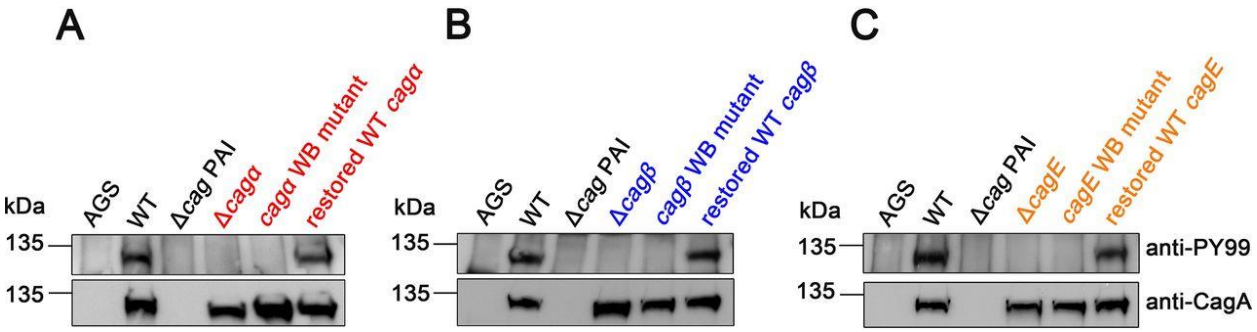

Figure 2.7: Functional Walker motifs in individual Cag T4SS ATPases are required for CagA translocation into AGS gastric epithelial cells. Strains containing mutations in Walker motifs of Cagα, Cagβ, or CagE (*cagα* WB, *cagβ* WB, and *cagE* WB mutants, corresponding to ASL11.1, ASL13.1, or ASL 15.1, respectively, in **Table 2.1**) were generated as described in Materials and Methods. Wild-type (WT) strain 26695, a Δ*cag* PAI mutant strain, and the indicated mutant strains were cocultured with AGS cells. Genetically manipulated strains containing restored wild-type ATPase sequences (named ASL12.1, ASL14.1, and ASL16.1; **Table 2.1**) were tested as controls. Extracts from *H. pylori*-gastric epithelial cell cocultures were immunoblotted with an anti-CagA antibody to detect CagA and an anti-phosphotyrosine antibody (anti-PY99) to detect phosphorylated CagA.

Functional ATP-binding motifs in Cagα and CagE are required for NF-κB activation, IL-8 induction, and TLR9 activation

To test if functional Walker motifs in the ATPases are necessary for other Cag T4SS-dependent phenotypes, we analyzed IL-8 production, NF-κB activation, and TLR9 activation induced by the Walker box mutant strains (ASL11.1, ASL13.1, and ASL15.1). The *cagα* and *cagE* Walker box mutants were defective in inducing IL-8 and NF-κB, whereas the *cagβ* Walker box mutant stimulated IL-8 production and NF-κB activation similar to the WT strain (**Fig 2.8 A, B**). Similarly, the *cagα* and *cagE* Walker box mutants were defective in TLR9 activation compared to the WT strain (**Fig 2.8 C**). However, the *cagβ* Walker box mutant induced TLR9 activation similar to the wild-type strain (**Fig 2.8 C**). These data indicate that intact Walker box motifs in Cagα and CagE are required for all the phenotypes tested (NF-κB activation, IL-8 induction, and TLR9 activation), whereas intact Walker box motifs in Cagβ are not required for these phenotypes.

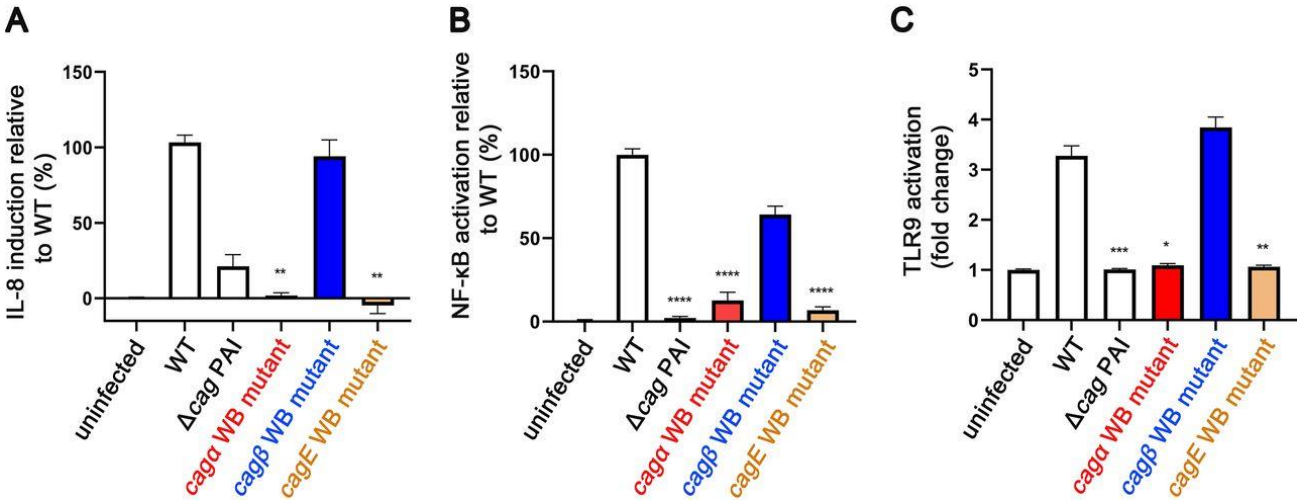

Figure 2.8: Functional Walker motifs in Cagα and CagE are required for three Cag T4SS-dependent phenotypes. Wild-type strain 26695, a Δ*cag* PAI mutant, and strains containing mutations in Walker motifs of Cagα, Cagβ, or CagE (ASL11.1, ASL13.1, or ASL 15.1; **Table 2.1**) were cocultured with AGS cells, AGS-NF-κB reporter cells, or HEK293-hTLR9 reporter cells. IL-8 production, NF-κB activation, or TLR9 activation were quantified as described in Materials and Methods. (A, B, and C) Functional Walker motifs in Cagα and CagE are essential for *H. pylori*-induced IL-8 induction, NF-κB activation, and TLR9 activation. The data represent results of three independent experiments with multiple technical replicates. Values represent mean ± standard error of the mean (SEM). Statistical significance among groups was determined by Kruskal-Wallis test with Dunnett's multiple comparison test. *, $P \leq 0.05$; **, $P \leq 0.01$; ***, $P \leq 0.001$; ****, $P \leq 0.0001$ compared to WT.

Discussion

H. pylori causes multiple alterations in gastric epithelial cells through processes dependent on the Cag T4SS (12, 13, 15, 80). Many Cag T4SS-dependent cellular alterations result from actions of CagA, whereas other Cag T4SS-dependent cellular alterations do not require CagA. For example, stimulation of IL-8 production by *H. pylori* has been attributed to the entry of lipopolysaccharide metabolites (HBP or ADP heptose) and/or peptidoglycan into host cells (36, 38-40, 81). HBP or ADP heptose activates alpha-kinase 1 (ALPK1) to phosphorylate tumor necrosis factor receptor-associated factor (TRAF)-interacting protein with forkhead-associated domain (TIFA) within host cells (36, 38, 81), and peptidoglycan is recognized by the intracellular host defense molecule NOD1 (40). Intracellular recognition of these pathogen-associated molecular patterns (PAMPs) leads to activation of multiple signaling pathways, including NOD1 signaling pathways and NOD-1 independent pathways that involve ALPK1 and TIFA, resulting in NF-κB activation (36, 38, 39, 81). Activation of TLR9 has been attributed to the entry of bacterial DNA into host cells (42). Since the Cag T4SS is required for phenotypes linked to the entry of multiple different types of *H. pylori* constituents into host cells, this provides an opportunity to undertake a comparative analysis of the processes by which different bacterial constituents are delivered into host cells.

To investigate the bacterial energetic requirements for CagA translocation and Cag T4SS-dependent cellular alterations in gastric epithelial cells, we generated mutant strains lacking individual ATPase components of the Cag T4SS. As a first step in analyzing the mutant strains, we investigated their capacity to assemble Cag T4SS core complexes. The *H. pylori* Cag T4SS core complex contains five proteins, all of which are required for T4SS function (50-52, 54). We successfully purified core complexes from each of the ATPase mutant strains, which indicates that these ATPases are not required for core complex assembly. This result is consistent with

the results of cryo-electron tomography studies of the *H. pylori* Cag T4SS (54) and the *Legionella* Dot/Icm T4SS (29).

To investigate the localization of the individual ATPases, we analyzed the architecture of the inner membrane complex in ATPase mutant strains along with wild-type strain and Δ cagPAI strain via cryo-ET analyses. The date suggests that CagE sits at the channel entrance of the inner membrane platform, followed by docking of Cagα right below CagE and finally, Cagβ and other unidentified Cag proteins assemble to form the inner membrane complex (54).

As a next step, we tested the ATPase mutant strains for the capacity to translocate CagA into host cells and found that all three ATPases are required for this activity. Previous studies used an insertional mutagenesis approach to disrupt Cag ATPases and reported that all three ATPases are required for the translocation of CagA protein into host cells (35). Analyses of unmarked deletion mutant strains (along with control strains) in the current study provide strong evidence that all three ATPases are required for CagA translocation, thereby indicating that the three ATPases are not functionally redundant.

We next tested the mutant strains for the capacity to stimulate IL-8 production. Consistent with the results of a previous study (35), we found that *H. pylori*-induced stimulation of IL-8 production requires CagE and Cagα but does not require Cagβ. The bacterial energetic requirements for *H. pylori*-induced NF-κB activation were identical to the requirements for IL-8 production, consistent with a current model in which NF-κB activation is required for IL-8 production (36, 48, 82-84).

A previous study reported that CagE was required for *H. pylori*-induced TLR9 activation (42), but the energetic requirements for this phenotype have not been previously studied in detail. We show that the energetic requirements for *H. pylori*-induced TLR9 activation are identical to requirements for IL-8 production and NF-κB activation (i.e., requiring CagE and Cagα but not

Cagβ). This finding differs from a requirement of the Cagβ homolog (VirD4) for delivery of DNA into recipient cells by *E. coli* conjugative T4SSs or the *A. tumefaciens* VirB/VirD4 T4SS (30, 31).

The observation that a Cagβ mutant is defective in CagA translocation but still capable of stimulating IL-8 production, NF-κB activation, and TLR9 activation provides important insights into the mechanisms by which these processes occur. Specifically, these results suggest that the *H. pylori* substrates mediating IL-8 induction, NF-κB activation, or TLR9 activation are recruited or delivered to host cells through one or more Cag T4SS-dependent pathways different from those used for recruitment and delivery of CagA. A current model proposes that CagA is recruited from the cytoplasm to the inner membrane complex of the T4SS through interactions with Cagβ, a VirD4 homolog (67). Similarly, in *E. coli* conjugative T4SSs and the *A. tumefaciens* T4SS, VirD4 acts as a coupling protein, responsible for recruiting DNA and protein substrates (30, 31). Since *H. pylori*-induced IL-8 secretion, NF-κB activation, and TLR9 activation do not require Cagβ, we speculate that lipopolysaccharide (LPS) metabolites, peptidoglycan, or DNA fragments might diffuse from the cytoplasm or periplasm into the T4SS apparatus through a nonspecific process that does not require recruitment by a coupling protein. Alternatively, we speculate that LPS metabolites, peptidoglycan, or DNA might transit the bacterial cell envelope through one or more mechanisms different from those used for secretion of CagA. For example, these nonprotein *H. pylori* constituents could potentially be released into the extracellular environment through bacterial autolysis, as components of outer membrane vesicles, or through other processes, and the Cag T4SS may then facilitate the entry of these PAMPs into host cells. Consistent with the latter hypothesis, treatment of *H. pylori*-host cell cocultures with DNase I partially reduced the level of TLR9 activation (42). In addition to the Cag T4SS, the *H. pylori* strain used in these studies harbors a second T4SS (ComB system), which is required for natural transformation and conjugative transfer of DNA (32). Cross talk among *H. pylori* T4SSs could potentially occur (for example, an ATPase from the ComB system

contributing to the function of the Cag T4SS), but there is no experimental evidence at present to support this possibility (42). In future studies, it will be important to determine whether *H. pylori* DNA, LPS metabolites, and peptidoglycan enter cells independently or if proteins analogous to the relaxosome utilized in conjugation systems and the *A. tumefaciens* VirB/VirD4 system are required.

ATPases (especially CagE) potentially have important roles in the assembly or stability of the T4SS inner membrane complex (54), independent of their enzymatic activity. If the ATPases contribute to T4SS activity through both enzymatic and nonenzymatic functions, it would not be possible to discriminate enzymatic and nonenzymatic functions through analysis of deletion mutant strains. In the current study, we generated *H. pylori* mutant strains harboring point mutations in sites predicted to be required for ATPase enzymatic activity and tested the hypothesis that these mutant strains might exhibit phenotypes different from those observed with deletion mutant strains. Previous studies have identified putative ATP-binding motifs in Cagα (55) and CagE (85), and mutagenesis of the Walker-A motif in the C-terminal portion of CagE abolished enzymatic activity of a recombinant protein produced in *E. coli* (85). Cag ATPase Walker box mutations have not previously been introduced into *H. pylori* chromosomal genes. In the current study, we found that each of the *H. pylori* mutant strains harboring point mutations in Walker boxes exhibited the same phenotypes as the deletion mutant strains. These data support a hypothesis that enzymatic activities of all three ATPases are required for CagA translocation.

In summary, this study indicates that the three Cag ATPases are components of the inner membrane complex and have nonredundant functions required for delivery of CagA into host cells and indicates that the energetic requirements for phenotypes associated with intracellular entry of nonprotein *H. pylori* constituents into host cells differ from the energetic requirements for translocation of CagA. In future studies, it will be important to further elucidate differences in

the mechanisms underlying the recruitment, secretion, and delivery of CagA into host cells compared to mechanisms underlying entry of nonprotein *H. pylori* constituents into host cells.

Chapter III

Temporal control of the *Helicobacter pylori* Cag type IV secretion system in a Mongolian gerbil model of gastric carcinogenesis

A modified version was previously published as:

Lin AS*, McClain MS*, Beckett AC, Caston RR, Harvey ML, Dixon BREA, Campbell AM, Sawhney N, Shuman JH, Loh JT, Piazuelo MB, Algood HM, Cover TL. Temporal control of the *Helicobacter pylori* Cag type IV secretion system in a Mongolian gerbil model of gastric carcinogenesis. mBio. Jun 2020. 11:e01296-20.

* co-first authors equally contributed to this work.

Introduction

Several lines of experimental evidence indicate that CagA contributes to gastric carcinogenesis. For example, experimental infection of Mongolian gerbils with a CagA-producing *H. pylori* strain containing an intact *cag* PAI can lead to the development of gastric cancer in infected animals, whereas infection with *cagA* mutant strains does not (59, 60, 86-88). Moreover, transgenic expression of CagA in mice results in tumor formation (24). In contrast to a wild-type strain containing an intact *cag* PAI, strains containing null mutations in several essential components of the Cag T4SS cause minimal gastric inflammation and do not cause gastric cancer in Mongolian gerbils (37, 62-66, 88). Thus far, studies of Cag T4SS and CagA in animal models have compared wild-type and mutant *H. pylori* strains but have not included testing of complemented mutant strains.

Although human epidemiologic studies and experiments with animal models indicate that *H. pylori* contributes to gastric carcinogenesis, it is not known if *H. pylori* has carcinogenic effects mainly during early stages of infection, during later stages of infection, or throughout infection. In the early stages of gastric colonization, *H. pylori* proliferates in the absence of a well-developed adaptive immune response, and during this time period, the bacteria might gain access to

gastric stem cell populations (89), causing mutations and other cellular alterations that initiate carcinogenesis (48, 90, 91). During later stages of infection, *H. pylori* resists clearance by immune defenses (92, 93) and provides a continual stimulus for gastric inflammation, which could contribute to neoplastic progression.

The hit-and-run model of carcinogenesis proposes that an infectious agent triggers carcinogenesis during initial stages of infection and that the ongoing presence of the infectious agent is not required for development of cancer (94-96). This model has been proposed for virus-induced cancers, including brain tumors (polyomavirus) (97-99), hepatocellular carcinoma (hepatitis viruses) (100), Schneiderian inverted papillomas (papillomaviruses) (101), and colorectal cancer (JC polyomaviruses) (102), and is potentially applicable to *H. pylori*-associated gastric cancer (18). Specifically, chronic *H. pylori* infection over a period of several decades can result in gastric histologic alterations (including intestinal metaplasia and atrophic gastritis) that render the stomach unsuitable for *H. pylori* colonization. Therefore, in some patients, *H. pylori* is no longer detected in the stomach at the time of gastric cancer diagnosis. It has been proposed that infection with CagA-positive *H. pylori* strains may act through a hit-and-run mechanism, whereby pro-oncogenic actions of CagA (translocated by the Cag T4SS) are followed by subsequent genetic or epigenetic alterations relevant to cancer pathogenesis (18). Thus far, there has been relatively little effort to experimentally test the hit-and-run model of carcinogenesis in the context of *H. pylori* infection, and there have not been studies to evaluate potential carcinogenic effects of CagA or Cag T4SS activity at specific time points during *H. pylori* infection.

Materials and methods

H. pylori culture methods

H. pylori strains used in this study are described in **Table 3.1**. *H. pylori* was maintained on Trypticase soy agar (TSA) plates containing 5% sheep blood incubated at 37°C in room air supplemented with 5% CO_2. Prior to infection of Mongolian gerbils, bacteria were inoculated into sulfite-free brucella broth supplemented with 10% fetal bovine serum (FBS) and grown to mid-log phase at 37°C in room air supplemented with 5% CO_2. For experiments to conditionally regulate Cag T4SS activity *in vitro*, *H. pylori* was cultured on TSA blood agar plates with or without anhydrotetracycline (ATc; Sigma-Aldrich) (100 ng/ml) for 24 to 48 h prior to assays (*cagU* gene expression, CagT production, and NF-κB activation) (103). *H. pylori* was grown in broth culture for 22 h in the presence of various concentrations of doxycycline prior to analysis of CagT production. Bacteria were also cultured with or without ATc prior to testing properties of gerbil output strains (NF-κB activation).

Generation of *H. pylori* strains in which Cag T4SS activity can be conditionally regulated

In a previous study, we reported methods for conditional expression of the *cagUT* operon and Cag T4SS activity in *H. pylori* 26695 based on use of the TetR/*tetO* system (103). In the current study, we introduced similar TetR/*tetO* elements into the gerbil-adapted *H. pylori* strain 7.13 (104). The resulting strains (VM202-203 [**Table 3.1**]) were then used for experimental infection of gerbils as described below.

Animal infection

Male Mongolian gerbils (less than 60 g weight) were purchased from Charles River Laboratories. Gerbils were fed AIN-93M rodent diets (Bio-Serv) containing a range of doxycycline hyclate concentrations (Sigma catalog no. D9891; 0 mg/kg to 175 mg/kg in chow), beginning 1 week prior to infection with *H. pylori*. After fasting overnight, gerbils were infected via oral gavage (day 0 and day 2) with 1×10^9 CFU of *H. pylori* VM202-203. To determine the optimal subantimicrobial concentration of doxycycline, the gerbils were fed diets containing different concentrations of doxycycline (range, 0 to 175 mg/kg doxycycline in chow). In

subsequent experiments, animals were fed a diet containing 25 mg/kg doxycycline or drug-free chow for specific time periods.

Processing of gastric tissue

At the end of the experiments, gerbil stomachs were excised and processed to retain glandular portions of the stomach (corpus and antrum), and the non-glandular portion of stomach (forestomach) was discarded. The glandular section of stomach was then cut open along the lesser curvature, and three longitudinal strips from each stomach were processed for *H. pylori* culture, analysis of gene expression, and histologic analysis as described below.

Bacterial colonization density

Longitudinal strips of stomach were homogenized with a tissue tearor (Biospec Products, Inc.) in sulfite-free brucella broth supplemented with 10% fetal bovine serum (FBS) until tissues were completely homogenized. *H. pylori* colonization density (CFU/gram of stomach tissue) was determined by plating serial dilutions of the tissue homogenates on TSA plates supplemented with 5% sheep blood, 50 µg/ml vancomycin, 100 µg/ml bacitracin, 10 µg/ml nalidixic acid, and 2 µg/ml amphotericin and culturing in microaerobic conditions (61). At least five single colonies of *H. pylori* output strains from each animal were pooled together and frozen for subsequent analyses.

Histology

Longitudinal strips of stomach tissue were fixed in 10% formalin overnight, embedded in paraffin, sectioned, and stained with hematoxylin and eosin. Histologic sections of gastric tissues were analyzed by a gastrointestinal pathologist in a blinded fashion. The tissue sections were evaluated for gastric inflammation (gastritis), presence of lymphoid follicles, gastric ulceration, dysplasia, and gastric adenocarcinoma in corpus and antrum (105). Histologic scoring data for gerbils experimentally infected with *H. pylori* are presented only for the gerbils

that were successfully colonized, based on culture and/or use of a modified Steiner stain. Histological scores (0, 1, 2, and 3 each representing absent, mild, moderate, and marked inflammation, respectively) were assigned to evaluate acute (neutrophils) and chronic (mononuclear leukocytes) inflammation in both the corpus and antrum, and these scores were added together to yield a cumulative score of 0 to 12 (59-61, 105, 106).

Analysis of *cagUT* expression

For analysis of gene expression in *H. pylori* cultured *in vitro,* strains were cultured for 16 hours in sulfite-free Brucella Broth supplemented with cholesterol. RNA was isolated using Trizol (Life Technologies) according to the manufacturer's protocol. Purified RNA (0.25 μg) was treated with Turbo DNA-free (Life Technologies). One half of each sample was used for first strand cDNA synthesis using Superscript III (Life Technologies) with random hexamer priming followed by RNase H treatment. The other half of each sample was treated in the same manner, except that reverse transcriptase was omitted. Quantitative real-time PCR (qRT-PCR) was performed using iQ SYBR Green Supermix (Bio-Rad) and oligonucleotide primers for *cagU* and control genes *lnt*, *lpxD*, and *prfA*. Control genes were chosen based on analysis of RNA-seq data, indicating stable expression of selected genes in response to *in vitro* stress (high salt conditions) and transcript abundance that was comparable (*lpxD* and *prfA*) to *cagU*, or approximately 0.1x as abundant (*lnt*) compared with *cagU*.

For analysis of gene expression from infected animal tissue, Trizol (Life Technologies) was added to stomach tissue along with 1 mm zirconium oxide (zirconia) beads (BioSpec Products). Samples were homogenized by vortexing for 5 minutes and then frozen at -70^{o}C. RNA was extracted from the homogenized samples using the manufacturer's instructions. Purified RNA (40 μg) was treated with Turbo DNA-free (Life Technologies). One half of each sample (approximately 20 μg) was used for first strand cDNA synthesis using Superscript III (Life

Technologies) with random hexamer priming followed by RNase H treatment. Duplicate samples (approximately 20 μg) were treated in the same manner, except that reverse transcriptase was omitted. Nucleic acids were then recovered in 60 μl water using AxyPrep Mag PCR Clean-up (Axygen). The recovered nucleic acids were then divided into 3 aliquots: 6 μl was used for qRT-PCR using gerbil GAPDH-specific primers (as one indicator of sample quality); 27 μl was used for 12 cycles of PCR using outer primers for nested PCR of *H. pylori lpxD*; and 27 μl was used for 12 cycles of PCR using outer primers for nested PCR of *H. pylori cagU*. The *H. pylori* outer PCR reaction products were purified using AxyPrep Mag PCR Clean-up (Axygen). The purified outer PCR products were then used for qRT-PCR of *lpxD* or *cagU* using inner primers, in triplicate. Quantitative RT-PCR was performed using iQ SYBR Green Supermix (Bio-Rad).

Western blot analysis

H. pylori strains were cultured with and without ATc or with various concentrations of doxycycline (0 to 40 ng/ml). *H. pylori* lysates were separated by sodium dodecyl sulfate-polyacrylamide gel electrophoresis (SDS-PAGE), and the proteins were transferred to a nitrocellulose membrane. Subsequently, the membrane was immunoblotted with a rabbit polyclonal anti-CagT antiserum and anti-Hsp60 antiserum (77), and developed using goat anti-rabbit IgG labeled with horseradish peroxidase (HRP) and enhanced chemiluminescence.

NF-κB activation

NF-κB activation was analyzed using AGS cells stably expressing a luciferase-based NF-κB reporter (58). Briefly, the reporter cell line was cocultured with *H. pylori* strains (multiplicity of infection [MOI] of 100:1) for 2 to 3 h at 37°C. *H. pylori* strains were cultured in the presence or absence of ATc for 24 to 48 h prior to testing NF-κB activation. Luminescence was measured using the Steady-Glo kit (Promega) on a BioTek FLx800 plate reader.

CagA translocation assay

CagA translocation into AGS gastric epithelial cells was analyzed using previously described methods (71-76). Briefly, *H. pylori* strains were cocultured with AGS cells at a MOI of 100:1 for 4 to 6 h at 37°C. CagA translocation was detected using an anti-phosphotyrosine antibody (anti-PY99; Santa Cruz Biotechnology) for tyrosine phosphorylation of CagA, and CagA was detected using anti-CagA antibody (Santa Cruz Biotechnology).

Statistical analyses

GraphPad Prism and R were used to perform the statistical analyses. A Mann-Whitney test was used to assess differences among groups in inflammation (two groups) or NF-κB activation. The Kruskal-Wallis test with Dunn's multiple-comparison test was used to assess differences among groups in inflammation (multiple groups) and bacterial burden (multiple groups). Fisher's exact test with Benjamini-Hochberg multitest correction was used to analyze differences among groups in incidence of gastric diseases. An unpaired *t* test with Welch's correction was used to evaluate numbers of lymphoid follicles/aggregates.

Bayesian z-scores and a standard z-test (multiple test correction using the Benjamini-Hochberg method) were used to evaluate gene expression RT-PCR data. Specifically, quantitative RT-PCR data were analyzed using generalized linear mixed models based on log-normal Poisson error distribution and fitted using Markov chain Monte Carlo analysis (107). Data were fit using informed models and data from control genes. Amplification efficiencies were determined based on analysis of amplification of targets over a 6-log range of template concentrations using purified *H. pylori* genomic DNA and optimized primer annealing temperatures. The credible intervals were determined by the MCMC.qpcr package in R. Based on the Bayesian framework, a credible interval (or credible limit) is an analog of a confidence interval in frequentist statistics.

The 95% credible limit indicates there is a 95% probability of the true value falling with this parameter.

Ethics statement: All animal experiments were approved by the Vanderbilt University Institutional Animal Care and Use Committee (protocol M1700055-00).

Results

Regulation of Cag T4SS activity *in vitro*

In a previous study, we developed a system that allowed conditional expression of Cag T4SS activity in *H. pylori* strain 26695, based on insertion of the *tet* repressor (*tetR*) in the *ureA* locus and insertion of *tet* operator (*tetO*) sites upstream of the *cagUT* operon (103). To facilitate experiments designed to conditionally regulate Cag T4SS in an animal model of *H. pylori*-induced gastric disease, we modified *H. pylori* strain 7.13 (a strain capable of colonizing Mongolian gerbils) so that it contained *tetR* in a locus nonessential for colonization (instead of the *ureA* locus) and *tetO* sites upstream of the *cagUT* operon (**Fig 3.1**). Pools of the resulting strains are designated *H. pylori* VM202-203 (**Table 3.1**). When strain VM202-203 was cultured in the presence of anhydrotetracycline (ATc), a derivative of tetracycline that lacks antibacterial activity, *cagU* expression was upregulated (while transcript levels of control genes remained stable), and CagT protein was produced **(Fig 3.2 A, B**). Accordingly, a Cag T4SS-dependent phenotype (NF-κB activation in AGS gastric epithelial cells) and CagA translocation into AGS cells were detected (**Fig 3.2 C, D**). When the strain was cultured in the absence of ATc, CagT protein was not produced, NF-κB activation was not detected, and CagA was not translocated into AGS gastric epithelial cells (**Fig 3.2 B-D**). Administration of ATc to Mongolian gerbils for prolonged time periods is not readily feasible due to the high cost of the drug. Therefore, we examined CagT expression in strains grown in the presence of doxycycline (another derivative of tetracycline). VM202-203 was grown in various concentrations of doxycycline. Growth was

not inhibited by doxycycline concentrations up to 40 ng/ml, whereas growth was inhibited by ≥80 ng/ml (data not shown). CagT protein was produced when *H. pylori* was cultured in the presence of doxycycline, and the CagT levels in strains grown in 10 to 40 ng/ml doxycycline were similar to levels produced by wild-type strain 7.13 (**Fig 3.2 E, F**).

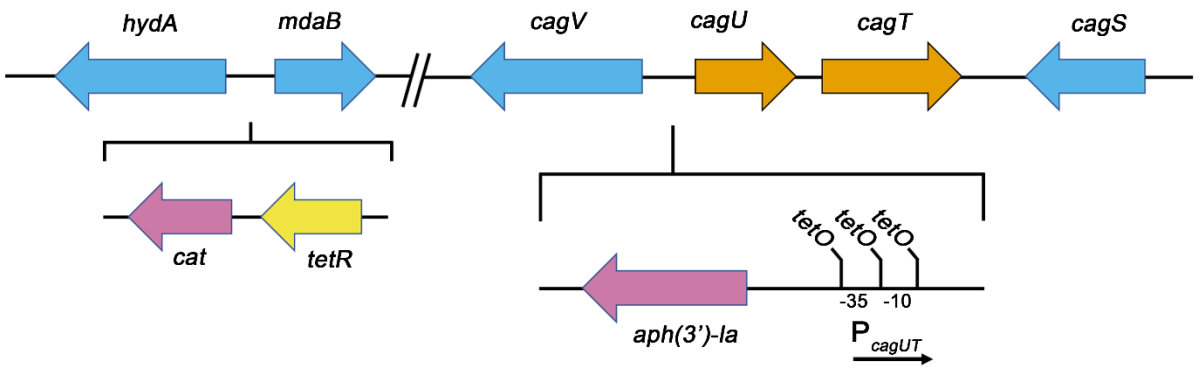

Figure 3.1: Introduction of *tetR* and *tetO* in the engineered strain VM202-203. The codon-optimized *tetR* was introduced into the intergenic region between *mdaB* and *hydA* derived from strain G27. Three copies of *tetO* were introduced upstream of the *cagUT* operon to regulate *cagUT* gene expression.

Table 3.1: *H. pylori* strains used in this study

Strain name	Description
7.13	Gerbil-adapted *H. pylori* strain 7.13
VM127	7.13 was transformed with plasmid pMM685, in which *tetR* and a chloramphenicol resistant determinant from pMM682 (103) were cloned into the region between *mdaB* and *hydA*.
VM127-Mu	Gerbils were infected with *H. pylori* VM127 and the output strain was designated VM127-Mu.
VM196	VM127-Mu in which a kanamycin resistant determinant was inserted within *cagU* (*cagU* mutant strain).
VM197-201	7.13 containing *tetR* inserted into the region between *mdaB* and *hydA* and three copies of *tetO* in proximity of the *cagUT* promoter.
VM202-203	A pool of VM197-201 was used to infect gerbils. Pools of *H. pylori* colonies cultured from two infected gerbils were designated VM202-203.

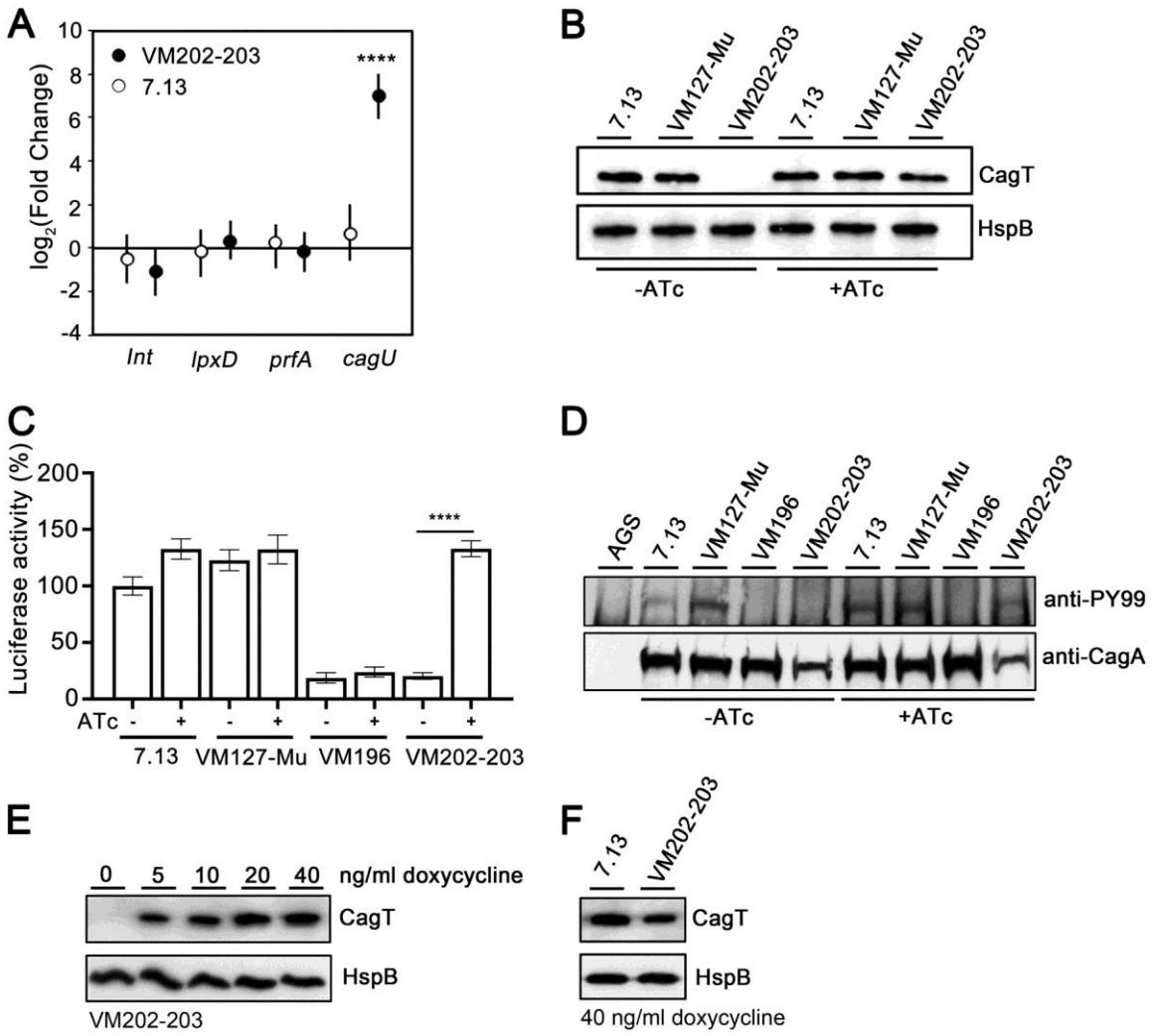

Figure 3.2: Regulatory control of *cagU* expression and Cag T4SS activity *in vitro*. (A) Transcript abundance of *cagU* and control genes (*Int*, *lpxD*, and *prfA*) were determined as described materials and methods. Fold change values compare transcript levels of the indicated genes in *H. pylori* strain VM202-203 or 7.13 grown in the presence of anhydrotetracycline (ATc) to corresponding transcript levels in the same strains grown in the absence of ATc. Values represent the means and 95% credible limits (error bars). Among the genes tested, only *cagU* expression changed significantly in the presence of ATc compared with the absence of ATc. Significance was determined by calculating Bayesian z-scores, and a standard z-test was performed to derive two-tailed *P* values which were corrected for multiple testing using the Benjamini-Hochberg method (with a false discovery rate of 5%). ****, $P \leq 0.0001$. (B) Western blot detection of CagT protein in the indicated strains in the presence (+) or absence (-) of ATc. Heat shock protein (HspB) was analyzed as a loading control. (C) NF-κB activation induced by the indicated strains in AGS reporter cells. Wild-type strains 7.13 and VM127-Mu (containing *tetR* but not *tetO*) (**Table 3.1**) were used as positive controls and VM196 (*cagU* mutant) as a negative control. The data represent results of three independent experiments with multiple technical replicates. Values represent means ± standard errors of the means (SEM). Significance was determined using the Mann-Whitney test. (D) CagA translocation into AGS gastric epithelial cells. 7.13 and VM127-Mu strains were used as positive

controls and VM196 as a negative control. (E) Western blot detection of CagT in VM202-203 in the presence of subinhibitory concentrations of doxycycline (0 to 40 ng/ml). (F) Western blot detection of CagT in VM202-203 and wild-type strain 7.13 grown in the presence of 40 ng/ml doxycycline.

Regulation of *cagUT* expression *in vivo*

We formulated rodent chow containing doxycycline as described in Materials and Methods. We first investigated if *H. pylori* VM202-203 could persistently colonize the gerbil stomach in animals receiving a diet containing doxycycline. Gerbils were experimentally infected with VM202-203, and the animals were fed chow containing a range of doxycycline concentrations (0, 50, 100, 150, or 175 mg/kg in chow) for 3 months. The animals were euthanized, and the stomachs were processed as described in Materials and Methods. In this pilot experiment, strain VM202-203 colonized the stomach in 2 out of 3 gerbils fed chow containing 50 mg/kg doxycycline and all 3 gerbils on a drug-free diet (0 mg/kg doxycycline). In contrast, *H. pylori* failed to colonize most of the animals fed chow containing >50 mg/kg doxycycline. The *cagU* transcript levels were higher in gastric tissue from *H. pylori*-infected animals receiving doxycycline than in tissue from infected control animals, based on quantitative real-time PCR (qRT-PCR) analysis (**Fig 3.3**), indicating that expression of the *cagUT* operon could be conditionally regulated *in vivo* by doxycycline.

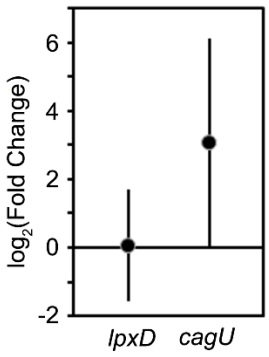

Figure 3.3: Pilot experiment analyzing transcript abundance of *cagU* and a control gene (*lpxD)* in stomach tissues of infected gerbils receiving chow containing 50 mg/kg doxycycline ($n = 2$) compared to infected gerbils receiving chow containing 0 mg/kg doxycycline ($n = 3$). Values represent the mean (and 95% credible limit) $\log_2$ fold change. Bayesian z-scores were calculated, and a standard z-test was performed to derive two-tailed *P* values. The *P* values (0.922 and 0.054 for *lpxD* and *cagU*, respectively) were corrected for multiple testing using the Benjamini-Hochberg method.

To further define the optimal sub-antimicrobial concentration of doxycycline in gerbil chow, we infected a larger cohort of gerbils with *H. pylori* and fed the animals chow containing a lower range of doxycycline concentrations (0, 10, 25, 50, or 75 mg/kg in chow) for 3 months (**Fig 3.4 A**). *H. pylori* was successfully cultured from most of the infected animals receiving chow containing 10 or 25 mg/kg doxycycline (**Fig 3.4 B**). The *H. pylori* colonization density in these animals was higher than the colonization density in animals receiving drug-free chow, but this trend was not consistently detected in subsequent experiments. Thus, consumption of chow containing 10 or 25 mg/kg doxycycline did not have a substantial antimicrobial effect on *H. pylori in vivo.* In contrast, *H. pylori* was not successfully cultured from many of the infected animals receiving chow containing 50 or 75 mg/kg doxycycline (**Fig 3.4 B**). qRT-PCR analysis of gastric tissue indicated that consumption of chow containing 10 or 25 mg/kg doxycycline was sufficient to derepress expression of *cagU in vivo* (**Fig 3.4 C**).

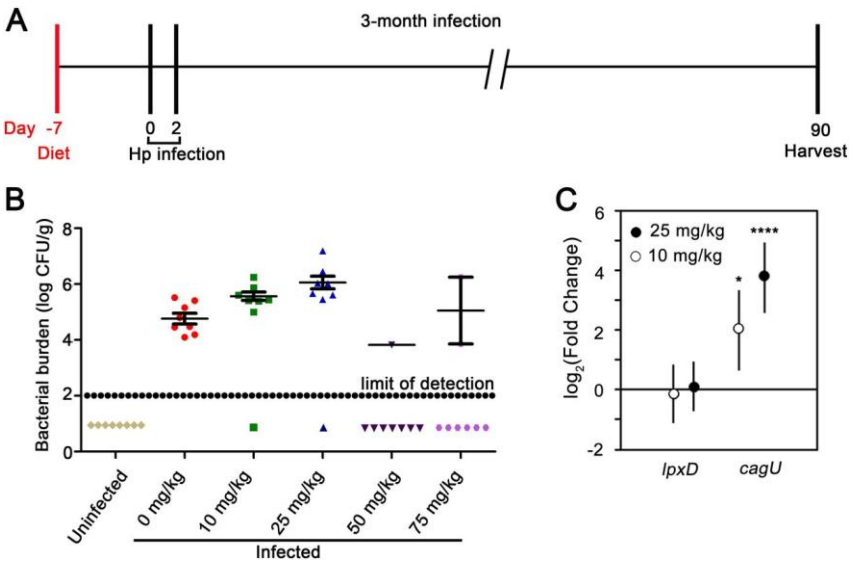

Figure 3.4: Regulatory control of *cagU* expression *in vivo*. (A) Mongolian gerbils were fed chow containing a range of doxycycline concentrations (0, 10, 25, 50, or 75 mg/kg) beginning 1 week prior to *H. pylori* (Hp) infection and continued for 3 months. The animals were infected with *H. pylori* VM202-203 via oral gavage on day 0 and day 2 and were euthanized 3 months postinfection. Uninfected animals that received drug-free chow were used as negative controls. (B) Bacterial colonization density in the stomachs of animals receiving chow containing the indicated doxycycline concentrations. The data represent values for individual animals. The data points below the limit of detection represent animals from which *H. pylori* could not be cultured. (C) Expression of *cagU* and a control gene (*lpxD)* in gastric tissues of infected animals fed chow containing the indicated doxycycline concentrations. Fold change values compare results for infected animals fed chow containing doxycycline compared to infected animals fed drug-free chow. Values represent the means and 95% credible limits. Transcript levels of *cagU* were significantly different in infected animals fed chow containing doxycycline (10 or 25 mg/kg) compared with animals fed a normal diet. Significance in panel C was calculated via Bayesian z-scores, and a standard z-test was performed to derive two-tailed *P* values which were corrected for multiple testing using the Benjamini-Hochberg method (with a false discovery rate of 5%). *, $P \leq 0.05$; ****, $P \leq 0.0001$.

Stability of the TetR/*tetO* system *in vivo*

We next tested if the TetR/*tetO*-dependent regulatory phenotype of *H. pylori* VM202-203 remained intact during colonization of the gerbil stomach for a 3-month time period (**Fig 3.5**). We analyzed the *H. pylori* strains cultured from the stomachs of successfully colonized gerbils by culturing the strains in the absence or presence of ATc and testing the capacity of these strains to activate NF-κB in AGS gastric epithelial cells (as a readout of Cag T4SS activity). Seven of 8 output strains harvested from infected gerbils fed a drug-free diet induced NF-κB activation in the presence of ATc but not in the absence of ATc (**Fig 3.5 A**). Similarly, 11 of 13 output strains collected from infected gerbils fed a diet containing 10 mg/kg or 25 mg/kg doxycycline stimulated NF-κB activation in the presence of ATc but not in the absence of ATc (**Fig 3.5 B**). One strain lacking this property (4_0D [animal number four fed chow containing 0 mg/kg doxycycline]) stimulated NF-κB activation in both the presence and absence of ATc (**Fig 3.5 A**) and contained a nonsense mutation in *tetR* (data not shown). Two strains with intact *tetR/tetO* sequences were defective in NF-κB activation in both the presence and absence of ATc (2_10D and 7_25D [animal number 2 and animal number 7 fed chow containing 10 mg/kg or 25 mg/kg doxycycline, respectively]) likely contain mutations in one or more *cag* PAI genes required for T4SS function (**Fig 3.5 B**). These results indicate that the TetR-dependent regulatory properties of the Cag T4SS remained intact in *H. pylori* strains from most animals after colonization of the gerbil stomach for a 3-month time period. A previous study that analyzed stability of *tetR*-containing *H. pylori* strains in mice reached a similar conclusion (108).

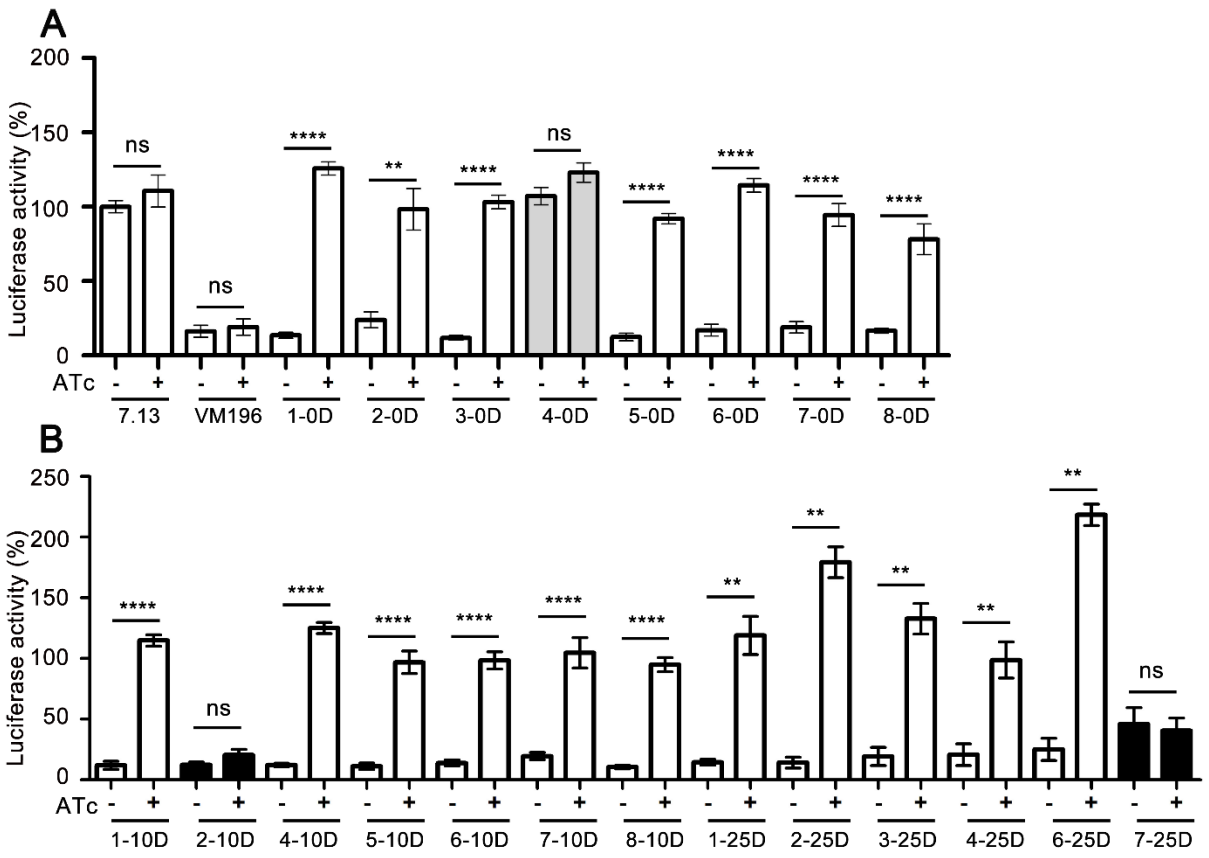

Figure 3.5: Stability of the Cag T4SS *in vivo*. Gerbils were infected with *H. pylori* VM202-203 and fed diets containing a range of doxycycline concentrations as described in the legend to **Fig 3.4**. (A) *H. pylori* strains cultured from infected animals fed a normal (drug-free) diet for 3 months were tested for capacity to stimulate NF-κB activation in AGS reporter cells. The label 1-0D indicates animal number 1 fed chow containing 0 mg/kg doxycycline. (B) NF-κB activation induced by output strains cultured from infected animals fed a diet containing 10 mg/kg or 25 mg/kg doxycycline for 3 months. The labels 1-10D and 1-25D indicate strains cultured from animals fed chow containing 10 mg/kg or 25 mg/kg doxycycline, respectively. Strain 7.13 was used as a positive control and VM196 as a negative control. The individual data represent results of two or three independent experiments with multiple technical replicates. Values represent means ± standard errors of the means (SEM). Significance was determined using Mann-Whitney test for panels A and B.*, $P \leq 0.05$; **, $P \leq 0.01$; ***, $P \leq 0.001$; ****, $P \leq 0.0001$.

Gastric inflammation in response to Cag T4SS activity

We next examined the gastric histology of the gerbils described above. To evaluate a potential impact of Cag T4SS activity on the severity of gastric inflammation, we used the histologic scoring system described in Materials and Methods. Gastric inflammation scores are reported for all uninfected gerbils, as well as experimentally infected gerbils from which *H. pylori* was successfully cultured and/or detected by use of a modified Steiner stain (**Fig 3.6 A**). Representative images of gastric histology are shown in **Fig 3.6 B**-**D**. As expected, gastric inflammation was not observed in tissues from uninfected animals (**Fig 3.6 A, B**). Similarly, we detected minimal gastric inflammation in *H. pylori*-infected animals fed a diet lacking doxycycline (**Fig 3.6 A, C**). In contrast, gastric inflammation was observed in most of the infected animals receiving chow containing 10 or 25 mg/kg doxycycline (**Fig 3.6 A, D**). The overall severity of gastric inflammation (combined analysis of antrum and corpus) in infected animals receiving doxycycline (10, 25, 50, or 75 mg/kg) was significantly greater than the severity of inflammation in infected animals receiving drug-free chow (**Fig 3.6 A**). Both acute and chronic inflammation scores (neutrophils and mononuclear cells, respectively) were significantly increased in the antrum of infected animals receiving doxycycline in chow, compared to infected animals receiving drug-free chow (data not shown). Dysplasia (a premalignant lesion) and/or gastric adenocarcinoma was detected in several of the *H. pylori*-infected animals receiving doxycycline (10, 25, or 50 mg/kg), but not in any of the infected animals receiving drug-free chow (**Table 3.2**). These data indicate that Cag T4SS activity contributes to the development of a gastric inflammatory response and suggest that Cag T4SS activity promotes the development of gastric adenocarcinoma.

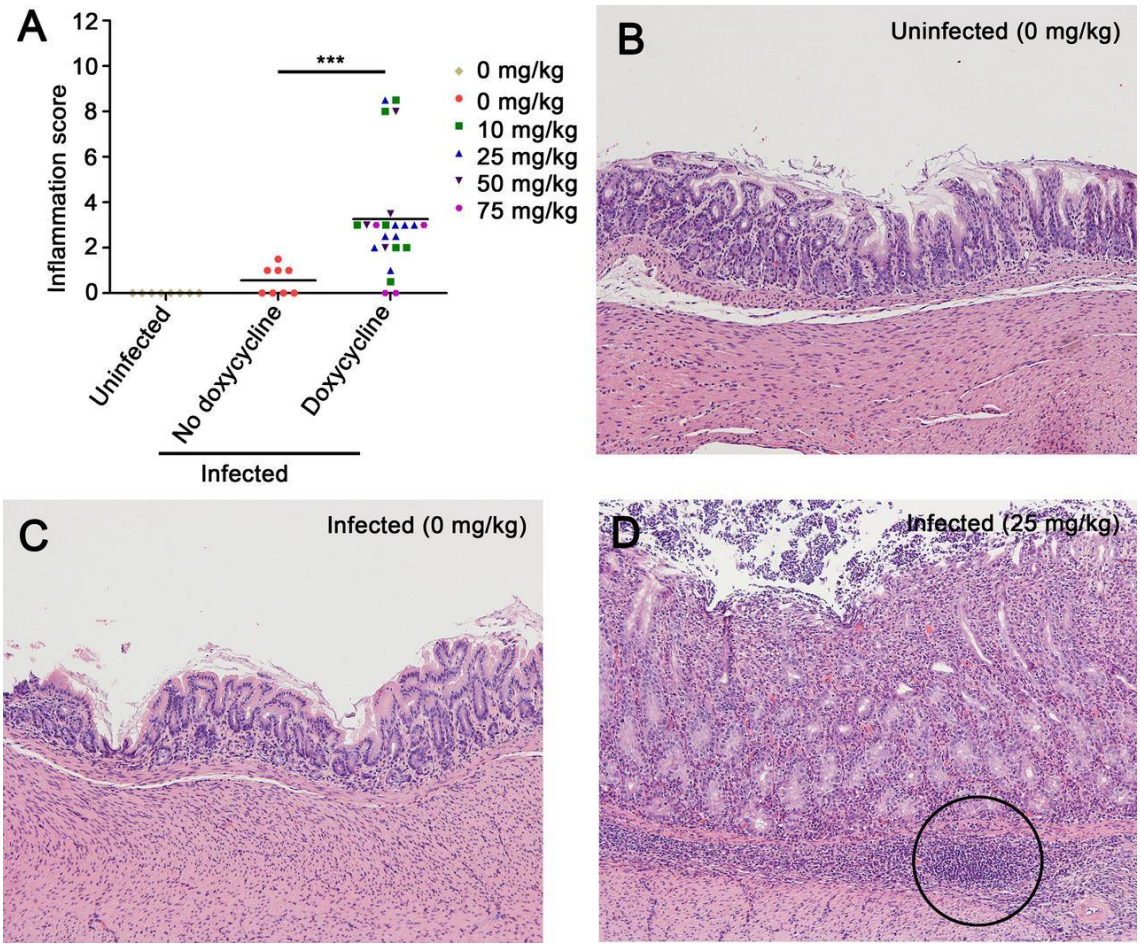

Figure 3.6: Gastric inflammation in *H. pylori*-infected animals in response to Cag T4SS activity. Gerbils were infected with *H. pylori* VM202-203 and fed diets containing a range of doxycycline concentrations as described in the legend to **Fig 3.4**. (A) Inflammation scores in gastric mucosa. Gastric inflammation was scored on a 12-point scale as described in Materials and Methods. The data represent results for individual animals. Significance was calculated using Mann-Whitney test. ***, $P \leq 0.001$. (B to D) Gastric antral histology from representative animals, showing normal histology in uninfected gerbils (B) and infected gerbils receiving a drug-free diet (C). (D) Severe gastric inflammation and lymphoid follicles (circle) were observed in infected gerbils receiving chow containing 25 mg/kg doxycycline. Magnification, 100×.

Table 3.2: Frequency of most severe diagnosis in uninfected and infected animals receiving various concentrations of doxycycline

Animal group[a]	Normal histology	Gastritis	Dysplasia	Cancer	No. of successfully colonized animals[b]	Total no. of animals used
Uninfected	8	0	0	0	0	8
Infected (0 mg/kg)	4	4	0	0	8	8
Infected (10 mg/kg)	1	4	2	1	7	8
Infected (25 mg/kg)	0	7	0	1	8	8
Infected (50 mg/kg)	1	6	0	1	4	8
Infected (75 mg/kg)	4	3	0	0	4	7

[a] Animals were infected with *H. pylori* VM202-203 and fed diets containing the indicated doxycycline concentrations. Uninfected animals in this experiment received drug-free chow.

[b] *H. pylori* colonization was evaluated by culturing *H. pylori* and/or Steiner stain.

Temporal regulation of Cag T4SS activity

To further evaluate a potential role of Cag T4SS activity in gastric cancer pathogenesis, we studied larger numbers of animals and fed the animals either chow containing a standardized concentration of doxycycline (25 mg/kg) or drug-free chow. We also sought to determine if Cag T4SS activity contributed to carcinogenesis during the early stages of infection, during later stages of infection, or continuously throughout infection. Specifically, we conducted experiments in which *cagUT* expression was derepressed only during an early stage of infection (prior to development of a robust adaptive immune response and gastric inflammatory response) (109) or only during later stages of infection (**Fig 3.7 A**). One group of animals received drug-free chow for the first 3 weeks and then were switched to chow containing doxycycline (25 mg/kg) for the remaining 10 weeks of the experiment. Another group of animals received doxycycline-containing chow (25 mg/kg) for the first 3 weeks of infection and then were switched to drug-free chow for the remaining 10 weeks of the experiment. Control animals received drug-free chow or chow containing doxycycline (25 mg/kg) throughout the 13-week experiment.

Most of the animals were successfully colonized (**Fig 3.7 B**). As expected, most of the output strains from infected gerbils retained the TetR-dependent regulatory properties of the T4SS (**Fig 3.8**). Eighteen of 20 strains induced NF-κB activation in AGS cells in the presence of ATc but not in the absence of ATc. Among the two strains lacking this property, one (8_0D [animal number eight fed chow containing 0 mg/kg doxycycline]) contained a nonsense mutation in *tetR* (data not shown), and the other (2_25D [animal number two fed chow containing 25 mg/kg doxycycline]) likely contained a mutation in a *cag* PAI gene required for T4SS activity (**Fig 3.8**). These data confirm that *H. pylori* strains from most animals retained the original Cag T4SS regulatory properties after colonization of the gerbil stomach for 3 months.

As expected, there was minimal gastric inflammation in uninfected animals receiving drug-free chow or chow containing 25 mg/kg doxycycline (**Fig 3.7 C**). Similarly, we detected minimal

inflammation in infected animals fed drug-free chow (**Fig 3.7 C**). The severity of gastric inflammation in infected animals receiving doxycycline for the entire 3-month time period was significantly increased compared to the severity of inflammation in infected animals receiving drug-free chow (**Fig 3.7 C**). Acute inflammation (neutrophils) and chronic inflammation (mononuclear cells) in the antrum and corpus were both significantly increased in infected animals receiving doxycycline compared to infected animals fed drug-free chow (data not shown). In animals receiving doxycycline for shorter time periods (only the first 3 weeks of infection or only the subsequent 10 weeks of infection), there was a trend toward increased gastric inflammation compared to infected animals receiving drug-free chow, but the differences were not statistically significant (**Fig 3.7 C**).

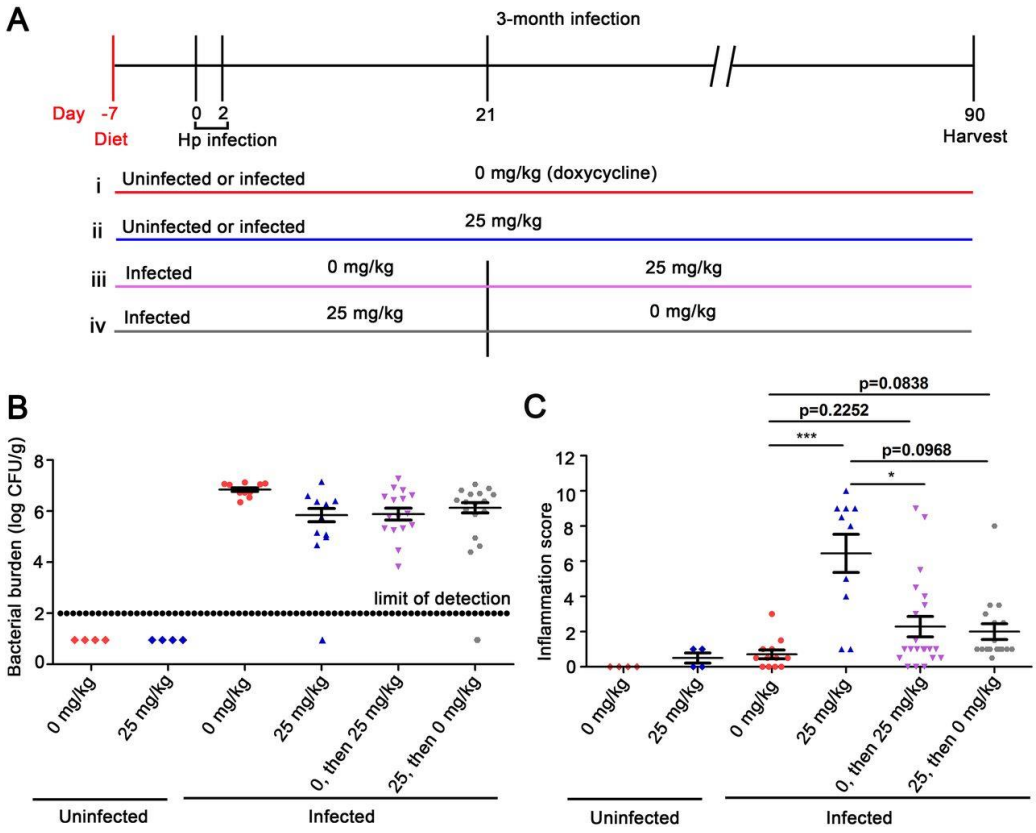

Figure 3.7: Gastric inflammation in response to Cag T4SS activity during specific stages of infection. (A) Gerbils were fed diets containing either 0 mg/kg or 25 mg/kg doxycycline 1 week prior to *H. pylori* infection and were infected with *H. pylori* VM202-203 via oral gavage on day 0 and day 2. (i and ii) *H. pylori*-infected gerbils or uninfected gerbils were fed diets containing either 0 mg/kg or 25 mg/kg doxycycline for the entire experiment. (iii) Gerbils were fed a diet containing 0 mg/kg doxycycline for the initial 3 weeks of infection and then switched to a diet containing 25 mg/kg doxycycline for the rest of the experiment (labeled “0, then 25” in subsequent panels). (iv) Gerbils were fed a diet containing 25 mg/kg doxycycline for the initial 3 weeks of infection and then changed to a diet containing 0 mg/kg doxycycline for the rest of the experiment (labeled “25, then 0” in subsequent panels). (B) Bacterial colonization density. (C) Inflammation scores in gastric mucosa. Significance was calculated using Kruskal-Wallis test with Dunn’s multiple-comparison test. The data represent results for individual animals. *, $P \leq 0.05$; ***, $P \leq 0.001$.

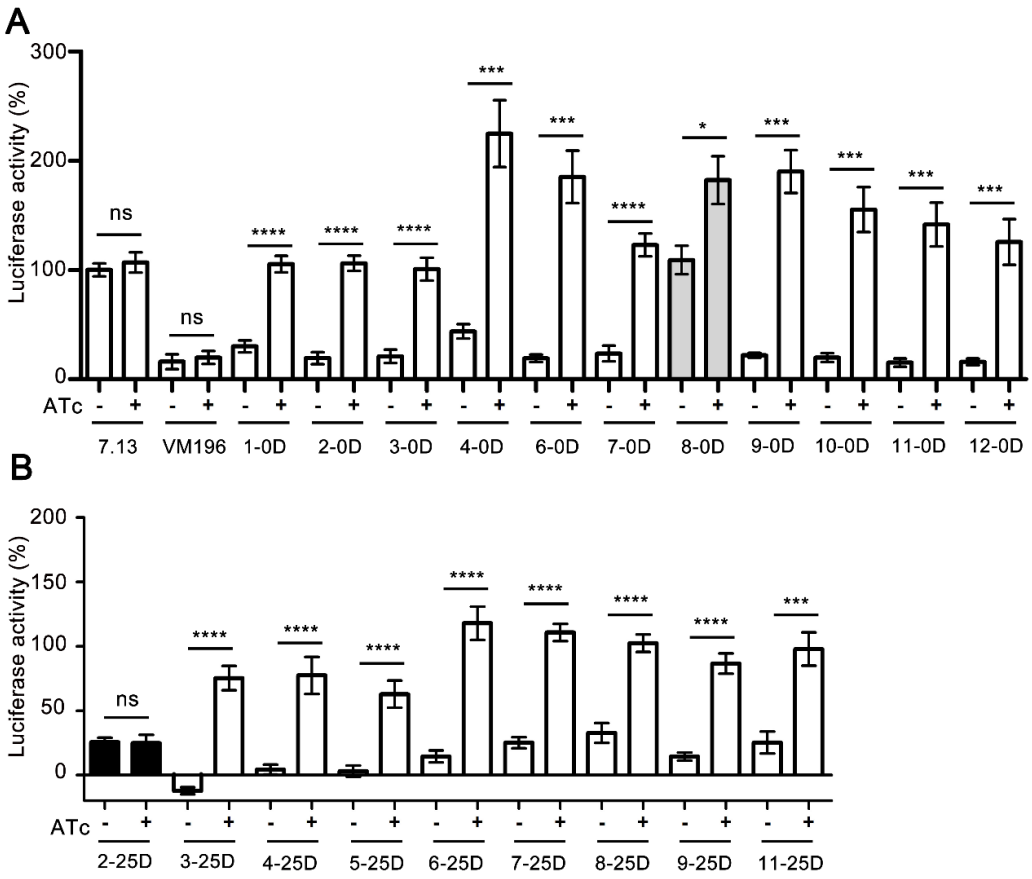

Figure 3.8: Stability of the TetR/*tetO* system *in vivo*. Gerbils were infected with *H. pylori* VM202-203 and fed various diets as described in the legend to **Fig 3.7**. (A) *H. pylori* strains cultured from infected animals fed a drug-free diet for 3 months were tested for their capacity to stimulate NF-κB activation in AGS cells. (B) NF-κB activation induced by output strains cultured from infected animals fed a diet containing 25 mg/kg doxycycline for 3 months. Strain 7.13 was used as a positive control and strain VM196 as a negative control. In parallel, the output strains from individual animals were grown in the absence or presence of ATc for 24 to 48 h prior to testing NF-κB activation. The data represent results of two or three independent experiments with multiple technical replicates. Values represent means ± standard errors of the means (SEM). Significance was determined using Mann-Whitney test. *, $P \leq 0.05$; **, $P \leq 0.01$; ***, $P \leq 0.001$; ****, $P \leq 0.0001$.

Dysplasia (a premalignant lesion) and/or gastric adenocarcinoma was detected in 63% of *H. pylori*-infected animals receiving doxycycline in chow for the entire 3-month time period (5/11 exhibited dysplasia, and 2/11 exhibited gastric cancer) (**Fig 3.9**). Among 12 infected animals receiving drug-free chow, none developed dysplasia or gastric cancer ($P = 0.0013$ when comparing infected animals receiving doxycycline with animals receiving drug-free chow). Dysplasia and/or cancer were not detected in animals receiving doxycycline for less than the entire 3-month time period (drug administration for the first 3 weeks of infection or weeks 4 to 13) (**Fig 3.9 A**). These findings indicate that Cag T4SS activity is required for development of dysplasia and/or gastric cancer.

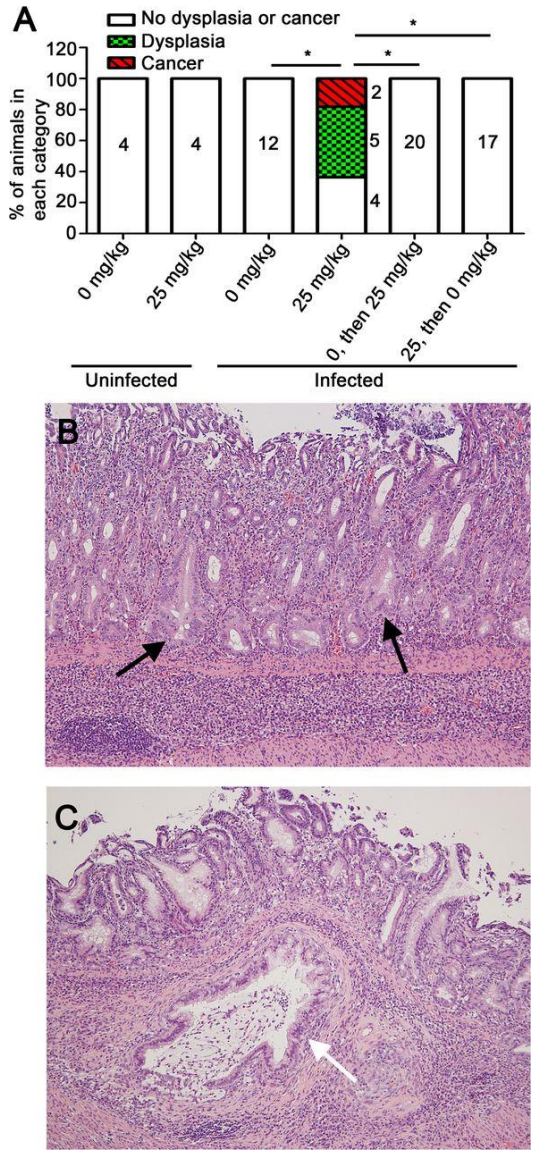

Figure 3.9: Dysplasia and gastric cancer in response to Cag T4SS activity. Gerbils were infected with *H. pylori* VM202-203 and fed various diets as described in the legend to **Fig 3.7**. (A) Frequency of dysplasia and/or cancer in uninfected and infected animals receiving chow containing the indicated concentrations of doxycycline at various time points. Significance was calculated using Fisher's exact test with Benjamini-Hochberg multitest comparison method (with a false discovery rate of 5%). *. $P < 0.0015$. (B and C) Representative gastric antral histology in infected animals, showing dysplastic glands (black arrows) and invasive carcinoma penetrating the muscularis mucosa and submucosa (white arrow). Magnification, 100×.

Since we did not detect dysplasia or gastric cancer in animals receiving doxycycline for the first 3 weeks of a 3-month infection, we did further experiments to evaluate the duration of Cag T4SS activity during early infection that is sufficient for development of dysplasia and/or gastric cancer. Animals were fed doxycycline-containing chow for 6 weeks and sacrificed at the 6-week time point (**Fig 3.10 A**). In addition, we analyzed a group of infected animals that received doxycycline during the initial 6 weeks of infection, followed by a drug-free diet for the next 7 weeks (**Fig 3.10 A**). Control groups were similar to the groups described previously. The *H. pylori* colonization density was lower at the 6-week time point compared to the 13-week time point (**Fig 3.10 B**). As expected, there was minimal gastric inflammation in uninfected animals receiving either drug-free chow or chow containing doxycycline (**Fig 3.10 C**). Gastric inflammation scores were higher in infected animals euthanized at the 3-month time point (either receiving doxycycline for the first 6 weeks of infection or the entire 3-month time period) than in infected animals receiving doxycycline and euthanized at the 6-week time point (**Fig 3.10 C**). Among the infected animals in which Cag T4SS activity was derepressed for 6 weeks and then repressed for weeks 7 to 13, one developed severe gastric inflammation and gastric cancer (**Fig 3.10 D**). These results suggest that Cag T4SS activity during the initial 6 weeks of infection results in gastric inflammation at a subsequent time point when the T4SS is no longer active and can result in gastric cancer at the later time point in a small proportion of animals.

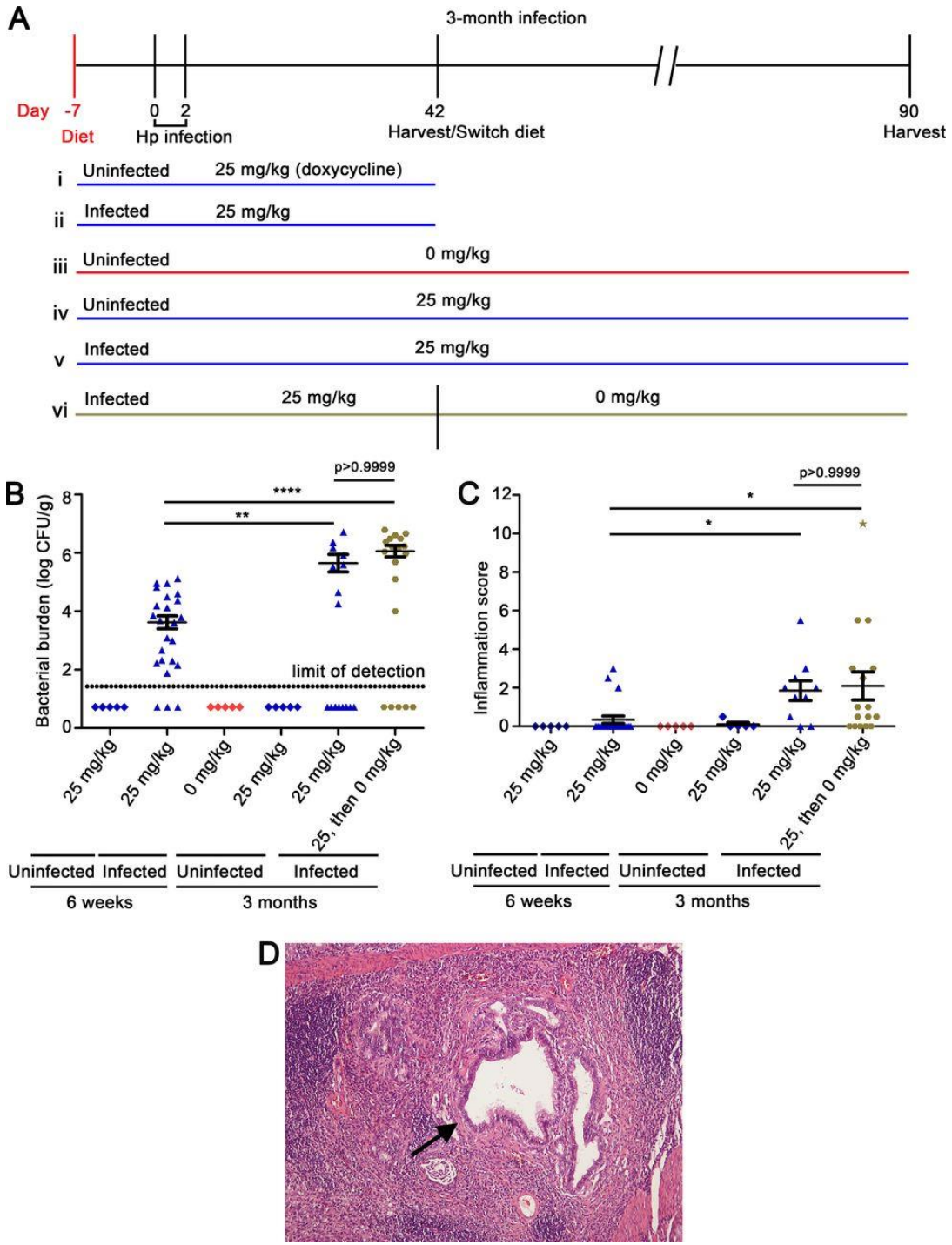

Figure 3.10: Gastric inflammation and gastric cancer in response to Cag T4SS activity during the initial 6 weeks of a 3-month infection. (A) Gerbils were fed diets containing either 0 mg/kg or 25 mg/kg doxycycline 1 week prior to infection and were infected with *H. pylori* VM202-203 via oral gavage on day 0 and day 2. (i and ii) *H. pylori*-infected or uninfected gerbils were fed diets containing 25 mg/kg doxycycline for 6 weeks. (iii and iv) Uninfected gerbils were fed diets containing either 0 mg/kg or 25 mg/kg doxycycline for the entire experiment. (v and vi) Infected gerbils were fed a diet containing 25 mg/kg doxycycline for the entire experiment or for the initial

6 weeks of infection, followed by switching to a diet containing 0 mg/kg doxycycline for weeks 7 to 13 (labeled “25, then 0” in subsequent panels). (B) Bacterial colonization density. The data represent results for individual animals. (C) Inflammation scores in gastric mucosa. The data represent results for individual animals. In this experiment, only one of the *H. pylori*-infected animals developed gastric adenocarcinoma (corresponding to the star-shaped data point). (D) Gastric antral histology in an infected animal (fed a doxycycline-containing diet for the initial 6 weeks of infection and then switched to a drug-free diet for the subsequent 7 weeks), showing invasive carcinoma in the submucosa. Significance was calculated using Kruskal-Wallis test with Dunn’s multiple-comparison test for panels B and C. *, $P \leq 0.05$; **, $P < 0.01$; ****, $P \leq 0.0001$.

Discussion

In this study, we utilized the TetR/*tetO* system to derepress the *H. pylori cagUT* operon, thereby allowing us to regulate Cag T4SS activity in a Mongolian gerbil model. We observed that derepression of Cag T4SS activity *in vivo* resulted in significantly higher levels of gastric inflammation than observed in infected control animals. Furthermore, dysplasia and gastric adenocarcinoma were detected only in animals in which Cag T4SS activity was derepressed. These results provide strong evidence that Cag T4SS activity contributes to development of a gastric mucosal inflammatory response and is required for development of gastric premalignant lesions and gastric cancer. Previous studies of *H. pylori cag* PAI mutant strains suggested that Cag T4SS activity contributes to gastric cancer pathogenesis in the gerbil model, but none of the previous studies tested complemented mutant strains. The approach used in the current study allowed us to overcome this limitation and also allowed us to temporally regulate Cag T4SS activity *in vivo*.

A previous study used the TetR/*tetO* system to conditionally regulate *H. pylori* urease in a mouse model and showed that urease is required for establishing gastric infection as well as persistence of infection (108). In the previous study, doxycycline or ATc was administered to mice in drinking water containing 5% sucrose (108). Mongolian gerbils are desert animals that drink relatively little water compared to mice. Therefore, in the current study, we fed the animals specially formulated chow containing doxycycline. Doxycycline has antibacterial activity and has been used in combination with other antibiotics for the treatment of *H. pylori* infection (110). In the current study, we were unable to culture *H. pylori* from many of the experimentally infected animals that consumed chow containing >50 mg/kg doxycycline. In contrast, administration of doxycycline in lower concentrations did not result in any detectable reduction in *H. pylori* colonization density compared to control gerbils receiving drug-free chow and was sufficient to derepress *cagUT* expression *in vivo*.

Although use of the TetR/*tetO* system and administration of doxycycline-containing chow allowed us to regulate Cag T4SS activity *in vivo* and detect histologic consequences of Cag T4SS activity, the incidence of premalignant changes and gastric cancer observed in the current study was somewhat lower than the corresponding incidence observed in several previous studies in which Mongolian gerbils were infected with wild-type strain 7.13 (59, 87). The lower rate of gastric cancer in the current study could potentially be due to variations among studies in study design (for example, differences in the duration of infection or differences in dietary composition). In addition, gerbils are outbred, so variations in outcomes of different studies (or variations in the severity of disease when comparing different gerbil cohorts in the current study) are potentially attributable to differences in the genetic characteristics of gerbil cohorts. Another possibility is that administration of doxycycline might modulate the severity of gastric disease that develops in response to *H. pylori*. For example, doxycycline administration might attenuate the severity of the gastric inflammatory response and/or lead to a reduced rate of gastric cancer.

Doxycycline can potentially have multiple activities *in vivo*, including anti-inflammatory activities (111) and effects on the intestinal microbiota (112). Doxycycline can induce esophageal ulceration mimicking a benign form of esophageal cancer (113-115), can cause gastrointestinal injury (116, 117), and can stimulate colonic tumor growth (118). On the other hand, doxycycline can also have antitumorigenic effects (119-122). In the current study, administration of doxycycline to gerbils did not cause any detected gastric histologic alterations in the absence of *H. pylori* infection. Therefore, the main activity of doxycycline in these experiments is attributed to its role in regulating *cagUT* expression and Cag T4SS activity.

Gastric cancer in humans is thought to arise through a multistep progression of histologic alterations (chronic gastritis, atrophic gastritis, intestinal metaplasia, dysplasia, gastric adenocarcinoma) (123). It is not known if *H. pylori* has carcinogenic effects mainly during early stages of infection, during later stages of infection, or throughout infection. The hit-and-run

model of carcinogenesis proposes that an infectious agent triggers carcinogenesis during initial stages of infection and that the ongoing presence of the infectious agent is not required for development of cancer. This model of carcinogenesis has been implicated in multiple types of virus-induced carcinogenesis (94, 96, 124). In the current study, we experimentally tested if the hit-and-run model of carcinogenesis is applicable to Cag T4SS activity and gastric cancer, and we investigated the temporal features of Cag T4SS activity that are relevant for carcinogenesis. The results suggest that continuous Cag T4SS activity throughout a 3-month time period leads to higher rates of gastric cancer incidence than the rates observed when Cag T4SS activity is limited to early or late stages of infection. Animals in which the Cag T4SS was derepressed for a 10-week time period during later stages of infection (weeks 4 to 13) did not develop dysplasia or gastric cancer, although these animals exhibited a trend toward increased gastric inflammation compared to control infected animals receiving drug-free chow. Animals in which Cag T4SS was derepressed for the initial 3 weeks of a 3-month infection also did not develop dysplasia or cancer, but we again noted a trend toward increased gastric inflammation. Among animals in which Cag T4SS activity was derepressed for the initial 6 weeks of infection and repressed for the remainder of the 3-month experiment, one animal developed severe gastric inflammation as well as gastric cancer. The development of gastric cancer in only 1 of 19 gerbils (~5%) in this experimental group might seem relatively low. On the other hand, fewer than 3% of *H. pylori*-infected humans develop gastric cancer during an entire lifetime (10). Therefore, the current results suggest that Cag T4SS activity during the initial 6 weeks of infection is sufficient to initiate cellular alterations that can result in gastric cancer in a small proportion of animals at later time points when the T4SS is no longer active, consistent with the hit-and-run model of carcinogenesis.

Cag T4SS activity probably contributes to carcinogenesis through multiple mechanisms. T4SS-mediated delivery of CagA to gastric stem cells potentially occurs throughout *H. pylori* infection,

and likely promotes alterations in cell signaling that are pro-carcinogenic (89, 125). In support of this view, *in vivo* experiments indicate that *H. pylori* colonizes gastric glands, activates stem cells, and induces hyperplasia in mice in a CagA-dependent manner (89). During later stages of infection, Cag T4SS activity contributes to the development of a robust gastric mucosal inflammatory response (92). Enhanced gastric mucosal inflammation in the setting of persistent infection likely stimulates DNA damage through actions of reactive oxygen species and reactive nitrogen species, resulting in mutations in an assortment of genes, including p53 and genes involved in DNA repair pathways (48, 90, 91). The *H. pylori* Cag T4SS has also been implicated in repression of parietal cell H^+/K^+-ATPase expression, leading to inhibition of acid secretion during later stages of infection (126, 127). Therefore, the actions of CagA and Cag T4SS might lead to alterations in the gastric microbiome that are relevant for cancer pathogenesis (128-131). *In vitro* experiments suggest that *H. pylori* utilizes CagA to promote acquisition of nutrients, including iron, from the host (132). Therefore, we speculate that the Cag T4SS and CagA facilitate enhanced *H. pylori* replication and/or entry of *H. pylori* into gastric niches (for example, gastric glands adjacent to stem cells or the gastric corpus) that are less accessible in the absence of Cag T4SS activity. Further experiments will be required to decipher the precise actions of the Cag T4SS and CagA that are relevant to carcinogenesis at specific time points during infection.

The current study focused on temporal features of *H. pylori* Cag T4SS activity that are relevant for gastric carcinogenesis in the Mongolian gerbil model. A previous study evaluated the effect of antibiotic treatment on *H. pylori*-induced gastric cancer in the gerbil model (133). Specifically, Mongolian gerbils were infected with *H. pylori* strain 7.13 for 4 or 8 weeks, followed by treatment with antimicrobial agents for 8 weeks (133). No premalignant and malignant lesions were observed in the group of animals infected for 4 weeks and then treated with antibiotics (133). Among animals infected for 8 weeks prior to receiving antibiotics, treatment resulted in a

reduced proportion of animals with premalignant or malignant lesions but did not completely prevent development of these lesions. Our finding that Cag T4SS activity for 6 weeks is sufficient for development of gastric cancer in a small proportion of animals is consistent with the results of the previous antimicrobial treatment study. In contrast to the previous study, the current study focuses specifically on the contribution of the Cag T4SS to gastric carcinogenesis.

Several studies have suggested that eradication of *H. pylori* with antibiotics can prevent development of gastric cancer in humans if administered prior to the development of preneoplastic gastric lesions (134). Thus, individuals with a high risk of gastric cancer can potentially benefit from antibiotic treatment if it is administered prior to the development of intestinal metaplasia and atrophic gastritis. One study suggested that antibiotic administration could prevent development of gastric cancer if administered at late stages when *H. pylori* is no longer present (135, 136). This effect was attributed to antibiotic-induced changes in non-*H. pylori* constituents of the gastric microbiome. There are several important differences between the model system used to test the hit-and-run hypothesis in this study and corresponding features in *H. pylori*-infected humans. *H. pylori* probably colonizes the human stomach for several decades prior to the development of gastric cancer. Therefore, the time period required for development of gastric cancer in *H. pylori*-infected humans is probably much longer than the time period required for development of gastric cancer in the gerbil model. In addition, the current study was designed to allow regulation of the Cag T4SS in animals that were continuously infected with *H. pylori*. In contrast, studies of the temporal relationship between *H. pylori* and gastric cancer in humans have been based on assessing the presence or absence of *H. pylori* infection.

In summary, this study demonstrates the utility of using the TetR/*tetO* system to regulate Cag T4SS activity in animal models and highlights the important role of the Cag T4SS in gastric cancer pathogenesis. Moreover, this study supports the hit-and-run model of carcinogenesis in

the context of *H. pylori* infection, Cag T4SS activity, and development of gastric cancer. In future studies, we anticipate that use of the TetR/*tetO* system will allow investigation of the actions of additional *H. pylori* genes *in vivo* during different stages of infection.

Chapter IV

Gastric lipid alterations in response to *Helicobacter pylori*

Introduction

H. pylori colonization of the human stomach consistently results in a gastric mucosal inflammatory response characterized by infiltration of neutrophils, lymphocytes, and macrophages (92). Subsequently, a series of premalignant changes can arise, including atrophic gastritis, intestinal metaplasia, and dysplasia (106, 123). Atrophic gastritis in the corpus is characterized by loss of acid-secreting parietal cells, resulting in hypochlorhydria and loss of gastric acidity (123).

Our understanding of the pathogenesis of *H. pylori* infection has been aided by the availability of animal models. Two of the most commonly used models are mice and Mongolian gerbils (57). *H. pylori* can colonize the stomach in both rodent species, but there are notable differences in the gastric responses. Both mice and Mongolian gerbils develop gastric mucosal inflammation in response to *H. pylori*, but the inflammation is typically more severe in gerbils than in mice (57). Under most circumstances, *H. pylori*-infected wild-type mice do not develop gastric ulcers or gastric cancer (57). In contrast, *H. pylori*-infected Mongolian gerbils can develop gastric ulcers, hyperplasia, premalignant pathology (parietal cell loss, and dysplasia), and gastric cancer (63, 64).

The most commonly used approach for evaluating gastric histologic features and pathology is hematoxylin and eosin staining of fixed, paraffin-embedded tissue. In the current study, we used MALDI Imaging mass spectrometry (MALDI-IMS) and Liquid Chromatography Tandem Mass Spectrometry (LC-MS/MS) to test the hypothesis that *H. pylori* infection causes alteration in gastric lipids in the Mongolian gerbil model. Untargeted lipidomics based on IMS allows an assessment of the spatial distribution of lipid species within tissue based on molecular ion

confirmation. LC-MS/MS methods provide a more comprehensive analysis of lipids present in the tissues along with the ability to identify unique structures. By using these two methods, we identified multiple lipids that change in abundance in gastric tissue in response to *H. pylori* infection. Importantly, we identify gastric lipids that are localized to the gastric corpus and that change in abundance exclusively in *H. pylori*-infected animals exhibiting atrophic gastritis (a premalignant condition characterized by inflammation and loss of parietal cells and chief cells in the gastric corpus).

Materials and methods

Animal infection

Male Mongolian gerbils (35-45 g weight) were obtained from Charles River Laboratories. Gerbils were fasted overnight and then were infected via oral gavage (Day 0 and Day 2) with 1×10^9 CFU of *H. pylori* strain 7.13. Gerbils were fed an AIN-93M rodent diet (Bio-Serv), beginning 7 days prior to infection and throughout the remainder of the experiment. In parallel, uninfected gerbils received the same diet. Animals were euthanized at 3 months post-infection.

Processing of gastric tissue

Gerbil stomachs were processed to retain the glandular portion of the stomach (corpus and antrum) and the non-glandular portion (forestomach) was discarded. The glandular portion was cut open along the lesser curvature and laid flat (**Fig 4.1**). Half of the glandular section of stomach was frozen and used for subsequent mass spectrometry analysis, and another portion was used for conventional histology analysis as described below (**Fig 4.1**).

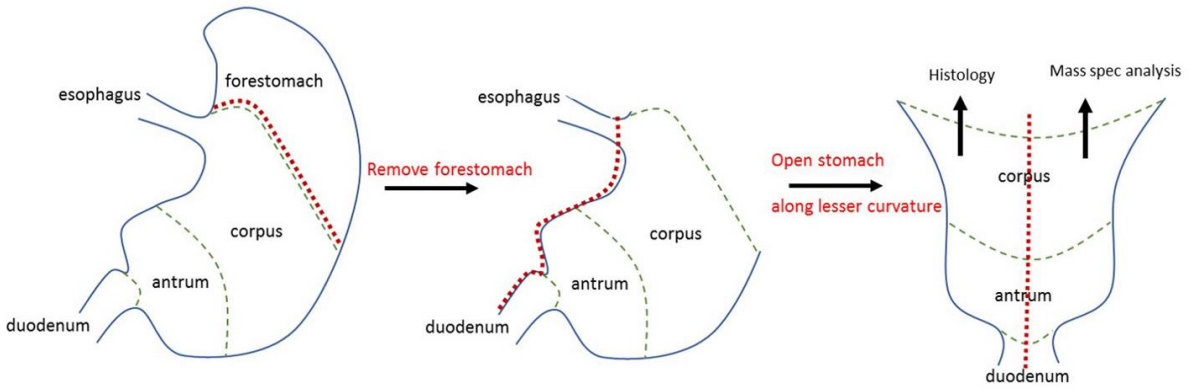

Figure 4.1: Processing of stomachs from Mongolian gerbils. After harvesting the stomach, the non-glandular forestomach was removed (red dotted line). Then, the stomach was cut open along the lesser curvature (red dotted line) and laid flat. The gastric tissue was cut into halves (red dotted line), each containing corpus and antrum, which were used for histology or imaging mass spectrometry analysis.

Histology

Longitudinal strips of stomach tissues were fixed in 10% formalin overnight, embedded in paraffin, sectioned, and stained with hematoxylin and eosin. Histologic sections of gastric tissues were analyzed by a gastrointestinal pathologist in a blinded fashion. Inflammation scores (0, 1, 2 and 3, corresponding to absent, mild, moderate, or marked inflammation, respectively) were assigned to evaluate both acute (neutrophils) and chronic (mononuclear leukocytes) inflammation. The inflammation was evaluated in both the corpus and antrum, and these scores were added together to yield a cumulative score of 0 to 12 (59-61, 105, 106, 137). The histologic evaluation also included an evaluation of whether gastric ulceration, dysplasia or gastric adenocarcinoma were present (105, 106). Finally, the abundance of parietal cells and chief cells in the gastric corpus was scored, using a previously described method (61).

Mass spectrometry imaging

Thin sections (12 μm) of fresh frozen glandular portion were obtained from a cryostat (Leica CM 1900) and thaw-mounted onto indium-tin oxide (ITO)-coated glass slides. Serial sections were obtained for lipid imaging (positive and negative ion mode) and H&E staining. DAN (1,5-diaminonaphthalene) was used as the matrix for MALDI imaging and was applied to the tissues by sublimation. Briefly, approximately 100 mg DAN was applied to the bottom of the custom sublimation apparatus and was allowed to sublimate onto the tissues at 130°C and ~25 mTorr for 4 minutes. Lipid images were acquired on a 15T FT-ICR MS (Bruker) at 75 μm spatial resolution.

Chemicals

HPLC grade chloroform, methanol, isopropanol, acetonitrile and water were purchased from Fisher Scientific (Pittsburg, PA). Formic acid and ammonium formate were obtained from Sigma-Aldrich (St. Louis, MO). tert-Butyl methyl ether (MTBE) was purchased from Honeywell

(Charlotte, NC). SPLASH® LIPIDOMIX® Mass Spec Standard was purchased from Avanti Polar Lipids, Alabaster, AL, U.S.

Lipid extraction for liquid chromatography-mass spectrometry (LC-MS/MS) procedure

12 µm of fresh frozen tissue sections were used for the lipid extraction. The corpus and antrum tissues were carefully scraped using razer and placed on a 1.5ml HPLC glass vial. One ml of MMC extraction mixture (138) (1.3:1:1, methanol: tert-Butyl methyl ether (MTBE): chloroform) spiked with 10 µl of lipid standard mixture was added to the same vial and the preparations were centrifugated at 3000 rpm for 10 minutes. The supernatant was transferred to a separate HPLC vial and was evaporated to dryness under nitrogen. The sample was then reconstituted with 30 µl methanol and 10µl was subjected for LC-MS/MS analysis.

Chromatographic separation (139) was achieved using an ACQUITY UPLC BEH C-18 column (2.1 X 150mm, 1.7 µm particle size) (Waters Corporation, Milford, MA, USA) held at 50°C coupled to a Vanquish binary pump (Thermo Fisher Scientific, San Jose, CA). A gradient mobile phase was maintained for 55 minutes with a flow rate of 250µL/min and was comprised of 10mM ammonium formate in 40:60 (v/v) water: acetonitrile with 0.1% formic acid and 10mM ammonium formate in 90:10 v/v) isopropanol: acetonitrile with 0.1% formic acid. The gradient elution profile was as follows: 32% B (0-1.5min), 32-45% B(1.5-4 min), 45-52% B(4-6min), 52-58% B(6-10min), 58-66% B (10-16 min), 66-70% B (16-22min), 70-75% B(22-30min), 75-97% B(30-38min), 97%B (38-48min), 97-32% B(48-50min), 32% B(50-55 min. Ten µL of sample was injected via the Vanquish autosampler maintained at 4°C and ionized by a HESI heated ESI source, and analyzed using Q-Executive HF instrument (Thermo Scientific, San Jose, CA, USA). Data were acquired at both full (MS1) and data dependent MS2 (ddMS2) scan modes using positive and negative polarities. The full scan mode had a mass resolution of 60000, mass range of m/z 400-1200 in positive polarity and m/z 240-1600 in negative polarity and a maximum trap fill time of 100 ms. ddMS2 data were acquired at 15,000 resolution with a

maximum trap fill time of 160ms. The isolation window of selected MS1 ions was ± 1.4 m/z with a normalized collision energy (NCE) of 20 and 25. LC-MS/MS data were acquired using Xcalibur version 4.0.

Data processing for LC-MS/MS

Raw data files (Thermo .raw files), consisting of blanks and samples, were converted to mgf files using the MSConvert function of ProteoWizard. Filters for peak picking were set for vendor specific algorithm to MS level 1. Mgf, mzXML input files were searched using the spectrum searcher feature of LipiDex[35] software v1.0.2 for lipid identifications using LipiDex_HCD_Acetate and LipiDex_Splash_ISTD_Acetate libraries. Precursor mass-to-charge (m/z), fragmentation spectra, chromatographic retention time and identification were integrated using LipiDex. The fragmentation patterns of individual lipid standards were manually interpreted and then matched against LipiDex (140) library results.

Results

Gastric inflammation and disease outcomes in response to *H. pylori*

Mongolian gerbils were experimentally infected with *H. pylori*, and a group of animals from the same cohort were maintained as uninfected controls. Gerbils were euthanized at 3 months post-infection. A longitudinal strip of gastric tissue from each animal was processed for conventional hematoxylin and eosin (H&E) staining and an additional strip of tissue was frozen for subsequent imaging mass spectrometry analysis (**Fig 4.1**). Gastric inflammation and epithelial alterations were evaluated by analyzing the H&E-stained tissue, using the histologic scoring system described in Methods.

When choosing gastric tissues for imaging mass spectrometry analysis, we selected stomachs from 4 *H. pylori*-infected animals that exhibited severe gastric disease (severe gastric inflammation along with dysplasia or gastric cancer), one infected animal with milder gastric

disease (mild gastric inflammation without detectable dysplasia or gastric cancer), and 5 control animals (uninfected). Gastric inflammation was graded for severity using the scoring system described in Methods. All 5 of the stomachs from infected animals exhibited gastric inflammation and increased numbers of gastric lymphoid follicles compared to uninfected animals (**Fig 4.2, 4.3**). Dysplasia was detected in two stomachs from infected animals (**Fig 4.2 C, D**), corresponding to I1 and I8 colored in blue in **Fig 4.3**, and invasive adenocarcinoma was detected in stomachs from two additional infected animals (**Fig 4.2 E, F**), corresponding toI2 and I5 colored in red in **Fig 4.3**. These latter four stomachs were larger in size than the stomachs from uninfected animals, consistent with hyperplasia (**Fig 4.5 A**). Four of the five stomachs from *H. pylori*-infected animals exhibited inflammation in both the antrum and the corpus, whereas one exhibited inflammation only in the antrum (**Fig 4.3 A-D**). The overall severity of gastric inflammation (combined analysis of antrum and corpus) and number of lymphoid follicles in infected animals was significantly greater than the severity of inflammation in uninfected animals (**Fig 4.3 E, F**). Atrophic gastritis (characterized by inflammation in the gastric corpus, loss of parietal cells and loss of chief cells) was detected in 4 of the 5 infected animals (examples shown in **Fig 4.4**; **Table 4.1**).

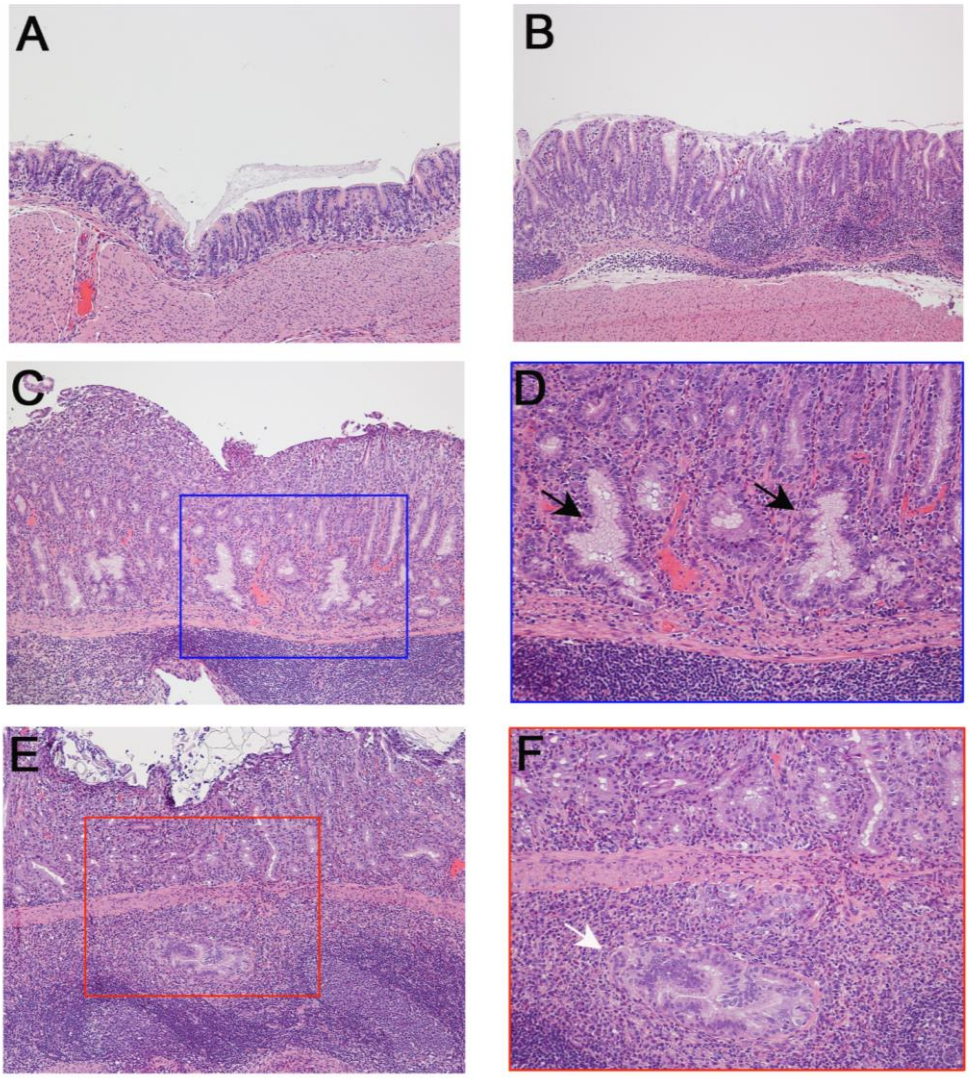

Figure 4.2: Gastric histology from representative animals. (A) Normal histology from control uninfected animal. Gastric tissue from *H. pylori*-infected animals demonstrating (B) gastric inflammation, (C, D) low-grade dysplasia, or (E, F) invasive adenocarcinoma. Panel D is an enlargement of panel C, showing dysplastic glands by black arrows and the panel F is an enlargement of panel E, showing invasive adenocarcinoma by white arrow. Magnification,100X (A, B, C, E), 200X (D, F).

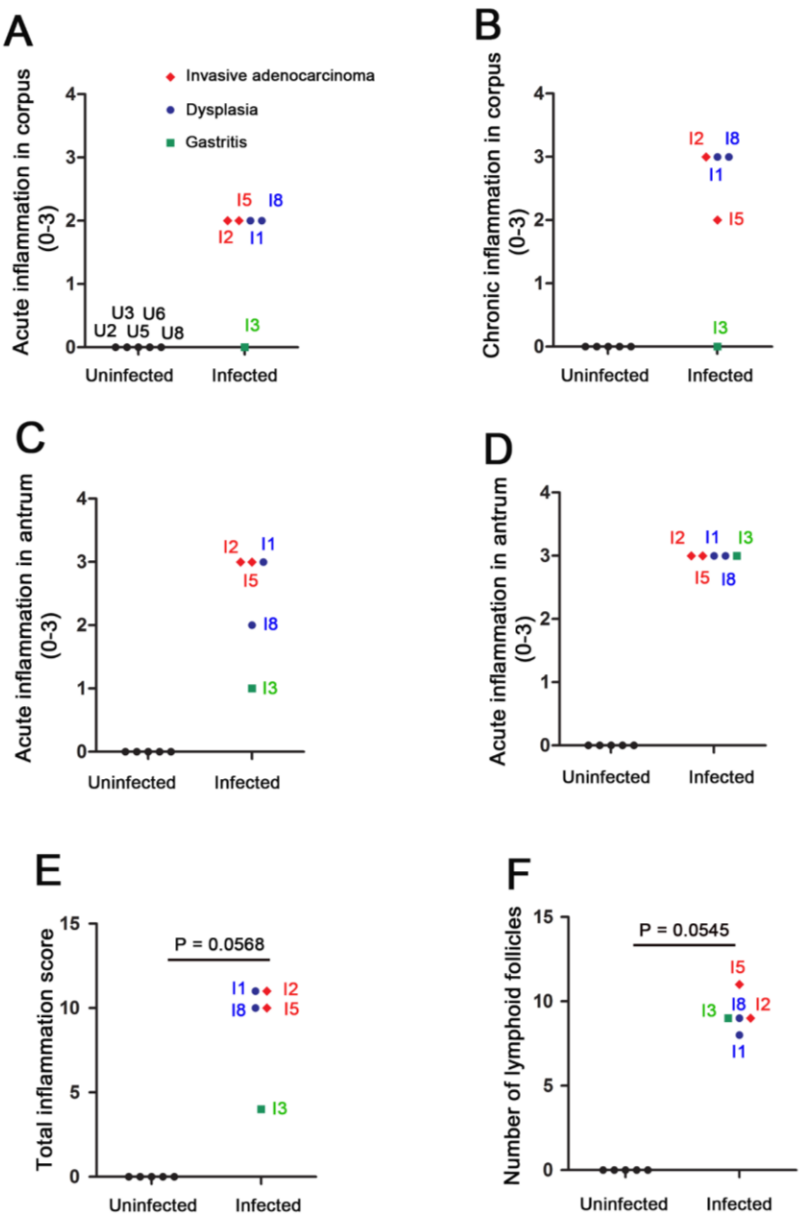

Figure 4.3: Gastric inflammation in response to *Helicobacter pylori* infection. (A, B) Acute and chronic inflammation in corpus. (C, D) Acute and chronic inflammation in antrum. (E) Total inflammation. (F) Number of lymphoid follicles present in gastric mucosa. The label “U” and subsequent numbers (2, 3, 5, 6, 8) represent designations of individual uninfected animals. The label “I” and subsequent numbers (1, 2, 3, 5, 8) represent designations of individual infected animals. Gastric inflammation was scored as described in Methods. Pathologic findings in individual animals are indicated by the color code.

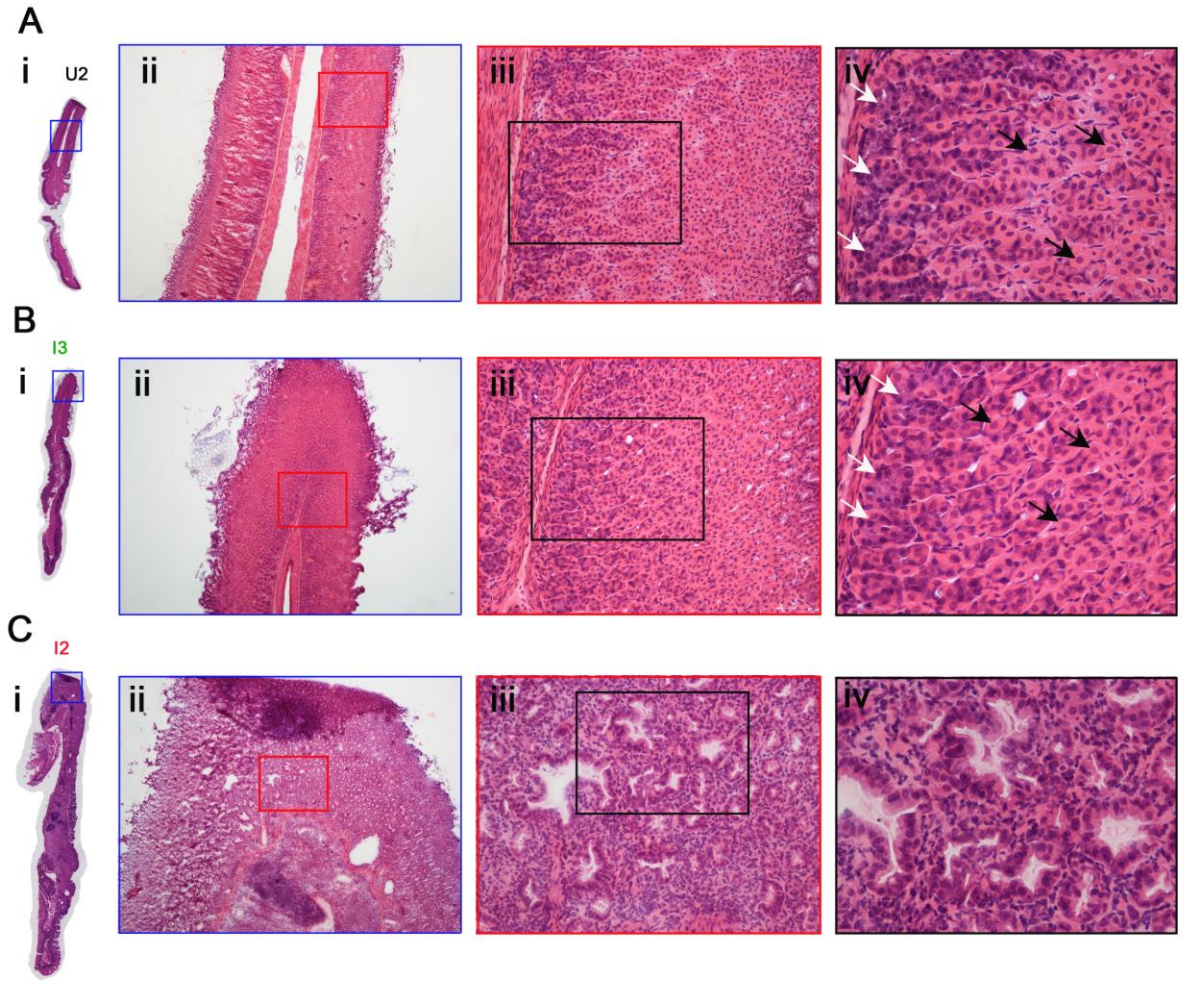

Figure 4.4: Loss of parietal cells and chief cells in response to *H. pylori* infection. (A) Normal gastric histology in a representative uninfected animal (U2), with intact parietal cells and chief cells in the corpus region. (B) Gastric corpus histology in an infected animal (I3), showing intact parietal cells and chief cells. (C) Atrophic gastritis in the corpus of infected animal I2, showing loss of parietal chief cells, replaced by dysplastic glands. White arrows indicate chief cells and black arrows parietal cells. Magnification, 40X (ii); 200X (iii); 400x (iv).

Table 4.1: Quantification of parietal cell loss and chief cell loss

Gerbil	% parietal loss	% chief loss	oxyntic gland atrophy[a]
U2	0	0	0
U3	0	0	0
U5	0	0	0
U6	0	0	0
U8	0	0	0
I1	100	100	3
I2	95	100	3
I3	0	0	0
I5	60	75	2
I8	100	100	3

[a] Oxyntic gland atrophy is a 0-3 score based on the combination of parietal and chief cell loss as follows:
0: no atrophy
0.5: <25% parietal and <25% chief cell loss
1.0: >25% parietal cell loss but <50% chief cell loss
1.5: 50% parietal cell loss & 50% chief cell loss
2.0: 75% parietal cell loss & 75% chief cell loss
2.5: 75% parietal cell loss & 90% chief cell loss
3.0: > 75% parietal cell loss & 100% chief cell loss

Visualization of gastric lipids by Imaging Mass Spectrometry (IMS)

To assess the relative abundance and spatial distribution of lipids in the gastric mucosa, the gastric tissues were subjected to IMS analysis. Lipid images were obtained on an FT-ICR MS (15T Bruker) at 75 μm spatial resolution in both positive and negative mode, as described in Methods. Lipid images were analyzed as described in Methods to identify ions that differed in abundance when comparing gastric tissues from infected animals with tissues from uninfected animals. We detected 72 ions in positive ion mode and 15 ions in negative ion mode that differed in abundance.This list was subsequently curated by eliminating likely isotopic signals as well as low-intensity signals. The m/z values were searched against the LipidMaps database to provide tentative identifications.

Identification of lipids by Liquid Chromatography-Mass Spectrometry (LC-MS/MS)

To provide a more definitive identification of differentially abundant lipids, several additional sections from one *H. pylori*-infected (I5) and one uninfected control stomach (U5) were homogenized and subjected to lipid extraction and analysis by HPLC-MS/MS, as described in Methods. A total of 8 lipids identified by the HPLC-MS/MS analysis (**Table 4.2**) were correlated, by accurate m/z, with the species detected during the IMS analyses. Differentially abundant ions identified by this approach include sphingomyelin species, phosphatidylcholine species, and lyso-phosphatidylethanolamine (**Table 4.2**).

Table 4.2: Lipids observed in positive or negative ion mode imaging mass spectrometry (IMS) and correlated with liquid chromatography tandem mass spectrometry (LC-MS/MS)

	IMS			LC-MS/MS		
Lipid class	**ID**	**FT m/z[a]**	**error**	**ID**	**LC-MS m/z[b]**	**error**
Sphingomyelin (SM)	SM d34:2	701.5605	2.0	SM (18:1/16:1) [M+H]+	701.5592	0.8
	SM d36:2	729.5924	2.6	SM (18:2/18:0) [M+H]+	729.5905	0.8
	SM d38:2	757.6238	2.6	SM (18:0/20:2) [M+H]+	757.6145	0.8
Phosphatidylcholine (PC)	PC (P-32:0)	718.5755	1.4	PC (P-32:0) [M+H]+	718.5745	0.8
	PC (O-32:0)	720.5917	2.1	PC (O-32:0) [M+H]+	720.5902	0.7
	PC (P-38:6)	790.5747	0.3	PC (P-38:6) [M+H]+	790.5745	0.8
	PC (O-38:6)	792.5916	1.8	PC (O-38:6) [M+H]+	792.5538	0.6
Lyso-phosphatidyl-ethanolamine (LPE)	LPE 18:1	478.2963	4.8	LysoPE 18:1 [M-H]-	478.2939	1.0

[a] Fourier-transform mass-to-charge ratio
[b] Liquid chromatography mass spectrometry mass-to-charge ratio

Spatial distribution of differentially abundant lipids identified by LC-MS/MS and IMS

We then analyzed the spatial distribution of the 8 differentially abundant lipids (**Table 4.2**) and compared the ion images with the respective histologic images (**Fig 4.5-4.7**). Multiple sphingomyelin species were decreased in abundance in stomachs from infected animals compared to uninfected animals (**Fig 4.5**). Specifically, SM d34:2, d36:2 and d38:2 (m/z 701.560, 729.592 and 757.624, respectively) were differentially abundant. SM d34:2 was detected mainly in superficial regions of the corpus mucosa (including the proliferative zone of the glands) (**Fig 4.5 C i, ii and iii**).

Multiple phosphatidylcholine species were upregulated in gastric tissues from the infected animals, compared to the tissues from the uninfected animals (**Fig 4.6**). Specifically, PC P-32:0, O-32:0, P-38:6 and O-38:6, corresponding to m/z 718.576, 720.592, 790.575 and 792.592, respectively, were differentially abundant. Several of these lipids were detected at very high levels in the stomach of an infected animal (I2) in regions exhibiting ulcerated mucosa, dysplasia and carcinoma (**Fig 4.6 C**).

Lyso-phosphatidylethanolamine (LPE 18:1) was detected predominantly in the gastric corpus (but not the gastric antrum) of uninfected animals (**Fig 4.7**). In comparison to the stomachs from uninfected animals, this lipid was reduced in abundance in the stomachs of 4 *H. pylori*-infected animals with atrophic gastritis but not altered in abundance in the stomach of an infected animal with inflammation restricted to the antrum and no evidence of atrophic gastritis (I3) (**Fig 4.7**). Moreover, this lipid was less abundant in gastric tissues from each of the infected animals exhibiting dysplasia or gastric cancer (I2, I5, I8 and I1), compared to the tissues from the uninfected animals (**Fig 4.7**).

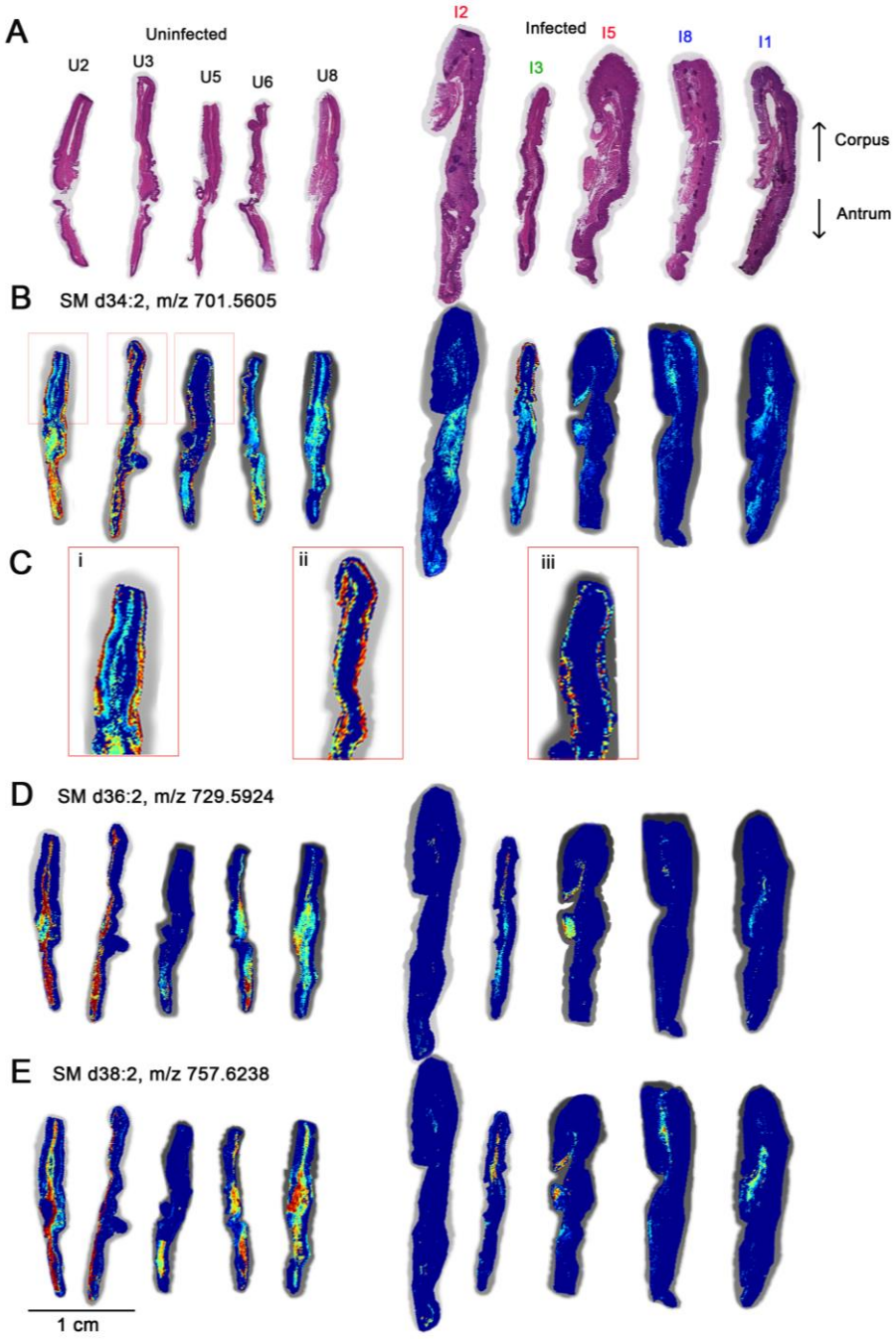

Figure 4.5: Imaging mass spectrometry analysis showing reduced abundance of multiple sphingomyelin species in gastric tissue from infected animals. (A) H&E staining of the gastric mucosae from uninfected and infected animals. (B-E) The respective ion images show localization of ions m/z 701.560, 729.592 and 757.624. Panel C shows higher magnification images depicting localization of SM d34:2 mainly in superficial portions of the mucosa.

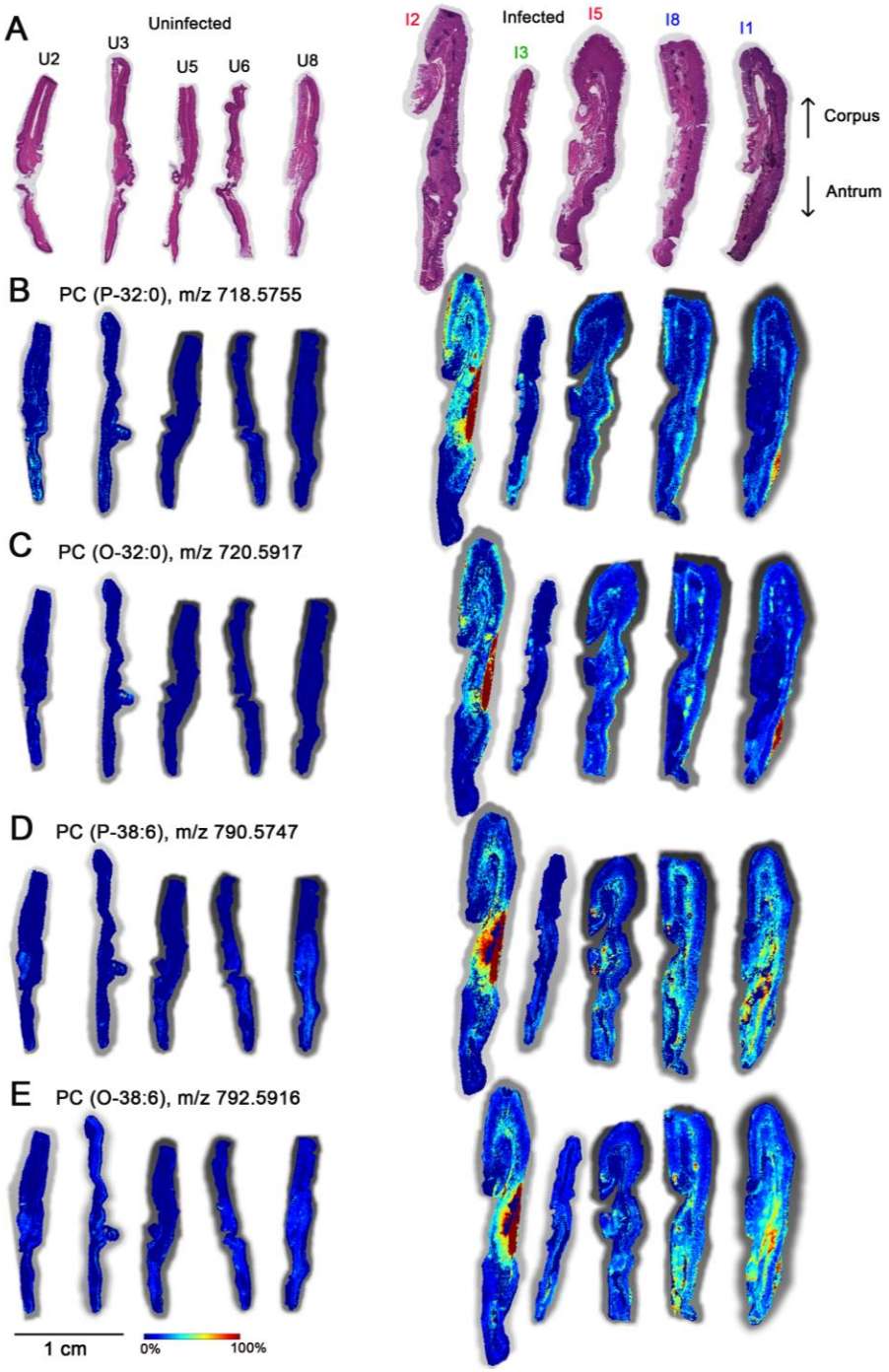

Figure 4.6: Imaging mass spectrometry analysis showing increased abundance of multiple phosphatidylcholine species in gastric tissues from infected animals. (A) H&E staining of the gastric mucosae from uninfected and infected animals. (B, C, D, E) The respective ion images show localization of phosphatidylcholine ions at m/z 718.576, 720.592, 790.575 and 792.592.

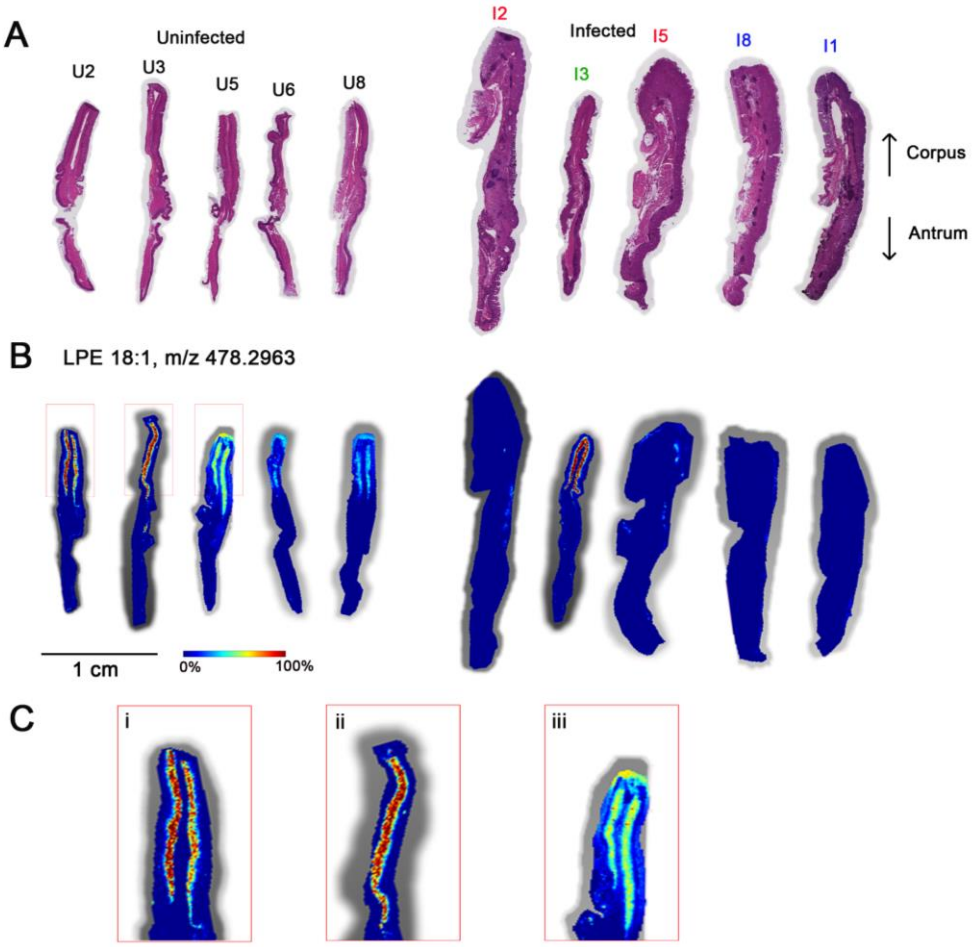

Figure 4.7: Imaging mass spectrometry analysis showing corpus localization of lyso-phosphatidylethanolamine 18:1 that is reduced in abundance in gastric tissues from infected animals. (A) H&E staining of the gastric mucosae from uninfected and infected animals. (B) The ion image shows localization of lyso-phosphatidylethanolamine 18:1 at m/z 478.29. This lipid is detected predominantly in the gastric corpus of uninfected animals. There is reduced abundance of this ion in the gastric corpus of 4 animals with atrophic gastritis. (C) Higher magnification images showing the presence of this lipid in the gastric corpus.

Spatial distribution of additional lipids by IMS

In addition to the lipids identified by both IMS and HPLC-MS/MS, we detected 5 lipids in the imaging experiments that differed in abundance when comparing gastric tissues from uninfected and infected animals, but that did not have corresponding signals detected in the HPLC-MS/MS experiment. These signals were tentatively identified by accurate mass alone.

The spatial distribution of an ion at m/z 813.5905, tentatively identified as triglyceride (TG) 48:8, was similar to that of lyso-phosphatidylethanolamine. It was less abundant in gastric tissues from the infected animals exhibiting dysplasia or gastric cancer, compared to the tissues from the uninfected animals (**Fig 4.8**). This lipid was detected predominantly in the gastric corpus of uninfected animals. In comparison to the stomachs from uninfected animals, this lipid was reduced in abundance in the stomachs of 4 *H. pylori*-infected animals with atrophic gastritis but not altered in abundance in the stomach of an infected animal with inflammation restricted to the antrum and no evidence of atrophic gastritis (I3) (**Fig 4.8**).

An ion at m/z 754.539, tentatively identified as phosphatidylcholine (PC) 34:4, was increased in abundance in gastric tissues from infected animals (**Fig 4.9 B**). This increased abundance was observed uniformly in tissues from both the antrum and corpus regions and seemed to match with regions that have abundant inflammation (**Fig 4.9 B**). Similarly, an ion tentatively identified as phosphatidylserine (PS) 38:5 at m/z 848.482 was increased in abundance in gastric tissues of infected animals (both antrum and corpus) (**Fig 4.9 C**).

Tentatively identified phosphatidylethanolamines (PE) 38:4 and PE 40:7 at m/z 806.5122 and m/z 828.4931, respectively, were increased in abundance in gastric tissues from infected animals (**Fig 4.10**). The increases were relatively uniform throughout the infected tissues. Interestingly, PE 38:4 was mainly increased in abundance in deeper gastric tissues in I5, I8 and I1 (**Fig 4.10 B**).

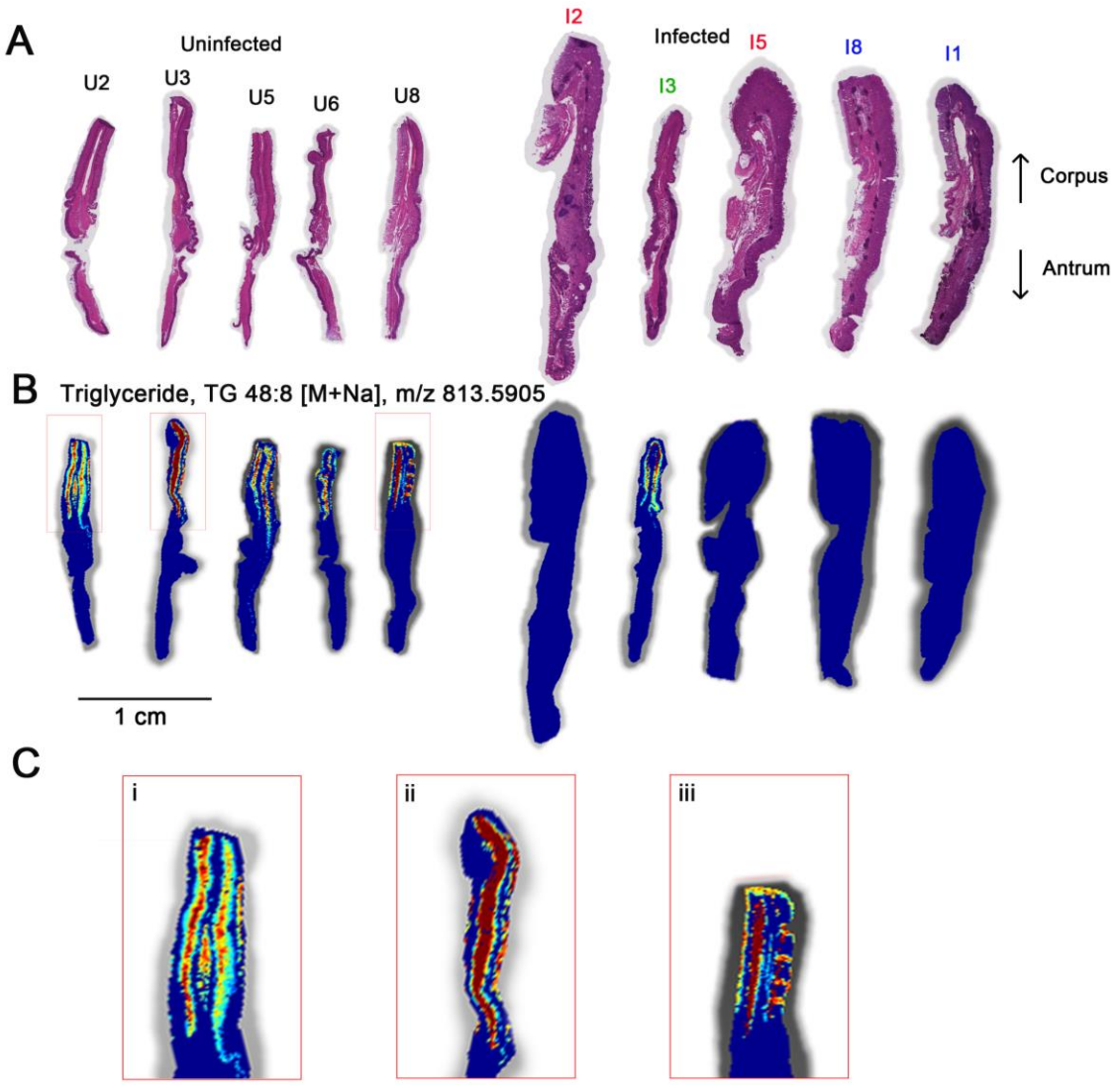

Figure 4.8: Imaging mass spectrometry analysis showing triglyceride 48:8 is reduced in abundance in gastric tissues from infected animals. (A) H&E staining of the gastric mucosae from uninfected and infected animals. (B) The ion image showing spatial contribution of triglyceride 48:8 at m/z 813.5905. This lipid is detected predominantly in the gastric corpus of uninfected animals and one infected animal exhibiting gastritis. (C) Higher magnification images, showing the presence of this lipid in the gastric corpus.

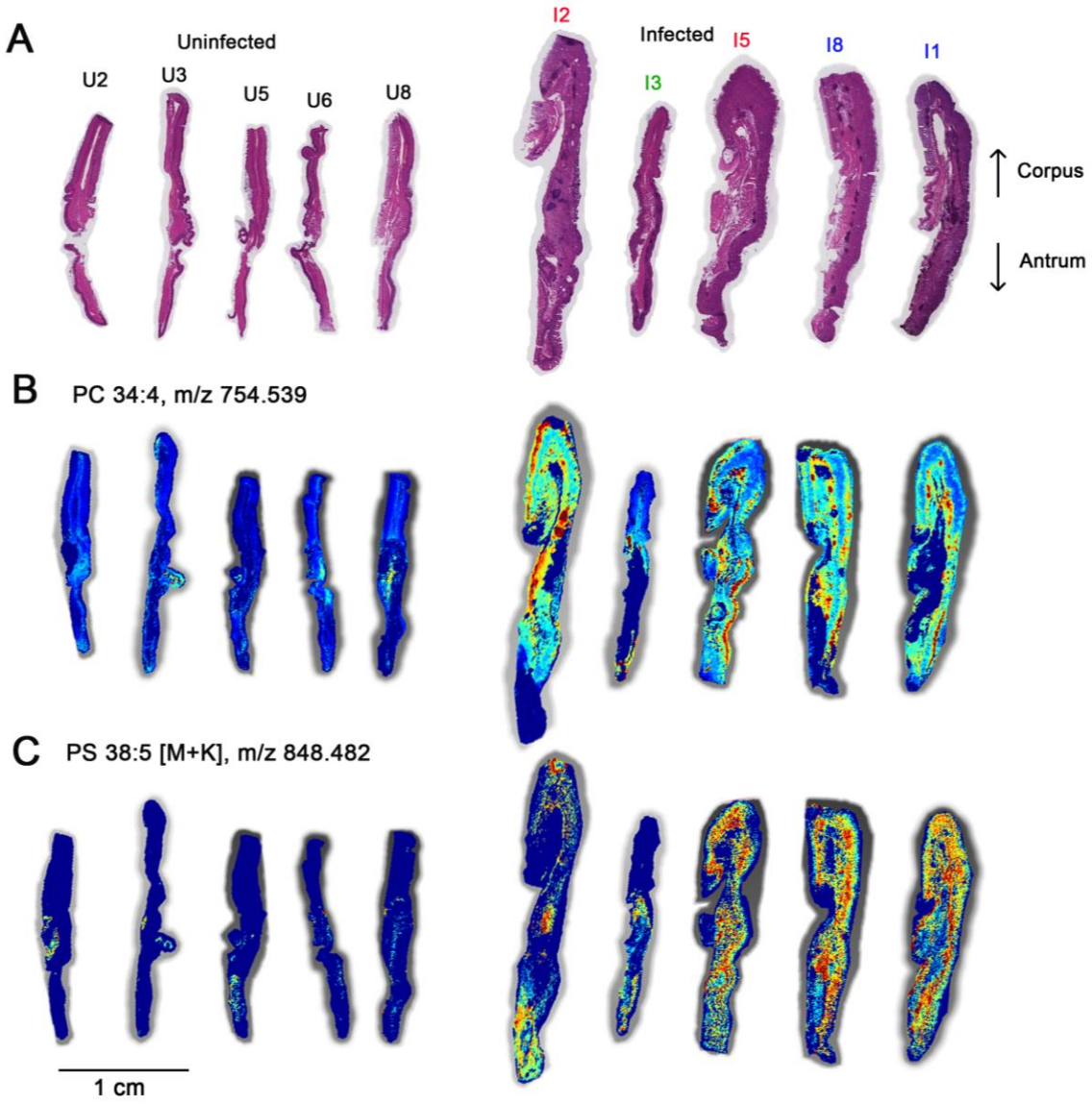

Figure 4.9: Imaging mass spectrometry analysis showing phosphatidylcholine and phosphatidylserine species are increased in abundance in gastric tissues from infected animals. (A) H&E staining of the gastric mucosae from uninfected and infected animals. (B, C) The respective ion images showing spatial contribution of PC 34:4 and PS 38:5 at m/z 754.539 and m/z 848.482, respectively.

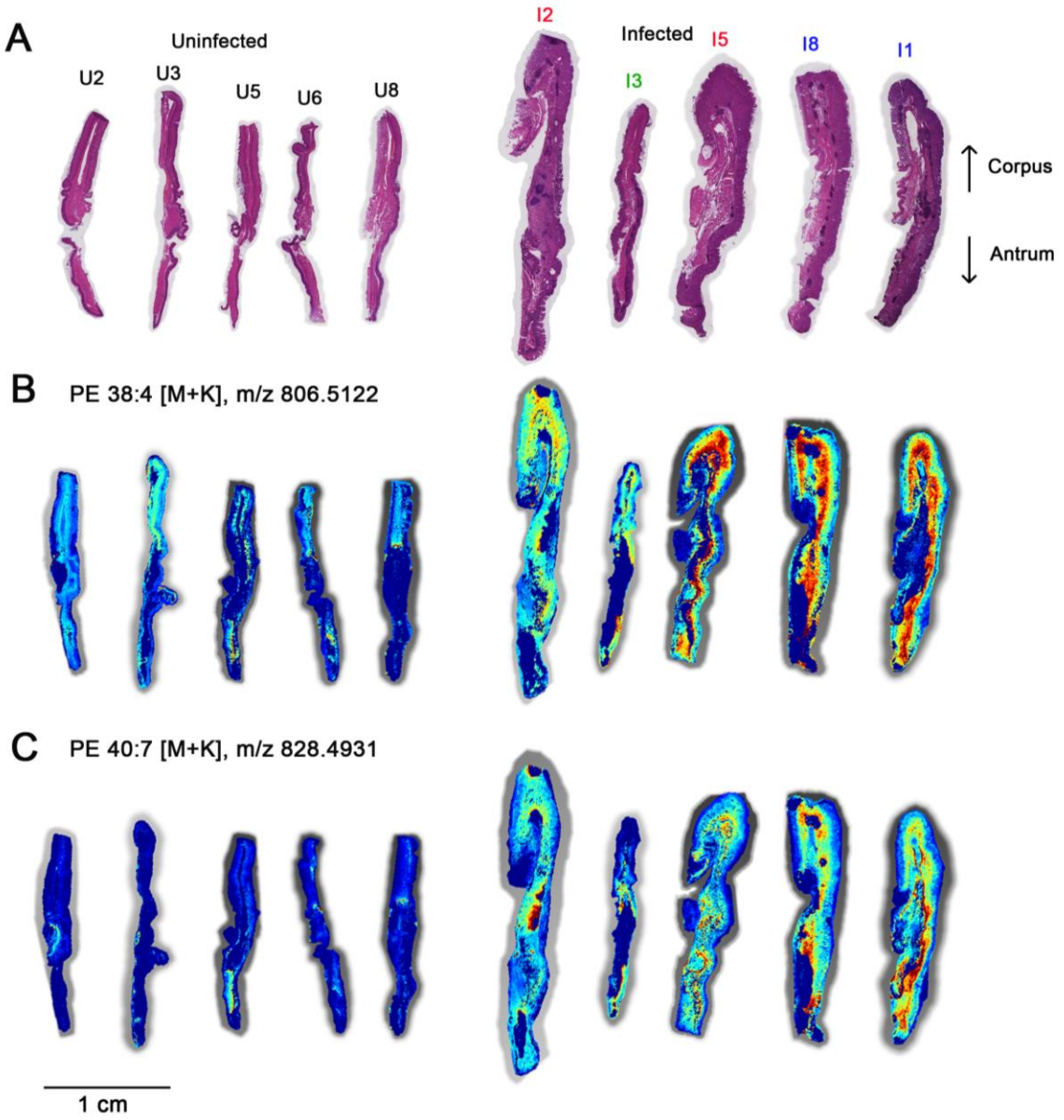

Figure 4.10: Imaging mass spectrometry analysis showing phosphatidylethanolamine species are increased in abundance in gastric tissues from infected animals. (A) H&E staining of the gastric mucosae from uninfected and infected animals. (B, C) The respective ion images showing spatial contribution of PE 38:4 at m/z 806.5122 and PE 40:7 at m/z 828.4931.

Discussion

In this study, we utilized imaging mass spectrometry as an unbiased approach to evaluate gastric molecular alterations that occur in response to *H. pylori* infection. Imaging mass spectrometry methodology can reliably detect a wide range of tissue lipids (141). Therefore, in the current study we focused specifically on analysis of gastric lipid alterations in response to *H. pylori* infection We observed that specific gastric lipids were increased in abundance in *H. pylori*-infected animals compared to uninfected animals, and others were decreased in abundance in response to *H. pylori* infection. The use of HPLC-MS/MS allowed us to determine the precise molecular identity of many of the altered lipids.

Imaging mass spectrometry allowed us to define the spatial distributions of individual lipids of interest within the stomach. For example, some of the differentially abundant lipids were localized specifically to the corpus or the antrum, whereas others were localized in both regions of the stomach. Some of the differentially abundant lipids were localized primarily at the luminal surface of the stomachs, whereas others were localized in deeper gastric tissues. Increased abundance of lipids in *H. pylori*-infected stomachs could potentially reflect lipid components of the *H. pylori* cell envelope, upregulated lipid production by gastric tissue, or lipids associated with infiltrating inflammatory cells. We believe the two latter explanations are more likely for several reasons. First, the distribution of many of the lipids in gastric tissue deeper than the epithelial layer seems more consistent with host-associated lipids than lipids associated with the bacteria, since *H. pylori* typically localizes in the gastric mucus layer without invading host tissue. Second, the relative abundance of *H. pylori* in gastric tissue is much lower than the abundance of host cells, and we speculate that the methodology used in this study might not have sufficient sensitivity to detect *H. pylori* lipids.

Lipids with decreased abundance in *H. pylori*-infected stomachs could potentially reflect loss of specific cell types in the setting of *H. pylori* infection or alterations in the membrane composition

of various cells in gastric tissue. Multiple sphingomyelin (SM), triglyceride (TG) and lyso-phosphatidylethanolamine (LPE) species were decreased in abundance in infected animals with severe disease compared to uninfected animals, whereas multiple phosphatidylcholine species (PC), phosphatidylethanolamine (PE) and phosphatidylserine (PS) were increased in abundance in response to *H. pylori* infection. Since closely related lipids exhibited similar patterns of change (increased or decreased) in infected stomachs compared to uninfected stomachs, this suggests that *H. pylori* infection stimulates extensive alterations in gastric lipid biology.

Several of the differentially abundant lipids (lyso-phosphatidylethanolamine and triglyceride) were detected specifically in the gastric corpus from uninfected animals but were reduced in abundance in tissue from infected animals exhibiting atrophic gastritis. The current analysis does not have sufficiently high spatial resolution to permit assignment of the lipids to specific host cell types, but we speculate that these lipids might be constituents of specialized cell types such as parietal cells or chief cells, which are present in the gastric corpus but not the gastric antrum. Parietal cells are characterized by a complex network of intracellular membranes, which might be a site for localization of distinctive lipids.

Lipids have vital roles in cellular systems. Phospholipids (PE and PC) act as gastric surfactants, protecting the gastric mucosae against luminal pathogens by forming a hydrophobic layer on the gastric luminal surface (142). Furthermore, they have a pivotal role in various cellular processes, including cell signaling, so alterations in cellular lipid composition could potentially lead to disruptions in cellular processes that are relevant for carcinogenesis (143, 144). Previous studies have shown that *H. pylori* can bind to PE on gastric cells (145). Therefore, alterations in gastric lipids might also influence adherence or other interactions of *H. pylori* with host cells.

In future studies, it will be important to analyze in more detail how the results of the current study (using an animal model) compare with gastric lipid alterations in *H. pylori*-infected humans. Previous studies have reported that *H. pylori* infection can dramatically reduce the levels of total phospholipids (PC and PE) in patients with chronic atrophic gastritis (146). In our study, we observed a reduction of PE and increased PC in gastric tissues of infected animals after a 3-month infection.

In summary, the study shows that there is a distinct pattern of differently expressed lipids in abundance in the gastric tissues in response to *H. pylori* infection. This study may serve a foundation to better understand relationships between bacterial infection and the lipid composition of host tissues.

Chapter V

Projects in progress

There are multiple Cag T4SS projects that are currently ongoing and not yet completed. These projects focus on investigating pilus-like structures that form when *H. pylori* is in contact with host cells, defining the structures of individual Cag ATPases, and investigating the composition of the Cag T4SS inner membrane complex.

Filamentous structures

Previous studies reported that filamentous structures termed “pili” form at the interface between gastric epithelial cells and *H. pylori* (53, 58, 75, 77, 147). The filaments have mainly been observed by scanning electron microscopy. Multiple studies reported that the formation of these pili is dependent on genes in the *cag* PAI. Specifically, several genes in the *cag* PAI that are required for Cag T4SS functions (for example, *cagT, cagX, cagV, cagM, cag3*, *cagH*, *cagE*) were reported to be essential for pilus formation (53, 58, 75, 77, 147).

A cryo-ET study also reported visualization of membranous tubes extending from *H. pylori* when in contact with gastric epithelial cells (53). The study reported that these tubes were not produced by *cag* PAI mutant strain (53). It seems likely that the membranous tubes visualized by cryo-ET are identical to the pili visualized by scanning EM. These studies led me to hypothesize that specific Cag ATPases might be essential for pilus/tube formation.

To investigate these filamentous structures, I cultured AGS gastric epithelial cells on electron microscopy grids, and then infected the adherent cells with *H. pylori* strains. The strains I used included control strains (wild-type strain 26695 and a Δ*cag* PAI mutant as positive and negative controls, respectively) and Cag ATPase mutant strains. In collaboration with Evan Krystofiak, EM Research Specialist Senior, Vanderbilt Cell Imaging Shared Resource (CISR) Core, we analyzed the co-cultured samples by scanning EM.

We took SEM images of 20 different randomly selected AGS cells and analyzed production of filamentous structures by bacteria that were attached to these AGS cells (ranging from 3 to 25 bacteria per cell). An evaluation of filamentous structures was performed by an individual who was blinded to the identity of the *H. pylori* strains. We observed the filamentous structures in all the Cag ATPases mutants (**Fig 5.1 C-E**), suggesting that the Cag ATPases are not required for formation of filamentous structures. Interestingly and surprisingly, we also observed the filamentous structures at the interface of epithelial cells and the *cag* PAI mutant (**Fig 5.1 B**). The quantification was based on two biological replicates in a blinded fashion. To ensure that the *cag* PAI mutant used in this experiment retained other expected phenotypes, I confirmed that the *cag* PAI was absent (by PCR), and that the strain was defective in Cag T4SS-dependent phenotypes (NF-κB activation and CagA translocation).

The unexpected phenotype could potentially be due to differences in methods for sample preparation or differences in techniques used to visualize the structures. Thus, I went back to the grids prepared more than 5 years ago. We again observed filamentous structures produced by the *cag* PAI mutant (**Fig 5.2**). I also went back to the published strains [TetR/*tetO* strain (103)] in which Cag T4SS-dependent phenotypes can be regulated by the TetR/*tetO* system via anhydrotetracycline (described in Chapter 3) (**Fig 5.3 A**). It was previously reported that “pili” were visible if the strain was exposed to an inducer (anhydrotetracycline) but not visible in the absence of anhydrotetracycline. However, to my surprise, we observed filamentous structures produced by the strain both in the presence and absence of anhydrotetracycline (**Fig 5.3 B, C**). Collectively, my results indicate that formation of the filamentous structures does not require genes in the *cag* PAI or Cag T4SS activity. The reasons for the discrepancy between the current results and previous results are not clear at present.

If these structures observed are not related to the *cag* PAI, what are they? *H. pylori* strains can harbor up to 4 different type IV secretion systems (32). Specifically, *H. pylori* strain 26695

harbors both the ComB system and the Cag T4SS. Therefore, there is a chance that filamentous structures observed could be associated with the ComB system. To date, there have not been any experiments to analyze structural features of the *H. pylori* ComB system. In future studies, it will be of interest to determine if *comB* mutant strains or double knock-out strains (both ComB system and Cag T4SS) produce filamentous structures. Alternatively, it is possible that the filaments represent an entirely different structure. For example, some bacteria are known to produce “nanotubes” (148) that have characteristics similar to the *H. pylori* filaments.

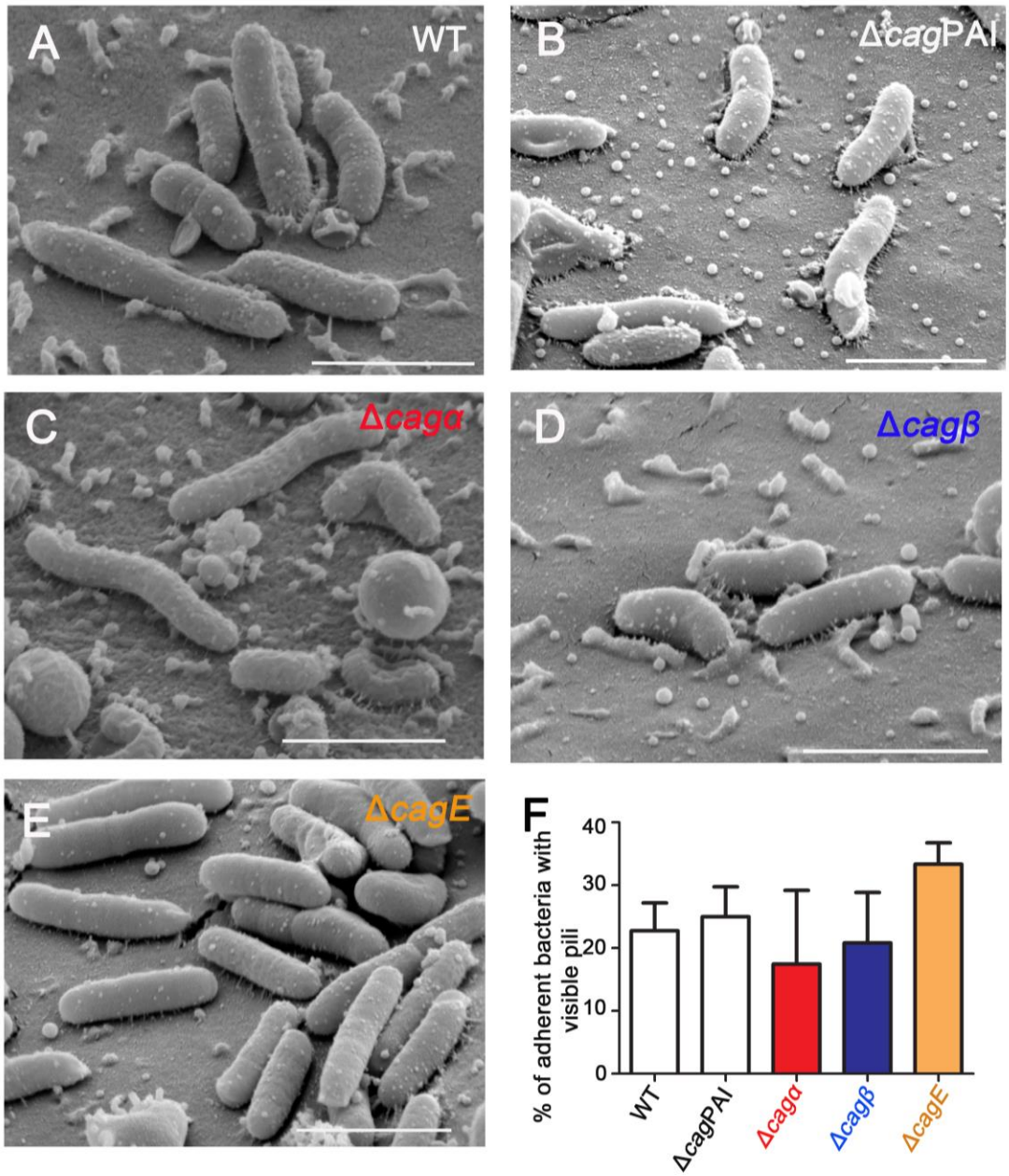

Figure 5.1: Individual Cag ATPases are not required for formation of "filamentous structures". Filamentous structures at the interface between gastric epithelial cells and *H. pylori* WT (A), Δ*cag*PAI (B), or mutant strains lacking individual *cag* ATPases - Cagα (C), Cagβ (D) or CagE (E). (F) Quantification of adherent bacteria with visible pili. The data represent results of two independent experiments with multiple technical replicates. Scar bar represents 2 µm.

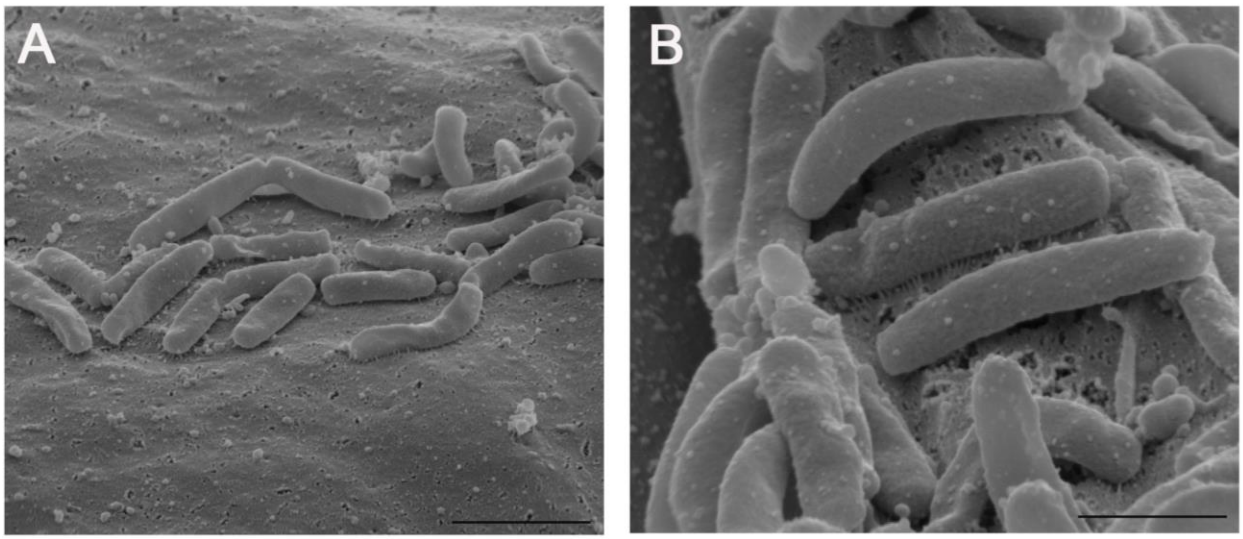

Figure 5.2: “Filamentous structures” are observed in images of a Δ*cag* PAI mutant strain when in contact with gastric epithelial cells. The grids were previously prepared as negative controls. (A, B) At the interface, “filamentous structures” are elaborated. Scar bar represents 2 µm in A, and 1 µm in B.

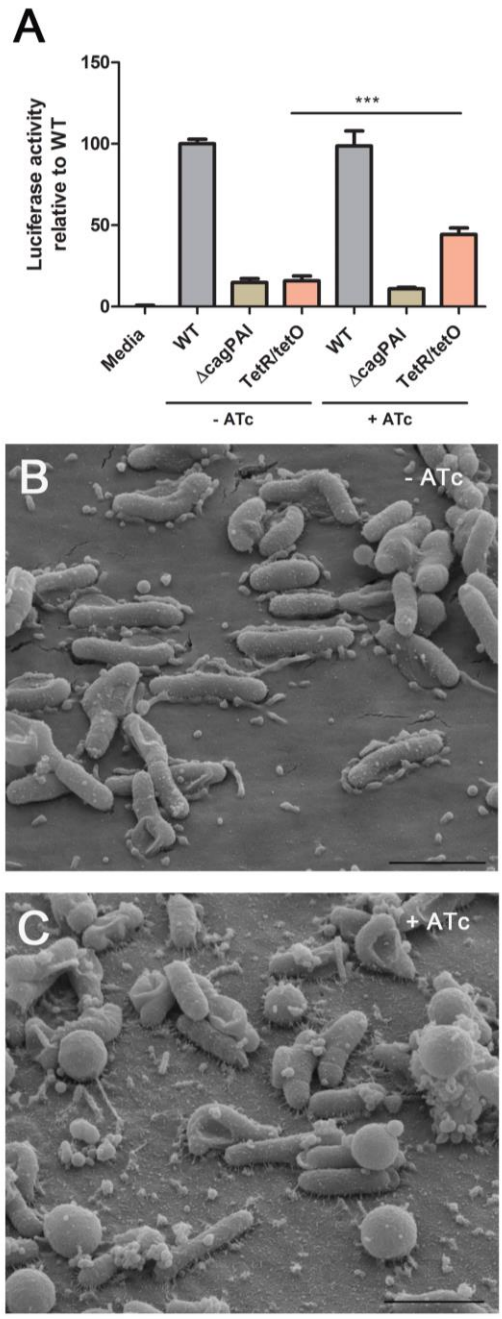

Figure 5.3: “Filamentous structures” are produced by the TetR/*tetO* strain in the presence or absence of anhydrotetracycline (ATc). (A) NF-κB activation induced by the strain in the presence or absence of ATc. (B, C) Observation of “pilus structures” produce in the presence or absence of ATc. Scar bar represents 2 µm.

Structure of Cagα

The Cagα crystal structure has been solved previously (55). Cagα can assemble into hexameric complexes, and each protomer consists of two domains (N- and C-terminal domains) (55, 149). Cagα undergoes nucleotide-dependent conformational changes (149). The crystal structure was solved by expressing the *cagα* gene recombinantly in *E. coli*. The endogenous structure of Cagα isolated from *H. pylori* has not been studied yet and might be slightly different from the structure of Cagα recombinantly expressed in *E. coli*.

Our laboratory has previously had success in isolating and purifying the Cag T4SS core complex from *H. pylori* by using epitope tags and immunoprecipitation (50-52). I utilized a similar approach for purification of Cagα. I successfully generated a strain producing HA-tagged Cagα, with the relevant gene inserted in the urease locus in both a wild-type strain and a Δ*cagα* strain (unmarked deletion mutant) (**Fig 5.4 A**). I confirmed that HA tagging does not disrupt Cag T4SS function, using an NF-κB activation assay (**Fig 5.4 B**). To investigate the interacting partners of Cagα, I employed an immuno-precipitation approach and tested three different detergent conditions – deoxycholate and NP40, NP40 alone or Tx100 (**Fig 5.4 C, D**). Mass spectrometry analyses showed that the target protein Cagα was successfully precipitated, but there were no significant spectral counts corresponding to other Cag proteins. Since Cagα has transmembrane domains (55), I wanted to test if I could potentially pull down any interacting partners if I focused on membrane fractions using the same detergents (**Fig 5.4 E, F**). However, the mass spectrometry analyses did not show any other proteins that were substantially enriched besides Cagα.

Thus far, I have performed immuno-precipitations of HA-Cagα from a strain that retains a wild-type unmodified copy of Cagα (with no HA tag), as well as a Δcagα/HA-Cagα strain (**Fig 5.5 A**). I was not able to pull down any other interacting partners from either strain. This led me to hypothesize that relevant protein-protein interactions might be transient and not readily detected

by the immuno-precipitation experiments. To test if I could “lock” possible transient interactions, I treated intact *H. pylori* with a water-soluble, cell membrane permeable cross-linker called dithiobis(succinimidyl propionate), DSP. I tested different concentrations of DSP (from 0.05 to 1 mM) (**Fig 5.5 B**) and found that 0.1 mM DSP concentration is the optimal concentration to form crosslinked species. Then, I performed immuno-precipitation using 0.1 mM DSP and found that there are cross-linked species that are larger in size than Cagα itself (**Fig 5.5 C**).

To identify the interacting partners of Cagα, the next logical follow-up experiment is to identify the cross-linked species via mass spectrometry analyses. To investigate the structure of Cagα, there are multiple experiments that need to be followed up in a step-wise manner: determining the optimal detergents for Cagα solubilization, purifying Cagα via affinity purification, visualizing the structure via negative-stain EM, performing single particle averaging to look for stable structural classes and ultimately optimizing vitrification conditions for cryo-EM structure determination.

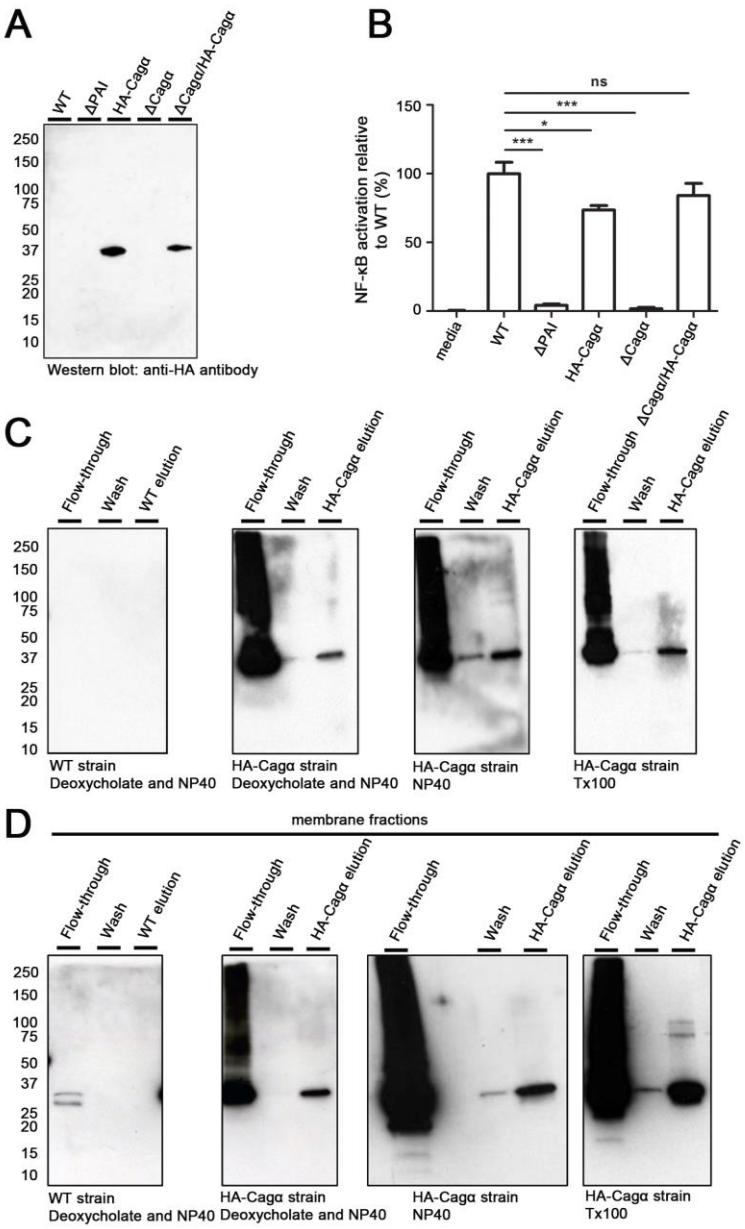

Figure 5.4: Modification of Cagα with an HA tag does not disrupt Cag T4SS function and allows affinity purification of Cagα via immunoprecipitation. (A) Cagα is tagged with HA. HA-Cagα is detected by using anti-HA antibody. (B) NF-κB activation detected by luciferase activity. (C) Immuno-precipitation of wild-type (WT) and HA-Cagα with three combination of detergents – deoxycholate and NP40, NP40 or Tx100. (C) Immuno-precipitation of the membrane fractions with three different detergent conditions.

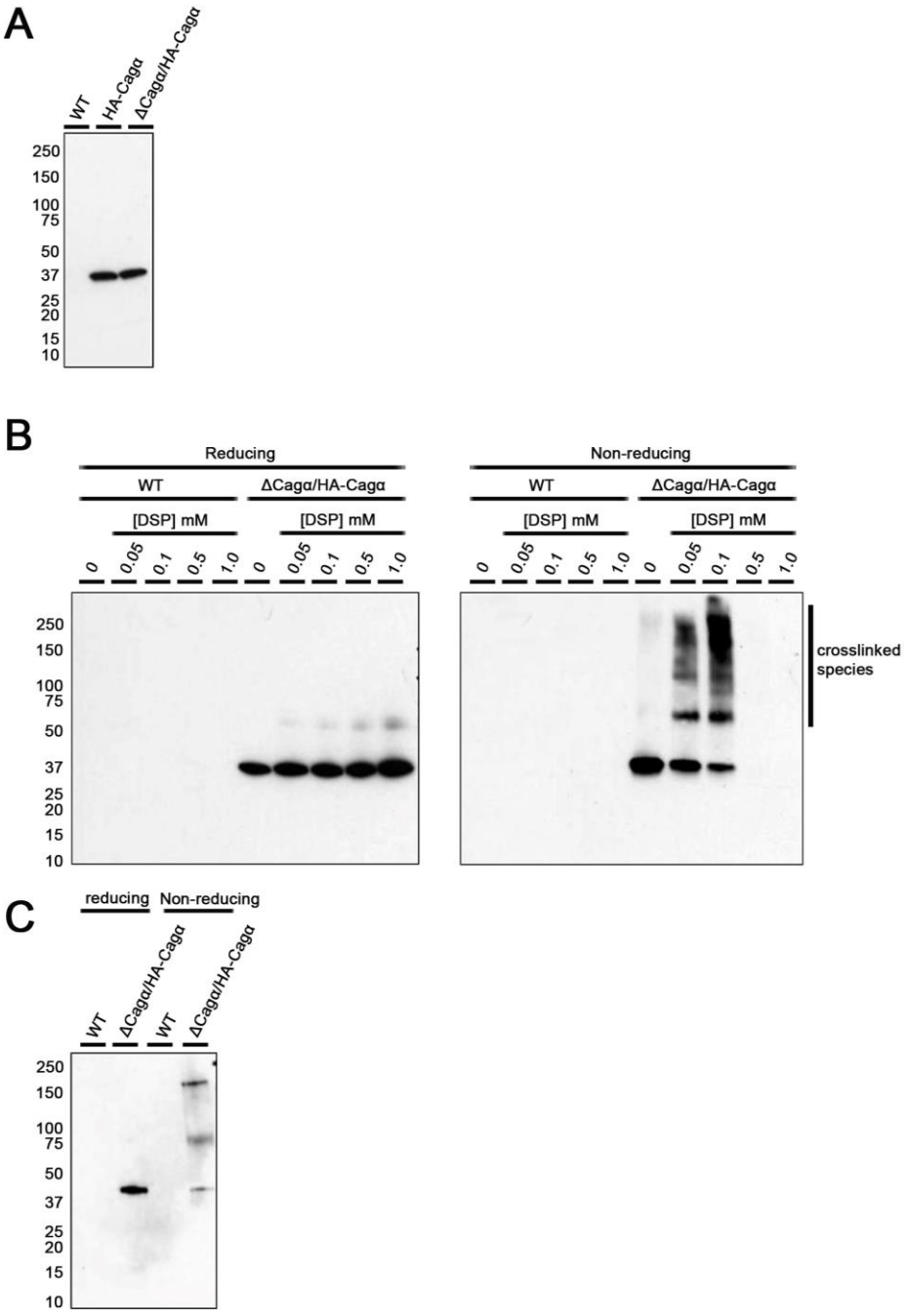

Figure 5.5: Crosslinking and immuno-precipitation of HA-Cagα from a ΔCagα/HA-Cagα strain. (A) Immuno-precipitation of two different types of strains – HA-Cagα (still has one copy of WT) and ΔCagα/HA-Cagα. (B) Different concentrations of DSP crosslinker. (C) Immuno-precipitation of HA-Cagα from cross-linked ΔCagα/HA-Cagα strain.

Structure of Cagβ

Thus far, the structure of Cagβ of *H. pylori* has not been reported. To investigate Cagβ structure, I have recombinantly expressed Cagβ in *E. coli* and also developed methods to affinity purify HA-tagged Cagβ from *H. pylori* (based on generating a strain containing the relevant gene in the urease locus). For production of the recombinant protein, I have tested variable temperatures (13°C, 20°C, 37°C), different inducing conditions (0.01 to 1 mM of IPTG), and different bacterial expression systems [BL21, ArcticExpress DE3, SoluBL21, C41(DE3)] for protein expression in *E. coli*. So far, I have not successfully optimized the conditions to over-express Cagβ in *E. coli*.

On the other hand, I have successfully tagged HA to Cagβ in *H. pylori* and performed immuno-precipitations using three detergent conditions – deoxycholate with NP40, NP40 alone or Tx100 (**Fig 5.6 A**). The mass spectrometry analyses consistently show that Cagβ interacts with CagZ (data not shown), which is consistent with a previous study (67). Based on the hypothesis that Cagβ would fully assemble and interact with more partners when in contact with host cells, I co-cultured the strains with gastric epithelial cells and then performed immuno-precipitation (**Fig 5.6 B**). However, I did not identify any additional interacting partners based on the spectral counts.

Since I want to identify more interacting partners and presume that some harsh detergents might be disrupting protein-protein interactions, I have recently tested different detergents (deoxycholate with NP40, decyl maltopyranoside, octyl glucopyranoside and fos-choline 12) (**Fig 5.7 A**). All the detergents tested were able to solubilize Cagβ protein. I chose deoxycholate with NP40 and fos-choline 12 for Cagβ purification from a larger scale of *H. pylori* culture, and observed a band corresponding to the expected size via colloidal blue staining and western blot approaches (**Fig 5.7 B, C**). This is the first time that the protein was abundant enough to be seen on the gel. Furthermore, the mass spectrometry analyses confirm that Cagβ interacts with

CagZ (data not shown). Since the purification process is optimized, it is crucial to follow up with the experiments to solve the structure of Cagβ, hopefully with CagZ bound by optimizing the conditions to visualize the structure by negative-stain EM, visualizing the structure in 2D classification, and ultimately determining the 3D cryo-EM structure.

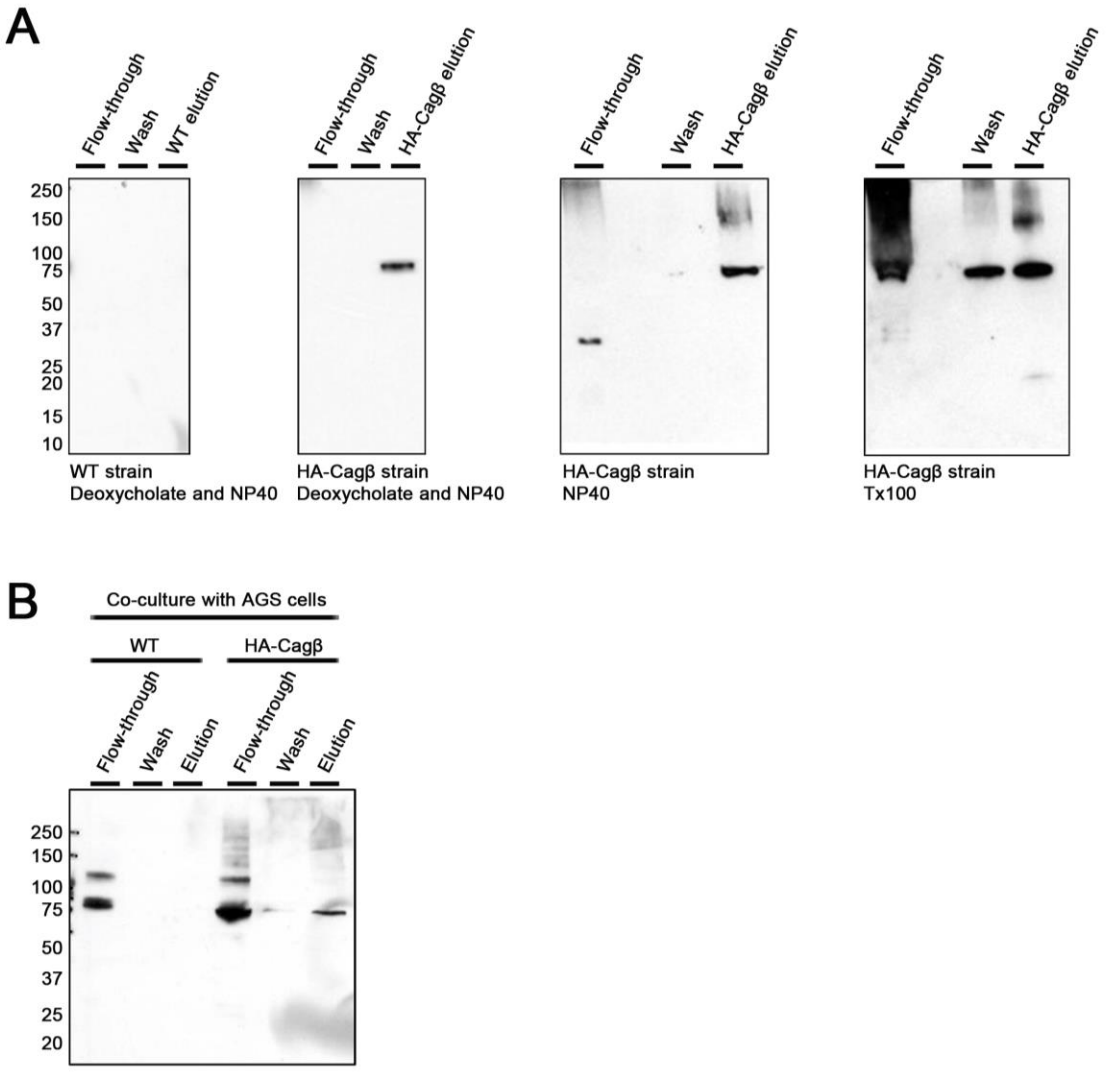

Figure 5.6: Immuno-precipitation of HA-Cagβ. (A) Immuno-precipitation of wild-type and HA-Cagβ strains in three detergent conditions – deoxycholate and NP40, NP40 or Tx100. (B) Immuno-precipitation of wild-type and HA-Cagβ strains in co-culture with gastric epithelial cells.

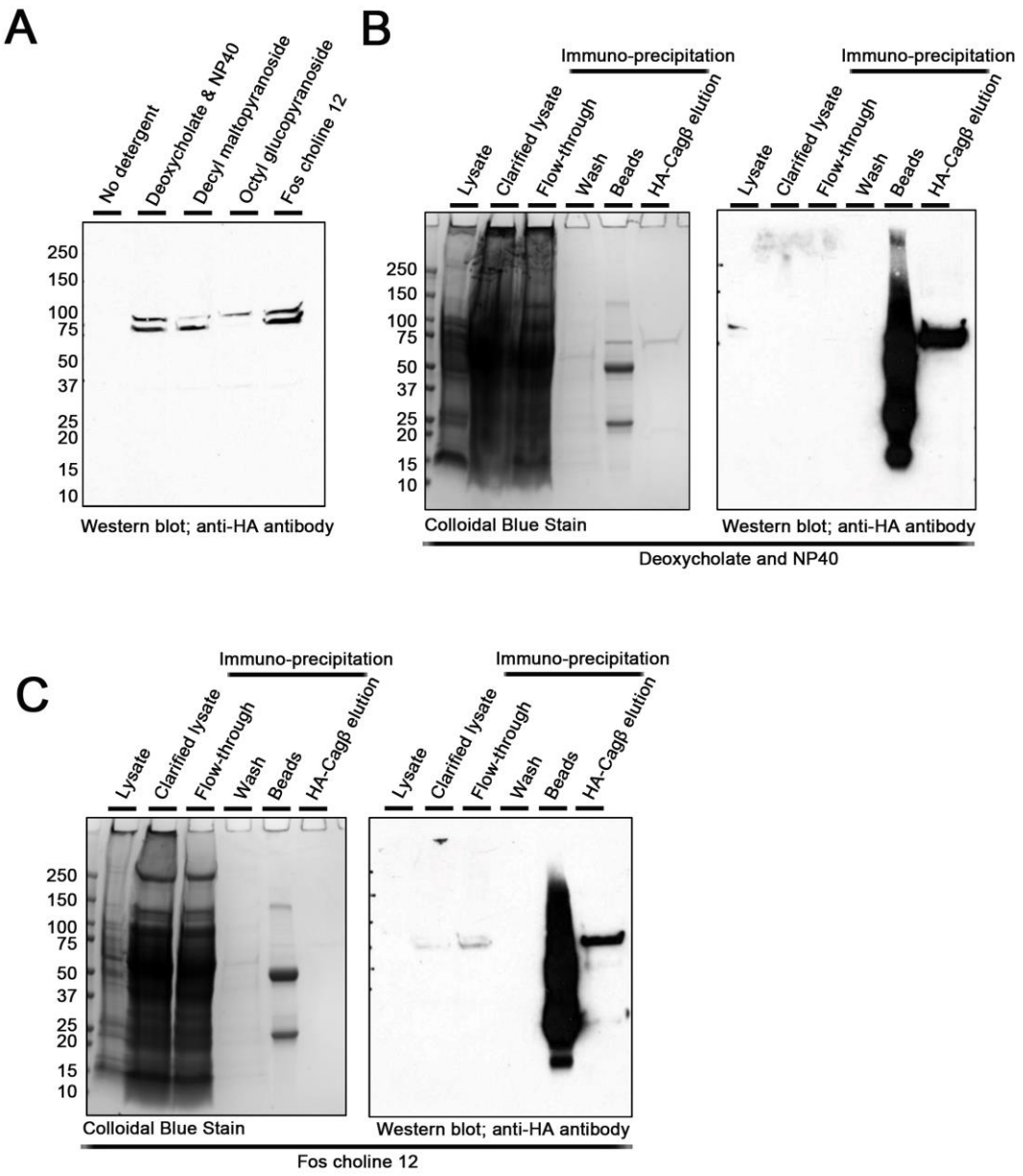

Figure 5.7: Purification of Cagβ from *H. pylori*. (A) Optimization of HA-Cagβ solubilization in different detergent conditions – deoxycholate with NP40, decyl maltopyranoside, octyl glucopyranoside or fos-choline 12. (B, C) Analysis of purified Cagβ using deoxycholate with NP40 and fos-choline 12 via colloidal blue stain and western blot using anti-HA antibody.

Structure of CagE

I have been actively working on investigating the structure of CagE recombinantly expressed in *E. coli*. In collaboration with Dr. Michael Sheedlo (a postdoctoral fellow in the Lacy Lab), we have successfully purified CagE by two steps of purification – GST purification followed by size exclusion column purification (**Fig 5.8 A, B**). At the first step of purification via GST, the CagE protein (111.8 kDa) was observed, along with many other contaminants including the GST protein (26 kDa) (**Fig 5.8 A**). The size exclusion column purification shows a nice separation of the CagE protein from GST and other contaminants (**Fig 5.8 B**). Negative stain EM analysis and 2D classification of the purified CagE protein (performed in collaboration with Dr. Sheedlo) shows that the particles have a diameter of ~250 Å (25 nm), and there are several "spikes" sticking out of what appears to be a globular core at the center of each class (**Fig 5.9**). We are at the stage of optimizing conditions for the vitrification process, which is necessary for determining a structure by cryo-EM. Thus, the follow-up experiments are to keep optimizing the vitrification process, to collect data, and analyze the structure.

Concurrently, I have successfully generated an *H. pylori* strain that produces HA-tagged CagE (containing the relevant gene inserted into the urease locus). I tested several different detergents to solubilize the CagE protein – decyl maltopyranoside, octyl glucopyranoside, fos-choline 12 and deoxycholate with NP40 (**Fig 5.10 A**), and all of them were equally able to solubilize the protein. I proceeded to purify CagE protein from *H. pylori* using deoxycholate with NP40 and fos-choline 12. I was able to purify CagE protein which migrates at the expected size on a gel with colloidal stain (**Fig 5.10 B, C**). The next follow-up experiment would be to visualize the protein via negative-stain EM, to perform 2D class averaging, and to optimize conditions for 3D cryo-EM analysis. While the project of solving recombinant CagE structure in *E. coli* is very promising and has solid preliminary data, it is also important to investigate the structure of CagE isolated from *H. pylori*.

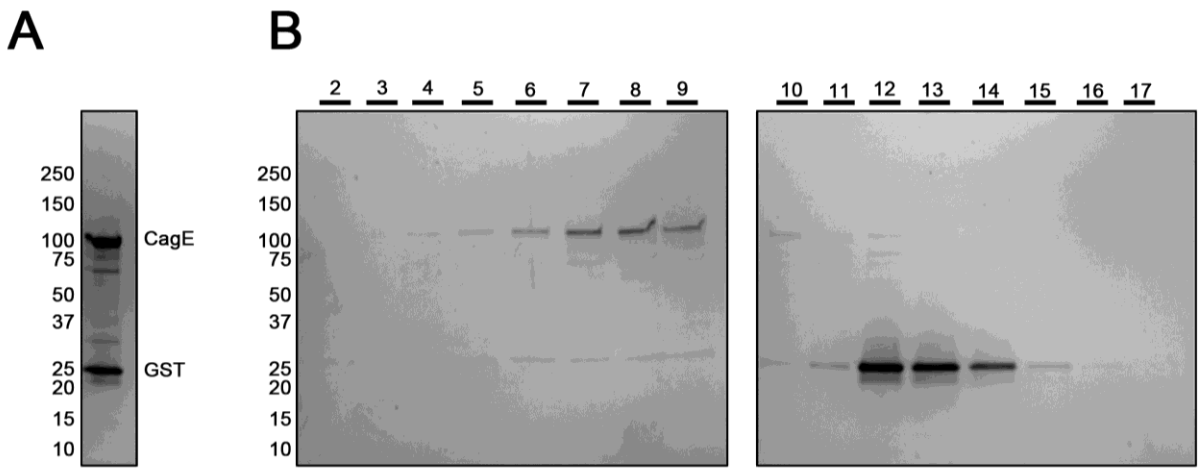

Figure 5.8: CagE purification via two steps using GST column and size exclusion column. (A) After GST column purification, CagE was purified along with many other contaminants including GST protein tag. (B) The size exclusion column purification separates CagE from other contaminants.

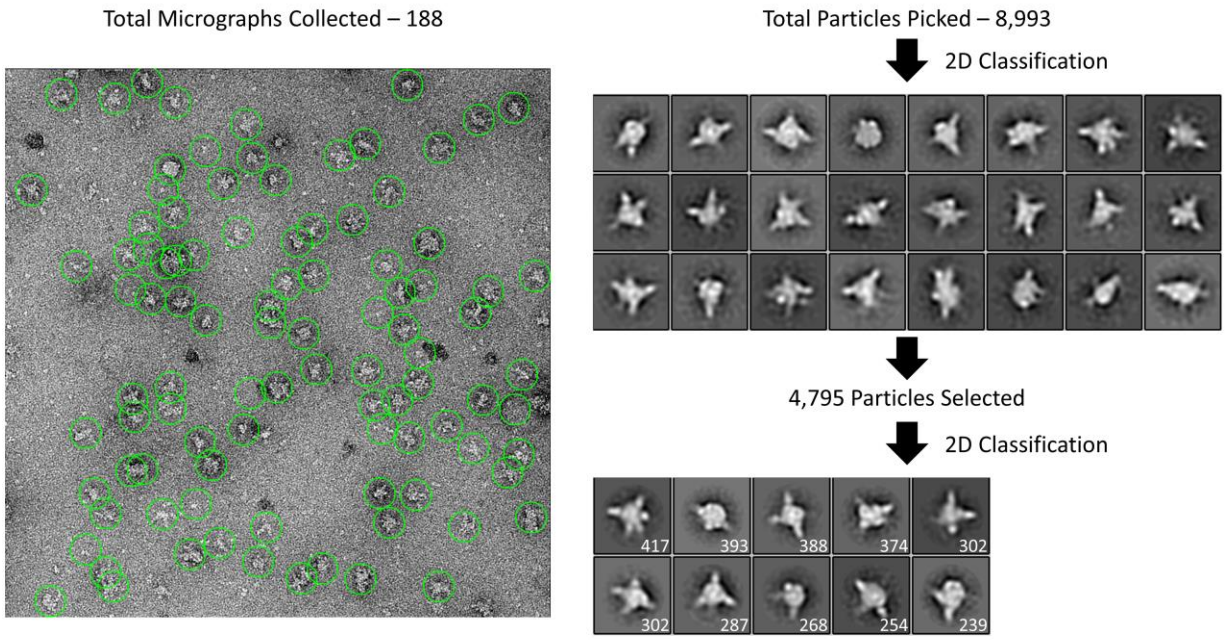

Figure 5.9: 2D class average of CagE structure showing spike features with a globular core at the center.

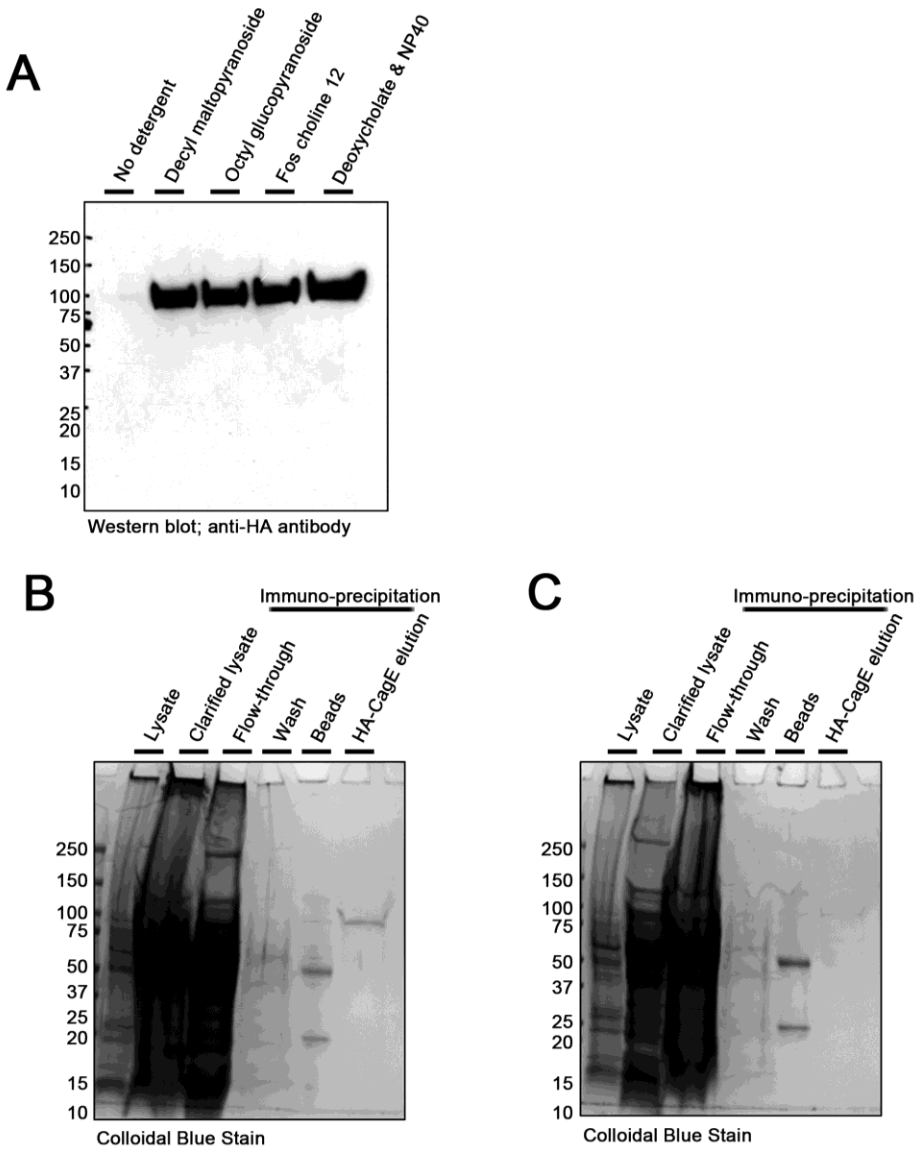

Figure 5.10: Purification of CagE from *H. pylori*. (A) Optimization of CagE solubilization with different detergents. (B, C) Analysis of purified CagE by colloidal blue stain.

Chapter VI

Conclusions and Future Directions

Conclusions

Type IV secretion systems (T4SSs) are present in a wide range of bacterial species (30, 31). One of the most common T4SS activities is transfer of plasmid DNA through conjugation, thus contributing to spread of antibiotic resistance genes among bacteria (30, 31). T4SSs can also facilitate translocation of effector proteins into target cells, thereby contributing to the pathogenesis of bacterial infections (30, 31). For example, T4SSs mediate secretion of *Bordetella pertussis* toxin, *Legionella pneumophila* effector proteins, and *Helicobacter pylori* CagA. The *H. pylori* Cag T4SS is made up of many components and traverses the bacterial cell envelope. The core complex is made up of three regions – an outer-membrane cap, a periplasmic ring and central stalk (51, 52). The inner membrane complex contains three putative Cag ATPases - Cagα, Cagβ and CagE, along with additional unidentified proteins (54). My thesis projects have focused on studies of the Cag ATPases, temporal control of the Cag T4SS *in vivo*, and *H. pylori*-induced alterations of gastric lipids, as summarized in the following sections.

Cag ATPases

Type IV secretion systems in many bacterial species possess three ATPases. My data showed that two ATPases are required for multiple *H. pylori* Cag T4SS-dependent phenotypes. In contrast, Cagβ is essential for CagA translocation but is not required for other Cag T4SS-dependent phenotypes. Although I have analyzed the requirement of individual Cag ATPases for several phenotypes, there are many other features of these proteins that still need to be investigated.

In prototypical T4SSs (*A. tumefaciens* VirB/VirD system and conjugation systems), VirD4 (Cagβ homolog) is required for DNA transfer and acts as a coupling protein for substrate recruitment (30, 68, 69). Since Cagβ is specifically required for CagA translocation, one likely function would be recruitment of CagA to the T4SS. Thus far, based on immunoprecipitation and mass spectrometry analyses, I have not detected an interaction of Cagβ with CagA. In contrast, a previous study reported the detection of an interaction based on analysis of recombinantly produced proteins (67). Further studies will be needed to be determine if Cagβ acts as a coupling protein to recruit CagA to the Cag T4SS.

In my study, I showed that each of the *H. pylori* strains harboring point mutations in Walker boxes of ATPases exhibited the same phenotypes as the deletion mutant strains. This finding suggests that each of the Cag ATPases has an enzymatic function. I successfully demonstrated that Cagα is able to hydrolyze ATP in a dose-dependent manner, and a Cagα mutant protein with Walker box mutations could not hydrolyze ATP (data not shown). These data are consistent with previous studies (149-151), showing that Cagα is indeed an ATPase. A previous study reported that a recombinantly expressed C-terminal domain of CagE exhibited ATPase activity, whereas a CagE mutant protein with a Walker box mutation in the C-terminal domain did not (85). Surprisingly, in this study a recombinantly expressed N-terminal domain of CagE exhibited ATPase activity even though the N-terminal domain does not have Walker box motifs (85). In contrast, I was unable to detect ATPase activity associated with full-length Cagβ or CagE. Future studies will need to investigate if full-length CagE or Cagβ is able to hydrolyze ATP.

My study shows that Cag ATPase are dispensable for core complex formation in *H. pylori,* and cryo-ET studies confirmed that the core complex is assembled *in situ* in *H. pylori* mutant strains lacking Cag ATPases (54). A current model proposes that the T4SS is assembled in a stepwise

manner with core complex assembly as an initial step, followed by inner membrane complex assembly.

Temporal control of the Cag T4SS *in vivo*

Several previous studies reported that CagA and the Cag T4SS contribute to gastric disease in animal models. The use of simple knock-out strains has revealed important roles of CagA and the Cag T4SS in the pathogenesis of *H. pylori*-induced gastric disease, but this approach does not allow an investigation of the actions of these proteins at specific stages of infection.

In my experiments, we used the well-established TetR/*tetO* system and synthesized a gerbil-adapted *H. pylori* strain in which the Cag T4SS activity can be conditionally regulated by an inducer. The successful engineering of this strain allowed us to investigate temporal features of Cag T4SS activity in an animal model. In addition, the availability of this strain allowed us to investigate if the Cag T4SS contributes to gastric carcinogenesis through a “hit-and-run” mechanism in an animal model of carcinogenesis.

A “hit-and-run” carcinogenesis mechanism has previously been proposed based on the results of experiments using animal models of virus-induced carcinogenesis. Our data show that Cag T4SS activity during initial stages of *H. pylori* infection (for at least 6 weeks) is sufficient to initiate a cascade of cellular alterations, leading to gastric inflammation and cancer. Several important questions still need to be answered. For example, it will be important to determine the molecular mechanisms by which CagA transforms gastric epithelial cells so they can continue to proliferate when CagA is no longer present.

None of the infected animals in which Cag T4SS activity was inactive during an initial 3 weeks of infection, and then active for a subsequent 10 weeks of infection, developed dysplasia or cancer. Additionally, the gastric inflammation in this group was not significantly increased, compared to inflammation in the infected group in which the Cag T4SS was active throughout

the entire 13-week infection. This is an interesting finding, suggesting that Cag T4SS activity during an early stage of infection is essential to cause subsequent severe gastric pathology. Further experiments, utilizing larger numbers of animals and longer time periods, will be needed to follow up on these results.

H. pylori-induced alterations of gastric lipids

An important goal of this project is to discover biomarkers for early signs of gastric adenocarcinoma. To identify molecular alterations that occur in gastric tissue in response to *H. pylori* infection, we utilized imaging mass spectrometry and liquid chromatography mass spectrometry approaches to analyze gastric tissue from Mongolian gerbils. These experiments showed that the abundance of specific gastric lipids was altered in response to *H. pylori* infection.

Additionally, I localized differentially abundant lipids to specific regions of the gastric tissues (for example, antrum versus corpus; surface mucous epithelium versus submucosal or muscle layers), based on the spatial distribution of the lipid signals in imaging mass spectrometry images. These experiments represent an unbiased approach for identifying *H. pylori*-induced alterations in gastric tissue. Importantly, we have identified several lipid species that are detected only in tissues exhibiting severe gastric disease (dysplasia and cancer), but not in tissue exhibiting gastric inflammation. Therefore, this is potentially a useful approach for identifying biomarkers for severe gastric pathology.

Future Directions

My work has provided important new insights into the Cag T4SS - the specific requirements of individual Cag ATPases for eliciting cellular alterations, the role of the Cag T4SS during specific stages of infection, and alterations in gastric lipid composition in response to *H. pylori* infection.

However, there is still much more that needs to be elucidated. My work provides a foundation for several new avenues of research that can be undertaken.

One of the important questions is to determine why many bacterial species have more than one ATPase component in their T4SSs. My experiments showed that Cagβ has a specific function in the translocation of CagA into host cells. This characteristic of Cagβ differs from the characteristics of the other two ATPases (Cagα and CagE). Previous studies proposed that Cagβ is a coupling protein that interacts with CagA and recruits CagA to the T4SS apparatus (67). On the other hand, Cagα and CagE have different non-redundant functions, essential for *H. pylori*-induced NF-κB activation, IL-8 induction and TLR9 activation in host cells. These phenotypes are linked to cellular uptake of non-protein bacterial constituents – lipopolysaccharide metabolites, peptidoglycan and DNA. We speculate that the mechanism by which *H. pylori* delivers CagA into host cells is different from the mechanism used for transfer of non-protein bacterial constituents. These pathways remain to be elucidated. Furthermore, the exact mechanistic functions of the individual Cag ATPases still need to be determined.

Another important question is to elucidate the mechanisms by which non-protein bacterial constituents are recruited to the T4SS, delivered into host cells, and activate signaling pathways in host cells. Previous studies showed that lipopolysaccharide metabolites activate alpha-kinase 1 (ALPK1), which leads to activation of the ALPK1/TIFA pathway (36-39). Peptidoglycan is recognized by the intracellular host defense molecule NOD1, leading to NOD1 signaling pathways (40). However, the exact mechanisms by which these bacterial constituents trigger transcription factor activation and cytokine production is not fully understood. Similarly, the exact mechanisms by which bacterial DNA is recognized by TLR9 receptors in the host cells is not fully understood.

Another important question is to elucidate the exact mechanism by which *H. pylori* translocates the CagA effector protein into host cells. CagA interacts with CagF and might interact with the

components of core complex (Cag3, CagT, CagM, CagX or CagY). Conversely, based on immunoprecipitation experiments and mass spectrometry analyses, I was not able to show that CagA interacts with Cagβ which is predicted to be a coupling protein. I was also unable to detect an interaction of CagA with the other two ATPases or other inner membrane components. Perhaps CagA interactions with inner membrane components or core complex components is transient and difficult to detect. Potentially CagA interactions with T4SS components could be detected more easily if studies were done using *H. pylori* co-cultured with gastric epithelial cells instead of *H. pylori* in the absence of host cells.

Another unresolved question is whether CagA is transported as a folded or unfolded protein within the secretion channel. A previous cryo-EM study showed that the type III secretion system of *Salmonella enterica* transports unfolded protein substrates (152). Future studies might be able to analyze CagA translocation at various stages of the secretion process via advanced imaging techniques.

Another avenue is to elucidate the composition of the inner membrane complex of the Cag T4SS system in further detail. In collaboration with the Christie lab and Hu lab (McGovern Medical School, Houston), we localized individual Cag ATPases in the inner membrane complex of *H. pylori* via cryo-ET (54). However, there are additional components of the inner membrane complex that have not been identified yet. It will be interesting to determine if Cag ATPases harboring substitution mutations in Walker box motifs can be incorporated into the inner membrane complex similar to the wild-type proteins.

Another future direction is to investigate if there is a conformational change in the inner membrane complex that initiates substrate translocation. A previous cryo-ET study visualized the *in vivo* structure of the Dot/Icm secretion system in *Legionella pneumophilia* (153). Importantly, this study reported that the cytoplasmic DotB (Cagα homolog, VirB11-like) ATPase complex docks on the DotO (Cage homolog, VirB4-like) ATPase complex, thus resulting in a

conformational change in the secretion system that results in the opening of a channel in the inner membrane (153). Similarly, within the inner membrane complex, *H. pylori* CagE forms a foundation at the channel entrance, and Cagα docks right under CagE, suggesting that the binding process may regulate the channel opening. This study leads me to hypothesize that there might be a conformational change dependent on either interactions among different components within the inner membrane complex or ATP hydrolysis by ATPases which leads to either opening or closing of the channel.

Another important future direction is to determine how the Cag T4SS interacts with host cells. What are the filamentous structures elaborated by bacteria when bacteria come into contact with host cells? Earlier studies proposed that these structures are pilus components of the Cag T4SS, but I consistently observed these structures in Δ*cag* PAI mutant strains.

Another key question is to understand the molecular events associated with the “hit-and-run” model of *H. pylori*-associated carcinogenesis. Several *in vitro* studies show that CagA can de-differentiate terminated cells into stem-like precursor cells by activating certain signaling pathways involved in programming (154). *In vivo* studies also show that *H. pylori* interacts with Lgr5+ stem cells in gastric glands in a CagA-dependent manner, causing hyperplasia (89). Furthermore, CagA stimulates production of H_2O_2, which causes oxidative DNA damage. CagA also enhances genotoxic stress by downregulating heme oxygenase-1 (HO-1) expression, a potent antioxidant and anti-inflammatory molecule (154). The resulting cumulative damage can potentially lead to carcinogenesis. However, the exact mechanisms by which CagA causes cellular changes or damage at genetic and epigenetic levels, and how these cellular changes are propagated when CagA is no longer present, are not well understood.

Finally, another interesting future direction is to investigate molecular changes in gastric tissues in response to *H. pylori* infection. This was a new territory of research when I started my dissertation. I detected several gastric lipid species that are altered in abundance in response to

H. pylori infection, especially in gastric tissues exhibiting severe disease (dysplasia or gastric cancer). Furthermore, by using imaging mass spectrometry methods, I was able to show the precise localization of these lipid changes in gastric tissues. This initial research has opened a Pandora's box of future research that can be undertaken. What are the changes in other molecules (including proteins and small molecule metabolites) in gastric tissues in response to *H. pylori* infection? What is the precise localization of these changes (corpus versus antrum; epithelial layer versus deeper gastric layers)? Most importantly, what are the mechanisms and functional consequences of these changes?

All in all, there are multiple future directions that can be undertaken. Investigating the mechanisms by which the Cag T4SS contributes to gastric disease is an important basic microbiology topic. Discovering biomarkers of gastric premalignant conditions is a more translational topic that can potentially lead to medical applications relevant to human health. Regardless of which direction is taken, all will contribute to new insights into the *H. pylori* Cag Type IV secretion system.

PUBLICATIONS

Lin AS, Kotnala A, Shaw JA, Beckett AC, Harvey J, Tuck M, Dixon BREA, Reyer ML, Algood HM, Schey KL, Piazuelo MB, Cover TL. Gastric lipid alterations in response to *Helicobacter pylori*. (manuscript in progress)

Harvey ML, **Lin AS**, Sun L, Koyama T, Shuman JH, Loh JT, Algood HM, Scholz M, McClain MS, Cover TL. Hop outer membrane proteins as determinants of *Helicobacter pylori* fitness. (manuscript submitted)

Lin AS*, McClain MS*, Beckett AC, Caston RR, Harvey ML, Dixon BREA, Campbell AM, Sawhney N, Shuman JH, Loh JT, Piazuelo MB, Algood HM, Cover TL. Temporal control of the *Helicobacter pylori* Cag type IV secretion system in a Mongolian gerbil model of gastric carcinogenesis. mBio. Jun 2020. 11:e01296-20.

* co-first authors equally contributed to this work.

Lin AS, Dooyema SDR, Frick-Cheng AE, Harvey ML, Suarez G, Loh JT, McDonald WH, McClain MS, Peek Jr. RM, Cover TL. Bacterial energetic requirements for *Helicobacter pylori* cag type IV secretion system-dependent alterations in gastric epithelial cells. Infect Immun. Jan 2020. 88:e00790-19.

Hu B, Khara P, Song L, **Lin AS**, Frick-Cheng AE, Harvey ML, Cover TL, Christie PJ. In situ molecular architecture of the *Helicobacter pylori* cag type IV secretion system. mBio. May 2019. 10:e00849-19.

Loh JT, **Lin AS**, Beckett AC, McClain MS, Cover TL. Role of a stem-loop structure in *Helicobacter pylori* cagA transcript stability. Infect Immun. Feb 2019. 87:e00692-18.

Beckett AC, Loh JT, Chopra A, Leary S, **Lin AS**, McDonnell WJ, Dixon B, Noto JM, Israel DA, Peek RM, Mallal S, Algood HM, Cover TL. *Helicobacter pylori* genetic diversification in the Mongolian gerbil model. PeerJ. May 2018. 6(1):e/4803.

REFERENCES

1. Hooi JKY, Lai WY, Ng WK, Suen MMY, Underwood FE, Tanyingoh D, Malfertheiner P, Graham DY, Wong VWS, Wu JCY, Chan FKL, Sung JJY, Kaplan GG, Ng SC. 2017. Global Prevalence of Helicobacter pylori Infection: Systematic Review and Meta-Analysis. Gastroenterology 153:420-429.

2. Gilbreath JJ, Cody WL, Merrell DS, Hendrixson DR. 2011. Change is good: variations in common biological mechanisms in the epsilonproteobacterial genera Campylobacter and Helicobacter. Microbiology and molecular biology reviews : MMBR 75:84-132.

3. Burkitt MD, Duckworth CA, Williams JM, Pritchard DM. 2017. Helicobacter pylori-induced gastric pathology: insights from in vivo and ex vivo models. Disease Models & Mechanisms 10:89-104.

4. Eusebi LH, Zagari RM, Bazzoli F. 2014. Epidemiology of Helicobacter pylori Infection. Helicobacter 19:1-5.

5. Burucoa C, Axon A. 2017. Epidemiology of Helicobacter pylori infection. Helicobacter 22:e12403.

6. Suerbaum S, Michetti P. 2002. Helicobacter pylori Infection. New England Journal of Medicine 347:1175-1186.

7. Cover TL, Blaser MJ. 2009. Helicobacter pylori in health and disease. Gastroenterology 136:1863-1873.

8. Ernst PB, Gold BD. 2000. The Disease Spectrum of Helicobacter Pylori: The Immunopathogenesis of Gastroduodenal Ulcer and Gastric Cancer. Annual Review of Microbiology 54:615-640.

9. Serin A, Tankurt E, Şarkış C, Simsek I. 2015. The prevalence of Helicobacter pylori infection in patients with gastric and duodenal ulcers - a 10-year, single-centre experience. Przeglad gastroenterologiczny 10:160-163.

10. Wroblewski LE, Peek RM, Jr., Wilson KT. 2010. Helicobacter pylori and gastric cancer: factors that modulate disease risk. Clinical microbiology reviews 23:713-739.

11. Backert S, Haas R, Gerhard M, Naumann M. 2017. The Helicobacter pylori Type IV Secretion System Encoded by the cag Pathogenicity Island: Architecture, Function, and Signaling. Current topics in microbiology and immunology 413:187-220.

12. Fischer W. 2011. Assembly and molecular mode of action of the Helicobacter pylori Cag type IV secretion apparatus. The FEBS Journal 278:1203-1212.

13. Terradot L, Waksman G. 2011. Architecture of the Helicobacter pylori Cag-type IV secretion system. The FEBS Journal 278:1213-1222.

14. Olbermann P, Josenhans C, Moodley Y, Uhr M, Stamer C, Vauterin M, Suerbaum S, Achtman M, Linz B. 2010. A Global Overview of the Genetic and Functional Diversity in the Helicobacter pylori cag Pathogenicity Island. PLOS Genetics 6:e1001069.

15. Bourzac KM, Guillemin K. 2005. Helicobacter pylori–host cell interactions mediated by type IV secretion. Cellular microbiology 7:911-919.

16. Park JY, Forman D, Waskito LA, Yamaoka Y, Crabtree JE. 2018. Epidemiology of Helicobacter pylori and CagA-Positive Infections and Global Variations in Gastric Cancer. Toxins 10:163.

17. Cover TL. 2016. Helicobacter pylori Diversity and Gastric Cancer Risk. mBio 7:e01869-15.

18. Hatakeyama M. 2014. Helicobacter pylori CagA and Gastric Cancer: A Paradigm for Hit-and-Run Carcinogenesis. Cell Host & Microbe 15:306-316.

19. Tegtmeyer N, Neddermann M, Asche CI, Backert S. 2017. Subversion of host kinases: a key network in cellular signaling hijacked by Helicobacter pylori CagA. Molecular Microbiology 105:358-372.

20. Hatakeyama M. 2004. Oncogenic mechanisms of the Helicobacter pylori CagA protein. Nature Reviews Cancer 4:688-694.

21. Backert S, Tegtmeyer N. 2017. Type IV Secretion and Signal Transduction of Helicobacter pylori CagA through Interactions with Host Cell Receptors. Toxins 9:115.

22. Stein M, Bagnoli F, Halenbeck R, Rappuoli R, Fantl WJ, Covacci A. 2002. c-Src/Lyn kinases activate Helicobacter pylori CagA through tyrosine phosphorylation of the EPIYA motifs. Molecular Microbiology 43:971-980.

23. Higashi H, Tsutsumi R, Muto S, Sugiyama T, Azuma T, Asaka M, Hatakeyama M. 2002. SHP-2 Tyrosine Phosphatase as an Intracellular Target of Helicobacter pylori CagA Protein. Science 295:683-686.

24. Ohnishi N, Yuasa H, Tanaka S, Sawa H, Miura M, Matsui A, Higashi H, Musashi M, Iwabuchi K, Suzuki M, Yamada G, Azuma T, Hatakeyama M. 2008. Transgenic expression of Helicobacter pylori CagA induces gastrointestinal and hematopoietic neoplasms in mouse. Proceedings of the National Academy of Sciences of the United States of America 105:1003-1008.

25. Alvarez-Martinez CE, Christie PJ. 2009. Biological diversity of prokaryotic type IV secretion systems. Microbiology and molecular biology reviews : MMBR 73:775-808.

26. Fronzes R, Christie PJ, Waksman G. 2009. The structural biology of type IV secretion systems. Nature Reviews Microbiology 7:703.

27. Wallden K, Rivera-Calzada A, Waksman G. 2010. Type IV secretion systems: versatility and diversity in function. Cellular microbiology 12:1203-1212.

28. Segal G, Feldman M, Zusman T. 2005. The Icm/Dot type-IV secretion systems of Legionella pneumophila and Coxiella burnetii. FEMS Microbiology Reviews 29:65-81.

29. Ghosal D, Jeong KC, Chang Y-W, Gyore J, Teng L, Gardner A, Vogel JP, Jensen GJ. 2019. Molecular architecture, polar targeting and biogenesis of the Legionella Dot/Icm T4SS. Nature Microbiology 4:1173-1182.

30. Christie PJ, Gomez Valero L, Buchrieser C. 2017. Biological Diversity and Evolution of Type IV Secretion Systems. Current topics in microbiology and immunology 413:1-30.
31. Waksman G. 2019. From conjugation to T4S systems in Gram-negative bacteria: a mechanistic biology perspective. EMBO reports 20:e47012.

32. Rohrer S, Holsten L, Weiss E, Benghezal M, Fischer W, Haas R. 2012. Multiple pathways of plasmid DNA transfer in Helicobacter pylori. PloS one 7:e45623-e45623.
33. Fischer W, Tegtmeyer N, Stingl K, Backert S. 2020. Four Chromosomal Type IV Secretion Systems in Helicobacter pylori: Composition, Structure and Function. Frontiers in Microbiology 11.

34. Hofreuter D, Odenbreit S, Haas R. 2001. Natural transformation competence in Helicobacter pylori is mediated by the basic components of a type IV secretion system. Molecular Microbiology 41:379-391.

35. Fischer W, Püls J, Buhrdorf R, Gebert B, Odenbreit S, Haas R. 2001. Systematic mutagenesis of the Helicobacter pylori cag pathogenicity island: essential genes for CagA translocation in host cells and induction of interleukin-8. Molecular Microbiology 42:1337-1348.

36. Gall A, Gaudet RG, Gray-Owen SD, Salama NR. 2017. TIFA Signaling in Gastric Epithelial Cells Initiates the cag Type 4 Secretion System-Dependent Innate Immune Response to Helicobacter pylori Infection. mBio 8:e01168-17.

37. Suarez G, Romero-Gallo J, Sierra JC, Piazuelo MB, Krishna US, Gomez MA, Wilson KT, Peek RM, Jr. 2017. Genetic Manipulation of Helicobacter pylori Virulence Function by Host Carcinogenic Phenotypes. Cancer research 77:2401-2412.

38. Zimmermann S, Pfannkuch L, Al-Zeer MA, Bartfeld S, Koch M, Liu J, Rechner C, Soerensen M, Sokolova O, Zamyatina A, Kosma P, Mäurer AP, Glowinski F, Pleissner K-P, Schmid M, Brinkmann V, Karlas A, Naumann M, Rother M, Machuy N, Meyer TF. 2017. ALPK1- and TIFA-Dependent Innate Immune Response Triggered by the Helicobacter pylori Type IV Secretion System. Cell Reports 20:2384-2395.

39. Pfannkuch L, Hurwitz R, Traulsen J, Sigulla J, Poeschke M, Matzner L, Kosma P, Schmid M, Meyer TF. 2019. ADP heptose, a novel pathogen-associated molecular pattern identified in Helicobacter pylori. FASEB journal : official publication of the Federation of American Societies for Experimental Biology 33:9087-9099.

40. Viala J, Chaput C, Boneca IG, Cardona A, Girardin SE, Moran AP, Athman R, Mémet S, Huerre MR, Coyle AJ, DiStefano PS, Sansonetti PJ, Labigne A, Bertin J, Philpott DJ, Ferrero RL. 2004. Nod1 responds to peptidoglycan delivered by the Helicobacter pylori cag pathogenicity island. Nature Immunology 5:1166-1174.

41. Varga MG, Peek RM. 2017. DNA Transfer and Toll-like Receptor Modulation by Helicobacter pylori. Current topics in microbiology and immunology 400:169-193.

42. Varga MG, Shaffer CL, Sierra JC, Suarez G, Piazuelo MB, Whitaker ME, Romero-Gallo J, Krishna US, Delgado A, Gomez MA, Good JAD, Almqvist F, Skaar EP, Correa P, Wilson KT, Hadjifrangiskou M, Peek RM. 2016. Pathogenic Helicobacter pylori strains translocate DNA and activate TLR9 via the cancer-associated cag type IV secretion system. Oncogene 35:6262-6269.

43. Lai C-H, Wang H-J, Chang Y-C, Hsieh W-C, Lin H-J, Tang C-H, Sheu JJ-C, Lin C-J, Yang M-S, Tseng S-F, Wang W-C. 2011. Helicobacter pyloriCagA-mediated IL-8 induction in gastric epithelial cells is cholesterol-dependent and requires the C-terminal tyrosine phosphorylation-containing domain. FEMS Microbiology Letters 323:155-163.

44. Lim JW, Kim KH, Kim H. 2009. αPix interacts with Helicobacter pylori CagA to induce IL-8 expression in gastric epithelial cells. Scandinavian Journal of Gastroenterology 44:1166-1172.

45. Kim S-Y, Lee Y-C, Kim HK, Blaser MJ. 2006. Helicobacter pylori CagA transfection of gastric epithelial cells induces interleukin-8. Cellular microbiology 8:97-106.

46. Brandt S, Kwok T, Hartig R, König W, Backert S. 2005. NF-κB activation and potentiation of proinflammatory responses by the Helicobacter pylori CagA protein. Proceedings of the National Academy of Sciences of the United States of America 102:9300-9305.

47. Gorrell RJ, Guan J, Xin Y, Tafreshi MA, Hutton ML, McGuckin MA, Ferrero RL, Kwok T. 2013. A novel NOD1- and CagA-independent pathway of interleukin-8 induction mediated by the Helicobacter pylori type IV secretion system. Cellular microbiology 15:554-570.

48. Sokolova O, Borgmann M, Rieke C, Schweitzer K, Rothkötter H-J, Naumann M. 2013. Helicobacter pylori induces type 4 secretion system-dependent, but CagA-independent activation of IκBs and NF-κB/RelA at early time points. International Journal of Medical Microbiology 303:548-552.

49. Crabtree JE, Xiang Z, Lindley IJ, Tompkins DS, Rappuoli R, Covacci A. 1995. Induction of interleukin-8 secretion from gastric epithelial cells by a cagA negative isogenic mutant of Helicobacter pylori. Journal of clinical pathology 48:967-969.

50. Frick-Cheng AE, Pyburn TM, Voss BJ, McDonald WH, Ohi MD, Cover TL. 2016. Molecular and Structural Analysis of the Helicobacter pylori Type IV Secretion System Core Complex. mBio 7:e02001-15.

51. Chung JM, Sheedlo MJ, Campbell AM, Sawhney N, Frick-Cheng AE, Lacy DB, Cover TL, Ohi MD. 2019. Structure of the Helicobacter pylori Cag type IV secretion system. eLife 8:e47644.

52. Sheedlo MJ, Chung JM, Sawhney N, Durie CL, Cover TL, Ohi MD, Lacy DB. 2020. Cryo-EM reveals species-specific components within the Helicobacter pylori Cag type IV secretion system core complex. bioRxiv:2020.09.01.277012.

53. Chang Y-W, Shaffer CL, Rettberg LA, Ghosal D, Jensen GJ. 2018. In Vivo Structures of the Helicobacter pylori cag Type IV Secretion System. Cell Reports 23:673-681.

54. Hu B, Khara P, Song L, Lin AS, Frick-Cheng AE, Harvey ML, Cover TL, Christie PJ. 2019. In Situ Molecular Architecture of the Helicobacter pylori Cag Type IV Secretion System. mBio 10:e00849-19.

55. Yeo H-J, Savvides SN, Herr AB, Lanka E, Waksman G. 2000. Crystal Structure of the Hexameric Traffic ATPase of the Helicobacter pylori Type IV Secretion System. Molecular Cell 6:1461-1472.

56. Backert S, Tegtmeyer N, Fischer W. 2015. Composition, structure and function of the Helicobacter pylori cag pathogenicity island encoded type IV secretion system. Future microbiology 10:955-965.

57. Zhang S, Moss SF. 2012. Rodent models of Helicobacter infection, inflammation, and disease. Methods in molecular biology (Clifton, NJ) 921:89-98.

58. Barrozo RM, Cooke CL, Hansen LM, Lam AM, Gaddy JA, Johnson EM, Cariaga TA, Suarez G, Peek RM, Jr., Cover TL, Solnick JV. 2013. Functional plasticity in the type IV secretion system of Helicobacter pylori. PLoS pathogens 9:e1003189-e1003189.

59. Gaddy JA, Radin JN, Loh JT, Zhang F, Washington MK, Peek RM, Jr., Algood HMS, Cover TL. 2013. High dietary salt intake exacerbates Helicobacter pylori-induced gastric carcinogenesis. Infection and immunity 81:2258-2267.

60. Noto JM, Gaddy JA, Lee JY, Piazuelo MB, Friedman DB, Colvin DC, Romero-Gallo J, Suarez G, Loh J, Slaughter JC, Tan S, Morgan DR, Wilson KT, Bravo LE, Correa P, Cover TL, Amieva MR, Peek RM, Jr. 2013. Iron deficiency accelerates Helicobacter pylori-induced carcinogenesis in rodents and humans. The Journal of clinical investigation 123:479-492.

61. Beckett AC, Piazuelo MB, Noto JM, Peek RM, Jr., Washington MK, Algood HMS, Cover TL. 2016. Dietary Composition Influences Incidence of Helicobacter pylori-Induced Iron Deficiency Anemia and Gastric Ulceration. Infection and immunity 84:3338-3349.

62. Akanuma M, Maeda S, Ogura K, Mitsuno Y, Hirata Y, Ikenoue T, Otsuka M, Watanabe T, Yamaji Y, Yoshida H, Kawabe T, Shiratori Y, Omata M. 2002. The Evaluation of Putative Virulence Factors of Helicobacter pylori for Gastroduodenal Disease b Use of a Short-Term Mongolian Gerbil Infection Model. The Journal of Infectious Diseases 185:341-347.

63. Ogura K, Maeda S, Nakao M, Watanabe T, Tada M, Kyutoku T, Yoshida H, Shiratori Y, Omata M. 2000. Virulence factors of Helicobacter pylori responsible for gastric diseases in Mongolian gerbil. The Journal of experimental medicine 192:1601-1610.

64. Rieder G, Merchant JL, Haas R. 2005. Helicobacter pylori cag-Type IV Secretion System Facilitates Corpus Colonization to Induce Precancerous Conditions in Mongolian Gerbils. Gastroenterology 128:1229-1242.

65. Saito H, Yamaoka Y, Ishizone S, Maruta F, Sugiyama A, Graham DY, Yamauchi K, Ota H, Miyagawa S. 2005. Roles of virD4 and cagG genes in the cag pathogenicity island of Helicobacter pylori using a Mongolian gerbil model. Gut 54:584-590.

66. Wiedemann T, Loell E, Mueller S, Stoeckelhuber M, Stolte M, Haas R, Rieder G. 2009. Helicobacter pylori cag-Pathogenicity island-dependent early immunological response triggers later precancerous gastric changes in Mongolian gerbils. PloS one 4:e4754-e4754.

67. Jurik A, Haußer E, Kutter S, Pattis I, Praßl S, Weiss E, Fischer W. 2010. The Coupling Protein Cagβ and Its Interaction Partner CagZ Are Required for Type IV Secretion of the Helicobacter pylori CagA Protein. Infection and immunity 78:5244-5251.

68. Cascales E, Christie PJ. 2004. Definition of a Bacterial Type IV Secretion Pathway for a DNA Substrate. Science 304:1170-1173.

69. Redzej A, Ukleja M, Connery S, Trokter M, Felisberto-Rodrigues C, Cryar A, Thalassinos K, Hayward RD, Orlova EV, Waksman G. 2017. Structure of a VirD4 coupling protein bound to a VirB type IV secretion machinery. The EMBO journal 36:3080-3095.

70. Grohmann E, Christie PJ, Waksman G, Backert S. 2018. Type IV secretion in Gram-negative and Gram-positive bacteria. Molecular Microbiology 107:455-471.

71. Backert S, Ziska E, Brinkmann V, Zimny-Arndt U, Fauconnier A, Jungblut PR, Naumann M, Meyer TF. 2000. Translocation of the Helicobacter pylori CagA protein in gastric epithelial cells by a type IV secretion apparatus. Cellular microbiology 2:155-164.

72. Busler VJ, Torres VJ, McClain MS, Tirado O, Friedman DB, Cover TL. 2006. Protein-protein interactions among Helicobacter pylori cag proteins. Journal of bacteriology 188:4787-4800.

73. Loh JT, Torres VJ, Cover TL. 2007. Regulation of Helicobacter pylori cagA Expression in Response to Salt. Cancer research 67:4709-4715.

74. Odenbreit S, Püls J, Sedlmaier B, Gerland E, Fischer W, Haas R. 2000. Translocation of Helicobacter pylori CagA into Gastric Epithelial Cells by Type IV Secretion. Science 287:1497-1500.

75. Shaffer CL, Gaddy JA, Loh JT, Johnson EM, Hill S, Hennig EE, McClain MS, McDonald WH, Cover TL. 2011. Helicobacter pylori exploits a unique repertoire of type IV secretion system components for pilus assembly at the bacteria-host cell interface. PLoS pathogens 7:e1002237-e1002237.

76. Stein M, Rappuoli R, Covacci A. 2000. Tyrosine phosphorylation of the Helicobacter pylori CagA antigen after cag-driven host cell translocation. Proceedings of the National Academy of Sciences 97:1263-1268.

77. Johnson EM, Gaddy JA, Voss BJ, Hennig EE, Cover TL. 2014. Genes required for assembly of pili associated with the Helicobacter pylori cag type IV secretion system. Infection and immunity 82:3457-3470.

78. Loh JT, Lin AS, Beckett AC, McClain MS, Cover TL. 2019. Role of a Stem-Loop Structure in Helicobacter pylori cagA Transcript Stability. Infection and immunity 87:e00692-18.

79. Styer CM, Hansen LM, Cooke CL, Gundersen AM, Choi SS, Berg DE, Benghezal M, Marshall BJ, Peek RM, Borén T, Solnick JV. 2010. Expression of the BabA Adhesin during Experimental Infection with *Helicobacter pylori*. Infection and Immunity 78:1593-1600.

80. Brown LM. 2000. Helicobacter Pylori : Epidemiology and Routes of Transmission. Epidemiologic Reviews 22:283-297.

81. Stein SC, Faber E, Bats SH, Murillo T, Speidel Y, Coombs N, Josenhans C. 2017. Helicobacter pylori modulates host cell responses by CagT4SS-dependent translocation of an intermediate metabolite of LPS inner core heptose biosynthesis. PLoS pathogens 13:e1006514-e1006514.

82. Liu T, Zhang L, Joo D, Sun S-C. 2017. NF-κB signaling in inflammation. Signal transduction and targeted therapy 2:17023.

83. Zhang Q, Lenardo MJ, Baltimore D. 2017. 30 Years of NF-κB: A Blossoming of Relevance to Human Pathobiology. Cell 168:37-57.

84. Keates S, Hitti YS, Upton M, Kelly CP. 1997. Helicobacter pylori infection activates NF-kappa B in gastric epithelial cells. Gastroenterology 113:1099-1109.

85. Shariq M, Kumar N, Kumari R, Kumar A, Subbarao N, Mukhopadhyay G. 2015. Biochemical Analysis of CagE: A VirB4 Homologue of Helicobacter pylori Cag-T4SS. PloS one 10:e0142606-e0142606.

86. Ferreira Júnior M, Batista SA, Vidigal PVT, Cordeiro AAC, Oliveira FMS, Prata LO, Diniz AET, Barral CM, Barbuto RC, Gomes AD, Araújo ID, Queiroz DMM, Caliari MV. 2015. Infection with CagA-positive Helicobacter pylori strain containing three EPIYA C phosphorylation sites is associated with more severe gastric lesions in experimentally infected Mongolian gerbils (Meriones unguiculatus). European journal of histochemistry : EJH 59:2489-2489.

87. Franco AT, Johnston E, Krishna U, Yamaoka Y, Israel DA, Nagy TA, Wroblewski LE, Piazuelo MB, Correa P, Peek RM, Jr. 2008. Regulation of gastric carcinogenesis by Helicobacter pylori virulence factors. Cancer research 68:379-387.

88. Shibata W, Hirata Y, Maeda S, Ogura K, Ohmae T, Yanai A, Mitsuno Y, Yamaji Y, Okamoto M, Yoshida H, Kawabe T, Omata M. 2006. CagA protein secreted by the intact type IV secretion system leads to gastric epithelial inflammation in the Mongolian gerbil model. The Journal of Pathology 210:306-314.

89. Sigal M, Rothenberg ME, Logan CY, Lee JY, Honaker RW, Cooper RL, Passarelli B, Camorlinga M, Bouley DM, Alvarez G, Nusse R, Torres J, Amieva MR. 2015. Helicobacter pylori Activates and Expands Lgr5+ Stem Cells Through Direct Colonization of the Gastric Glands. Gastroenterology 148:1392-1404.e21.

90. Gagnaire A, Nadel B, Raoult D, Neefjes J, Gorvel J-P. 2017. Collateral damage: insights into bacterial mechanisms that predispose host cells to cancer. Nature Reviews Microbiology 15:109-128.

91. Toller IM, Neelsen KJ, Steger M, Hartung ML, Hottiger MO, Stucki M, Kalali B, Gerhard M, Sartori AA, Lopes M, Müller A. 2011. Carcinogenic bacterial pathogen Helicobacter pylori triggers DNA double-strand breaks and a DNA damage response in its host cells. Proceedings of the National Academy of Sciences 108:14944-14949.

92. Algood HMS, Cover TL. 2006. Helicobacter pylori persistence: an overview of interactions between H. pylori and host immune defenses. Clinical microbiology reviews 19:597-613.

93. Salama NR, Hartung ML, Müller A. 2013. Life in the human stomach: persistence strategies of the bacterial pathogen Helicobacter pylori. Nature reviews Microbiology 11:385-399.

94. Ambinder RF. 2000. Gammaherpesviruses and "Hit-and-Run" oncogenesis. The American journal of pathology 156:1-3.

95. Galloway DA, McDougall JK. 1983. The oncogenic potential of herpes simplex viruses: evidence for a 'hit-and-run' mechanism. Nature 302:21-24.

96. Niller HH, Wolf H, Minarovits J. 2011. Viral hit and run-oncogenesis: Genetic and epigenetic scenarios. Cancer Letters 305:200-217.

97. Barbanti-Brodano G, Sabbioni S, Martini F, Negrini M, Corallini A, Tognon M. 2004. Simian virus 40 infection in humans and association with human diseases: results and hypotheses. Virology 318:1-9.

98. Khalili K, Del Valle L, Otte J, Weaver M, Gordon J. 2003. Human neurotropic polyomavirus, JCV, and its role in carcinogenesis. Oncogene 22:5181-5191.

99. Weggen S, Bayer TA, von Deimling A, Reifenberger G, von Schweinitz D, Wiestler OD, Pietsch T. 2000. Low Frequency of SV40, JC and BK Polyomavirus Sequences in Human Medulloblastomas, Meningiomas and Ependymomas. Brain Pathology 10:85-92.

100. Hessein M, Saad EG, Mohamed AA, Kamel EAM, Abdel Hady A, Amina M, Rogler CE. 2005. Hit-And-Run Mechanism of HBV-Mediated Progression to Hepatocellular Carcinoma. Tumori Journal 91:241-247.

101. Lawson W, Schlecht NF, Brandwein-Gensler M. 2008. The role of the human papillomavirus in the pathogenesis of Schneiderian inverted papillomas: an analytic overview of the evidence. Head and neck pathology 2:49-59.

102. Hori R, Murai Y, Tsuneyama K, Abdel-Aziz HO, Nomoto K, Takahashi H, Cheng C-m, Kuchina T, Harman BV, Takano Y. 2005. Detection of JC virus DNA sequences in colorectal cancers in Japan. Virchows Archiv 447:723-730.

103. McClain MS, Duncan SS, Gaddy JA, Cover TL. 2013. Control of gene expression in Helicobacter pylori using the Tet repressor. Journal of microbiological methods 95:336-341.

104. Franco AT, Israel DA, Washington MK, Krishna U, Fox JG, Rogers AB, Neish AS, Collier-Hyams L, Perez-Perez GI, Hatakeyama M, Whitehead R, Gaus K, O'Brien DP,

Romero-Gallo J, Peek RM. 2005. Activation of β-catenin by carcinogenic Helicobacter pylori. Proceedings of the National Academy of Sciences of the United States of America 102:10646-10651.

105. Boivin GP, Washington K, Yang K, Ward JM, Pretlow TP, Russell R, Besselsen DG, Godfrey VL, Doetschman T, Dove WF, Pitot HC, Halberg RB, Itzkowitz SH, Groden J, Coffey RJ. 2003. Pathology of mouse models of intestinal cancer: Consensus report and recommendations. Gastroenterology 124:762-777.

106. Piazuelo MB, Correa P. 2013. Gastric cáncer: Overview. Colombia medica (Cali, Colombia) 44:192-201.

107. Matz MV, Wright RM, Scott JG. 2013. No Control Genes Required: Bayesian Analysis of qRT-PCR Data. PloS one 8:e71448.

108. Debowski AW, Walton SM, Chua E-G, Tay AC-Y, Liao T, Lamichhane B, Himbeck R, Stubbs KA, Marshall BJ, Fulurija A, Benghezal M. 2017. Helicobacter pylori gene silencing in vivo demonstrates urease is essential for chronic infection. PLoS pathogens 13:e1006464-e1006464.

109. Scott Algood HM, Gallo-Romero J, Wilson KT, Peek RM, Jr, Cover TL. 2007. Host response to Helicobacter pylori infection before initiation of the adaptive immune response. FEMS Immunology & Medical Microbiology 51:577-586.

110. Niv Y. 2016. Doxycycline in Eradication Therapy of Helicobacter pylori - A Systematic Review and Meta-Analysis. Digestion 93:167-173.

111. Sapadin AN, Fleischmajer R. 2006. Tetracyclines: Nonantibiotic properties and their clinical implications. Journal of the American Academy of Dermatology 54:258-265.

112. Angelakis E, Million M, Kankoe S, Lagier J-C, Armougom F, Giorgi R, Raoult D. 2014. Abnormal Weight Gain and Gut Microbiota Modifications Are Side Effects of Long-Term Doxycycline and Hydroxychloroquine Treatment. Antimicrobial Agents and Chemotherapy 58:3342-3347.

113. Gencosmanoglu R, Kurtkaya-Yapicier O, Tiftikci A, Avsar E, Tozun N, Oran ES. 2004. Mid-esophageal ulceration and candidiasis-associated distal esophagitis as two distinct clinical patterns of tetracycline or doxycycline-induced esophageal injury. Journal of clinical gastroenterology 38:484-489.

114. Sasaki Y, Suzuki T, Zai H, Urita Y. 2017. Esophageal ulcer associated with inappropriately taken doxycycline: A benign mimicker of esophageal cancer. Journal of general and family medicine. 18(4):171-172. doi:10.1002/jgf2.55.

115. Tahan V, Sayrak H, Bayar N, Erer B, Tahan G, Dane F. 2008. Doxycycline-induced ulceration mimicking esophageal cancer. Cases journal. 1(1):144. doi:10.1186/1757-1626-1-144.

116. Affolter K, Samowitz W, Boynton K, Kelly ED. 2017. Doxycycline-induced gastrointestinal injury. Human Pathology 66:212-215.

117. Shih AR, Lauwers GY, Mattia A, Schaefer EAK, Misdraji J. 2017. Vascular Injury Characterizes Doxycycline-induced Upper Gastrointestinal Tract Mucosal Injury. The American journal of surgical pathology 41:374-381.

118. Nanda N, Dhawan DK, Bhatia A, Mahmood A, Mahmood S. 2016. Doxycycline Promotes Carcinogenesis & Metastasis via Chronic Inflammatory Pathway: An In Vivo Approach. PloS one. 11(3):e0151539. doi:10.1371/journal.pone.0151539.

119. Duivenvoorden WCM, Vukmirović-Popović S, Kalina M, Seidlitz E, Singh G. 2007. Effect of zoledronic acid on the doxycycline-induced decrease in tumour burden in a bone metastasis model of human breast cancer. British journal of cancer 96:1526-1531.

120. Mouratidis PXE, Colston KW, Dalgleish AG. 2007. Doxycycline induces caspase-dependent apoptosis in human pancreatic cancer cells. International Journal of Cancer 120:743-752.

121. Onoda T, Ono T, Dhar DK, Yamanoi A, Fujii T, Nagasue N. 2004. Doxycycline inhibits cell proliferation and invasive potential: combination therapy with cyclooxygenase-2 inhibitor in human colorectal cancer cells. Journal of Laboratory and Clinical Medicine 143:207-216.

122. Onoda T, Ono T, Dhar DK, Yamanoi A, Nagasue N. 2006. Tetracycline analogues (doxycycline and COL-3) induce caspase-dependent and -independent apoptosis in human colon cancer cells. International Journal of Cancer 118:1309-1315.

123. Correa P. 1992. Human Gastric Carcinogenesis: A Multistep and Multifactorial Process—First American Cancer Society Award Lecture on Cancer Epidemiology and Prevention. Cancer Research 52:6735-6740.

124. Furth PA. 2012. Cancer prevention as biomodulation: targeting the initiating stimulus and secondary adaptations. Annals of the New York Academy of Sciences 1271:1-9.

125. Wroblewski LE, Choi E, Petersen C, Delgado AG, Piazuelo MB, Romero-Gallo J, Lantz TL, Zavros Y, Coffey RJ, Goldenring JR, Zemper AE, Peek RM. 2019. Targeted mobilization of Lrig1+ gastric epithelial stem cell populations by a carcinogenic Helicobacter pylori type IV secretion system. Proceedings of the National Academy of Sciences 116:19652-19658.

126. Saha A, Hammond CE, Beeson C, Peek RM, Jr., Smolka AJ. 2010. Helicobacter pylori represses proton pump expression and inhibits acid secretion in human gastric mucosa. Gut 59:874-881.

127. Yao X, Smolka AJ. 2019. Gastric Parietal Cell Physiology and Helicobacter pylori-Induced Disease. Gastroenterology 156:2158-2173.

128. Noto JM, Peek RM, Jr. 2017. The gastric microbiome, its interaction with Helicobacter pylori, and its potential role in the progression to stomach cancer. PLoS pathogens 13:e1006573.

129. Noto JM, Zackular JP, Varga MG, Delgado A, Romero-Gallo J, Scholz MB, Piazuelo MB, Skaar EP, Peek RM. 2019. Modification of the Gastric Mucosal Microbiota by a Strain-

Specific Helicobacter pylori Oncoprotein and Carcinogenic Histologic Phenotype. mBio 10:e00955-19.

130. Pereira-Marques J, Ferreira RM, Pinto-Ribeiro I, Figueiredo C. 2019. Helicobacter pylori Infection, the Gastric Microbiome and Gastric Cancer, p 195-210. *In* Kamiya S, Backert S (ed), Helicobacter pylori in Human Diseases: Advances in Microbiology, Infectious Diseases and Public Health Volume 11. Springer International Publishing, Cham.

131. Schulz C, Schütte K, Mayerle J, Malfertheiner P. 2019. The role of the gastric bacterial microbiome in gastric cancer: Helicobacter pylori and beyond. Therapeutic Advances in Gastroenterology 12:1756284819894062.

132. Tan S, Noto JM, Romero-Gallo J, Peek RM, Jr., Amieva MR. 2011. Helicobacter pylori perturbs iron trafficking in the epithelium to grow on the cell surface. PLoS pathogens 7:e1002050-e1002050.

133. Romero-Gallo J, Harris EJ, Krishna U, Washington MK, Perez-Perez GI, Peek RM, Jr. 2008. Effect of Helicobacter pylori eradication on gastric carcinogenesis. Laboratory investigation; a journal of technical methods and pathology 88:328-336.

134. Choi IJ, Kim CG, Lee JY, Kim Y-I, Kook M-C, Park B, Joo J. 2020. Family History of Gastric Cancer and Helicobacter pylori Treatment. New England Journal of Medicine 382:427-436.

135. Freedberg DE, Abrams JA, Wang TC. 2014. Prevention of Gastric Cancer With Antibiotics: Can It Be Done Without Eradicating Helicobacter pylori ? JNCI: Journal of the National Cancer Institute 106.

136. Li W-Q, Ma J-L, Zhang L, Brown LM, Li J-Y, Shen L, Pan K-F, Liu W-D, Hu Y, Han Z-X, Crystal-Mansour S, Pee D, Blot WJ, Fraumeni JF, You W-C, Gail MH. 2014. Effects of Helicobacter pylori Treatment on Gastric Cancer Incidence and Mortality in Subgroups. JNCI: Journal of the National Cancer Institute 106.

137. Lin AS, McClain MS, Beckett AC, Caston RR, Harvey ML, Dixon BREA, Campbell AM, Shuman JHB, Sawhney N, Delgado AG, Loh JT, Piazuelo MB, Algood HMS, Cover TL. 2020. Temporal Control of the Helicobacter pylori Cag Type IV Secretion System in a Mongolian Gerbil Model of Gastric Carcinogenesis. mBio 11:e01296-20.

138. Pellegrino RM, Di Veroli A, Valeri A, Goracci L, Cruciani G. 2014. LC/MS lipid profiling from human serum: a new method for global lipid extraction. Analytical and Bioanalytical Chemistry 406:7937-7948.

139. Breitkopf SB, Ricoult SJH, Yuan M, Xu Y, Peake DA, Manning BD, Asara JM. 2017. A relative quantitative positive/negative ion switching method for untargeted lipidomics via high resolution LC-MS/MS from any biological source. Metabolomics 13:30.

140. Hutchins PD, Russell JD, Coon JJ. 2018. LipiDex: An Integrated Software Package for High-Confidence Lipid Identification. Cell Systems 6:621-625.e5.

141. Aichler M, Walch A. 2015. MALDI Imaging mass spectrometry: current frontiers and perspectives in pathology research and practice. Laboratory Investigation 95:422-431.

142. Lichtenberger LM. 2013. Role of Phospholipids in Protection of the GI Mucosa. Digestive Diseases and Sciences 58:891-893.

143. Sunshine H, Iruela-Arispe ML. 2017. Membrane lipids and cell signaling. Current opinion in lipidology 28:408-413.

144. Wymann MP, Schneiter R. 2008. Lipid signalling in disease. Nature Reviews Molecular Cell Biology 9:162-176.

145. Lingwood CA, Huesca M, Kuksis A. 1992. The glycerolipid receptor for Helicobacter pylori (and exoenzyme S) is phosphatidylethanolamine. Infection and immunity 60:2470-2474.

146. Nardone G, D'Armiento F, Corso G, Coscione P, Esposito M, Budillon G. 1994. Lipids of human gastric mucosa: Effect of Helicobacter pylori infection and nonalcoholic cirrhosis. Gastroenterology 107:362-368.

147. Kwok T, Zabler D, Urman S, Rohde M, Hartig R, Wessler S, Misselwitz R, Berger J, Sewald N, König W, Backert S. 2007. Helicobacter exploits integrin for type IV secretion and kinase activation. Nature 449:862-866.

148. Baidya AK, Rosenshine I, Ben-Yehuda S. 2020. Donor-delivered cell wall hydrolases facilitate nanotube penetration into recipient bacteria. Nature Communications 11:1938.

149. Savvides SN, Yeo H-J, Beck MR, Blaesing F, Lurz R, Lanka E, Buhrdorf R, Fischer W, Haas R, Waksman G. 2003. VirB11 ATPases are dynamic hexameric assemblies: new insights into bacterial type IV secretion. The EMBO journal 22:1969-1980.

150. Hilleringmann M, Pansegrau W, Doyle M, Kaufman S, MacKichan ML, Gianfaldoni C, Ruggiero P, Covacci A. 2006. Inhibitors of Helicobacter pylori ATPase Cagα block CagA transport and cag virulence. Microbiology 152:2919-2930.

151. Arya T, Oudouhou F, Casu B, Bessette B, Sygusch J, Baron C. 2019. Fragment-based screening identifies inhibitors of ATPase activity and of hexamer formation of Cagα from the Helicobacter pylori type IV secretion system. Scientific reports 9:6474-6474.

152. Radics J, Königsmaier L, Marlovits TC. 2014. Structure of a pathogenic type 3 secretion system in action. Nature Structural & Molecular Biology 21:82-87.

153. Park D, Chetrit D, Hu B, Roy CR, Liu J. 2020. Analysis of Dot/Icm Type IVB Secretion System Subassemblies by Cryoelectron Tomography Reveals Conformational Changes Induced by DotB Binding. mBio 11:e03328-19.

154. Takahashi-Kanemitsu A, Knight CT, Hatakeyama M. 2020. Molecular anatomy and pathogenic actions of Helicobacter pylori CagA that underpin gastric carcinogenesis. Cellular & Molecular Immunology 17:50-63.